EVAPORATED THIN FILM DISTRIBUTED RC NETWORKS

THEORETICAL AND EXPERIMENTAL STUDIES OF EVAPORATED THIN FILM DISTRIBUTED RC NETWORKS

By

JAMES A. CARSON, B. Eng.

A Thesis

Submitted to the Faculty of Graduate Studies

in Partial Fulfillment of the Requirements

for the Degree

Master of Engineering

McMaster University

December 1969

MASTER OF ENGINEERING (1969) McMASTER UNIVERSITY
(Electrical Engineering) Hamilton, Ontario.

TITLE: Theoretical and Experimental Studies of Evaporated Thin Film Distributed RC Networks.

AUTHOR: James Alexander Carson, B. Eng.
(McMaster University)

SUPERVISOR: Professor C. K. Campbell.

NUMER OF PAGES: (xi); 135.

SCOPE AND CONTENTS:

Thin film uniform and exponential distributed RC networks were fabricated and the network responses were investigated. It was necessary to take dielectric loss into consideration in the theoretical analysis before a close agreement could be obtained between the theoretical and experimental network responses.

ABSTRACT

Theoretical and experimental studies were carried out on evaporated thin film uniform and exponential distributed RC networks. Effects of finite dielectric losses were included in the theoretical analysis. Particular structures fabricated and tested were uniform and exponential RC networks of the type Aluminum/Silicon Monoxide/Nichrome. Notch filters incorporating such distributed networks exhibited notch attenuations of 71 db at 5.6 KH_Z and 62 db at 2.4 KH_Z respectively. An acceptable agreement was obtained between the experimental results and the theoretical predictions as extended to the lossy model.

ACKNOWLEDGEMENTS

The author wishes to show his appreciation to Dr. C.K. Campbell for his guidance and interest during this project.

Special thanks is given to Dr. H.I. Ralph for his suggestion of this topic and his guidance during the initial stages of the project.

In particular I wish to thank Mr. P.L. Swart for his continuous advice and encouragement throughout this work. I have also profited from discussions with Mr. F. Vallo whose suggestions proved to be invaluable.

Dr. S.S. Haykim kindly allowed the author the use of his research facilities which greatly aided in measurements carried out during this project.

The author also wishes to express his appreciation to those authorities of the Canadian Armed Forces who enabled him to proceed on the University program.

This project was financed through a grant-in-aid from the National Research Council of Canada to Dr. C.K. Campbell. The author is also indebted to McMaster University for financial support in the form of a McMaster Assistantship.

The author would also like to convey his sincere appreciation to Mrs. Intson for her help in the preparation of this manuscript.

TABLE OF CONTENTS

LIST OF FIGURES

CHAPTER I

INTRODUCTION

1.0 General

Current interest in integrated and thin film circuits has focused attention on the network properties of distributed RC networks. Increased reliability gained from a reduced number of interconnections between circuit components is one of the most important features of microcircuits. It has therefore become desirable to replace a lumped component circuit with a distributed circuit having an equivalent electrical performance if the number of interconnections can be reduced. Several papers have been published on distributed RC networks which were fabricated using semiconductor materials. It would seem, however, that there is a limited amount of material on distributed RC networks which were fabricated using evaporated thin film techniques.

Many methods are available for deposition of thin film components. Thin film deposition in this thesis was carried out by evaporation from resistively heated sources in a high vacuum. The vapor thus produced is condensed onto a flat insulating sheet called the substrate. The properties of the deposited film can be controlled by varying the substrate temperature, rate of deposition and

residual gas pressure. Another method of thin film deposition is "sputtering" where the material to be evaporated acts as the cathode and the substrate is the anode. It should also be noted that the desired pattern can be generated by using selective pattern etching. In this case the entire side of the substrate is coated with the desired material. Photo-resist techniques and etching are then used to produce the desired geometry.

1.1 Scope of this Thesis

Two types of distributed RC networks are investigated in this thesis; the uniform distributed RC network and the exponentially tapered distributed RC network. A one-dimensional analysis was used where the basic concept of "resistance per unit length" is meaningful. In most practical distributed circuits constructed by using the thin film or deposition techniques, the resistivity per unit square in the resistive film and the capacitance per unit area of a circuit are constant. This means that the parameters of "resistance and capacitance per unit length" must be controlled by varying the geometry of the network. However, one-dimensional analysis for an exponentially tapered distributed RC network is an approximation method which was found to be reasonably accurate. Other workers[6] in the field have derived a two-dimensional model for a network with an exponential taper, which was found to be more accurate.

It was found necessary in this thesis to take dielectric loss into consideration before a reasonable agreement between the theoretical and experimental network responses could be obtained. The theory for the dielectric loss pertaining to the different network responses is discussed in Chapter III.

CHAPTER II

Theory of Distributed Parameter Filters

2.0 Introduction

To get a clear understanding of the thin film distributed RC network, one must first look at the network properties. A distributed RC filter can be characterized if one knows the two-port driving point admittances and the transfer function of the filter. In this thesis, we are concerned with two types of distributed RC filters; the uniform distributed RC filter (referred to as the $\overline{URC}$ filter from here on) and the exponentially distributed RC filter (referred to as the $\overline{ERC}$ filter from here on).

2.1 $\overline{URC}$ Low Pass Filter[1,2]

The $\overline{URC}$ filter consists of a highly conducting layer, a dielectric layer and a resistive layer as shown in Figure 2:1. Assuming the highly conducting layer has zero resistance, the structure can be equated to a lossy transmission line as shown in Figure 2:2.

The incremental network representation is an approximation that becomes more accurate as $\Delta x \to 0$. The four distributed parameters characterizing the transmission

FIGURE 2:1

(a) Physical structure of a $\overline{\text{URC}}$ network

(b) Schematic symbol of a $\overline{\text{URC}}$ network

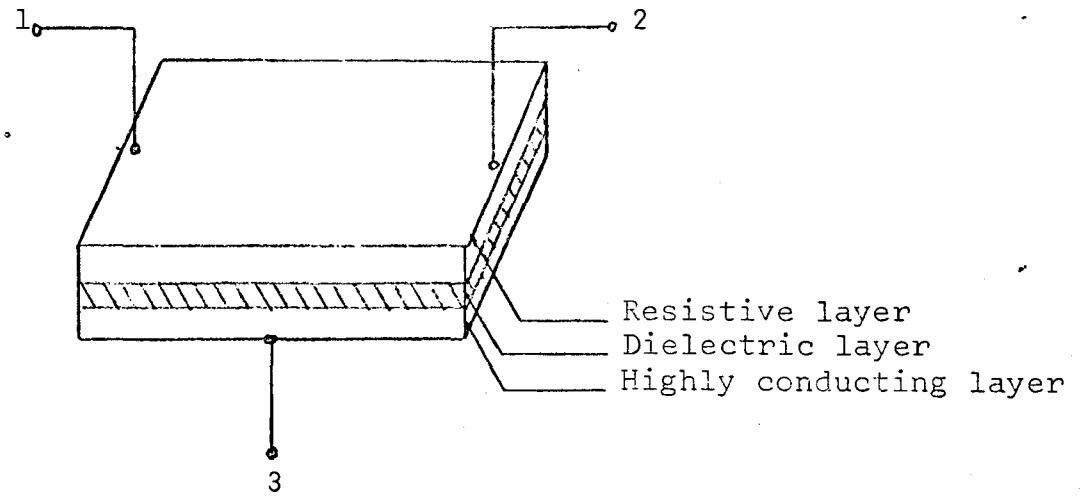
1
2
3
Resistive layer
Dielectric layer
Highly conducting layer

(a)

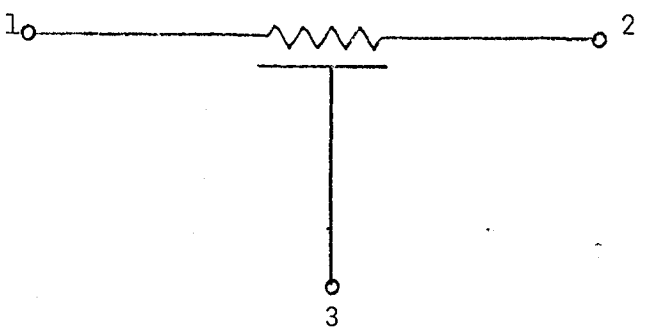
1
2
3

(b)

FIGURE 2:2

Incremental network model of a lossy transmission line

FIGURE 2:3

Linear two-port network

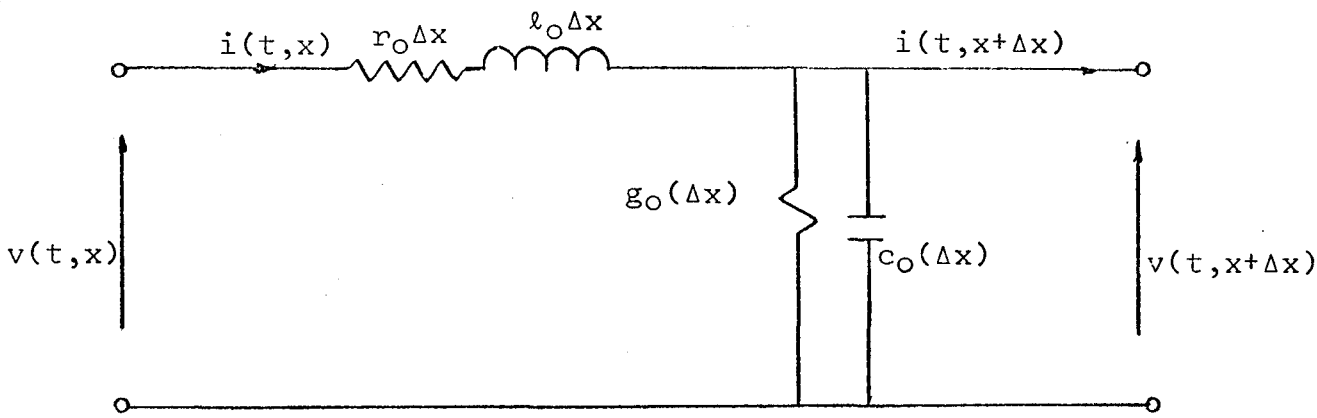

Figure 2:2

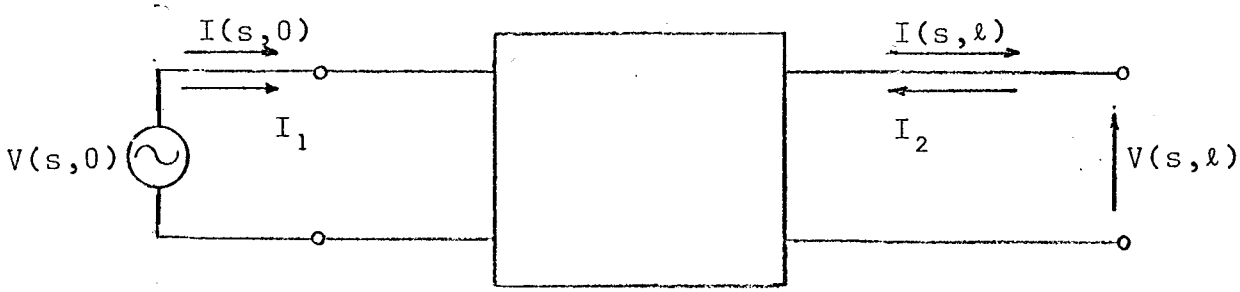

Figure 2:3

line are r_o [ohms/unit length], ℓ_o [henries/unit length], g_o [mhos/unit length] and c_o [farads/unit length]. The equilibrium equations of the circuit by Kirchoff's voltage and current laws are

$$v(t,x + \Delta x) - v(t,x) = - \Delta x[\ell_o \frac{\partial i(t,x)}{\partial t} + r_o i(t,x)] \qquad .....2.1$$

$$i(t,x + \Delta x) - i(t,x) = - \Delta x[c_o \frac{\partial v(t,x + \Delta x)}{\partial t} + g_o v(t,x + \Delta x)] \qquad .....2.2$$

Dividing by Δx and taking the limit as $\Delta x \to 0$ gives us the following partial differential equations:

$$\frac{\partial v(t,x)}{\partial x} = - \ell_o \frac{\partial i(t,x)}{\partial t} - r_o i(t,x) \qquad .....2.3$$

$$\frac{\partial i(t,x)}{\partial x} = - c_o \frac{\partial v(t,x)}{\partial t} - g_o v(t,x) \qquad .....2.4$$

By taking the Laplace transform of both sides of equations 2.3 and 2.4 we get

$$\frac{dV}{dx}(s,x) = - (\ell_o s + r_o) I(s,x) \qquad .....2.5$$

$$\frac{dI}{dx}(s,x) = - (c_o s + g_o) V(s,x) \qquad .....2.6$$

Differentiating 2.5 and 2.6 with respect to x gives

$$\frac{d^2V}{dx^2}(s,x) = - (\ell_o s + r_o) \frac{dI}{dx}(s,x) \qquad .....2.7$$

$$\frac{d^2I}{dx^2}(s,x) = - (c_o s + g_o) \frac{dV}{dx}(s,x) \qquad .....2.8$$

Substituting equation 2.6 in 2.7 gives

$$\frac{d^2V}{dx^2}(s,x) = (\ell_o s + r_o)(c_o s + g_o)V(s,x) \quad .....2.9$$

Similarly, substituting equation 2.5 in 2.8 gives

$$\frac{d^2I}{dx^2}(s,x) = (c_o s + g_o)(\ell_o s + r_o)V(s,x) \quad .....2.10$$

Equations 2.9 and 2.10 are second order linear differential equations and solutions are of the type

$$V(s,x) = A_1 \cosh\gamma_o x + A_2 \sinh\gamma_o x \quad .....2.11$$

$$I(s,x) = B_1 \cosh\gamma_o x + B_2 \sinh\gamma_o x \quad .....2.12$$

where

$$\gamma o = \sqrt{(\ell_o s + r_o)(c_o s + g_o)} \quad .....2.13$$

and is usually referred to as the propagation function. The terms A_1, A_2, B_1 and B_2 are not functions of x, but are determined from the boundary conditions. At this point we can consider the distributed RC network. The transmission line would become a distributed RC network when $\ell_o = 0$ and $g_o = 0$. In this work, dimensions of the physical structure are such that the inductance per unit length is negligible and will be ignored. However, the leakage conductance per unit length will be dependent on the properties of the dielectric. When the filter was fabricated by us, the leakage

resistance was measured and a program was run to determine its effect on the various parameters. These results are shown in Chapter 3 and it can be concluded that the leakage conductance in this case has no noticeable effect on the various parameters. We can now return to equation 2.13 and conclude that the propagation function is

$$\gamma_o = \sqrt{sc_or_o} \qquad .....2.14$$

Let us now return to equations 2.9 and 2.10. For a distributed RC network where $\ell_o = 0$ and $g_o = 0$ we obtain

$$\frac{d^2V}{dx^2}(s,x) - sc_or_oV(s,x) = 0 \qquad .....2.15$$

$$\frac{d^2I}{dx^2}(s,x) - sc_or_oI(s,x) = 0 \qquad .....2.16$$

A known general solution to equation 2.15 is

$$V(s,x) = A_1e^{\gamma_o x} + A_2e^{-\gamma_o x} \qquad .....2.17$$

where

$$\gamma_o = \sqrt{sc_or_o}$$

We shall assume that the structure has a length equal to λ and treat it as a two-port network with I_1, V_1 denoting the conditions at port 1-1' and I_2, V_2 the conditions at port 2-2'. The two port network is as shown in Figure 2:3.

Evaluating equation 2.17 at $x = 0$ and $x = \lambda$ we obtain

$$V_1 = V(s,o) = A_1 + A_2$$

$$V_2 = V(s,\lambda) = A_1 e^{\gamma_o \lambda} + A_2 e^{-\gamma_o \lambda} \qquad .....2.18$$

Solving equations 2.18 for A_1 and A_2 we obtain

$$A_1 = - \frac{e^{-\gamma_o \lambda} V_1}{e^{\gamma_o \lambda} - e^{-\gamma_o \lambda}} + \frac{V_2}{e^{\gamma_o \lambda} - e^{-\gamma_o \lambda}} \qquad .....2.19$$

$$A_2 = \frac{e^{\gamma_o \lambda} V_1}{e^{\gamma_o \lambda} - e^{-\gamma_o \lambda}} - \frac{V_2}{e^{\gamma_o \lambda} - e^{-\gamma_o \lambda}}$$

To determine the current flow, we set $\ell_o = 0$ in equation 2.5 obtaining

$$I(s,x) = - \frac{1}{r_o} \frac{dV(s,x)}{dx} \qquad .....2.20$$

Using equations 2.17 and 2.20 we obtain

$$I(s,x) = - \frac{1}{Z_o} [A_1 e^{\gamma_o x} - A_2 e^{-\gamma_o x}] \qquad .....2.21$$

Where Z_o is the characteristic impedance of the network defined by

$$Z_o = \sqrt{\frac{r_o}{sc_o}} \qquad .....2.22$$

Evaluating equation 2.21 at $x = 0$ and $x = \lambda$, we obtain

$$I_1 = I(s,o) = \frac{1}{Z_o} [A_1 - A_2] \qquad .....2.23$$

$$I_2 = -I(s,\lambda) = \frac{1}{Z_o}\left[A_1 e^{\gamma_o \lambda} - A_2 e^{-\gamma_o \lambda}\right]$$

Substituting values of A_1 and A_2 in equations 2.23 gives

$$\begin{bmatrix} I_1 \\ I_2 \end{bmatrix} = \frac{1}{Z_o}\begin{bmatrix} \coth\gamma_o\lambda & -\operatorname{csch}\gamma_o\lambda \\ -\operatorname{csch}\gamma_o\lambda & \coth\gamma_o\lambda \end{bmatrix}\begin{bmatrix} V_1 \\ V_2 \end{bmatrix} \qquad \ldots\ldots 2.24$$

The y-parameters of the $\overline{URC}$ network are therefore

$$y_{11} = y_{22} = \frac{\coth\gamma_o\lambda}{Z_o} = \frac{1}{Z_o}\frac{\cosh\gamma_o\lambda}{\sinh\gamma_o\lambda}$$

$$y_{12} = y_{21} = \frac{-\operatorname{csch}\gamma_o\lambda}{Z_o} \quad \frac{-1}{Z_o}\frac{1}{\sinh\gamma_o\lambda} \qquad \ldots\ldots 2.25$$

The open circuit impedance parameters can be shown to be

$$z_{11} = z_{22} = Z_o\coth\gamma_o\lambda = Z_o\frac{\cosh\gamma_o\lambda}{\sinh\gamma_o\lambda}$$

$$z_{12} = z_{21} = Z_o\operatorname{csch}\gamma_o\lambda = Z_o\frac{1}{\sinh\gamma_o\lambda} \qquad \ldots\ldots 2.26$$

Since only the y-parameters of the $\overline{URC}$ filter were measured, they will be the only parameters considered from here on. If the z-parameters are desired, they can easily be derived from the y-parameters through conversion.

The pole zero locations of the y-parameters may be determined by expanding equations 2.25 into product form. This can be done by making use of the relations

$$\frac{\sinh\theta}{\theta} = \prod_{n=1}^{\infty}\left(1+ \frac{\theta^2}{n^2\pi^2}\right) \qquad .....2.27$$

$$\cosh\theta = \prod_{n=1}^{\infty}\left[1 + \frac{4\theta^2}{(2n-1)^2\pi^2}\right]$$

Taking note that $\theta = \sqrt{SCR}$, the y-parameters of equation 2.25 may now be expressed in the form

$$y_{11}(s) = y_{22}(s) = \frac{1}{R}\prod_{n=1}^{\infty}\frac{\left(1 + \frac{4SCR}{(2n-1)^2\pi^2}\right)}{\left(1 + \frac{SCR}{n^2\pi^2}\right)} \qquad .....2.28$$

$$y_{12}(s) = y_{21}(s) = -\frac{1}{R}\prod_{n=1}^{\infty}\frac{1}{\left(1 + \frac{SCR}{n^2\pi^2}\right)}$$

where $R = r_o\lambda$ is the total resistance of the network and $C = c_o\lambda$ is the total capacitance of the network.

By considering equations 2.28, one can see that the poles and zeros of the short circuit driving point admittances are infinite in number, alternating along the negative real axis of the s-plane with a zero as the nearest critical frequency to the origin. This is shown in Figure 2:4(a). By considering the latter of equations 2.28, one can see that the transfer admittances have the same poles as the driving point admittances with no finite zeros as shown in Figure 2:4(b).

FIGURE 2:4

(a) Pole-zero diagram of $y_{11}(s) = y_{22}(s)$

(b) Pole-zero diagram of $y_{12}(s) = y_{21}(s)$

(c) Pole-zero diagram of $v_2(s)/v_1(s)$

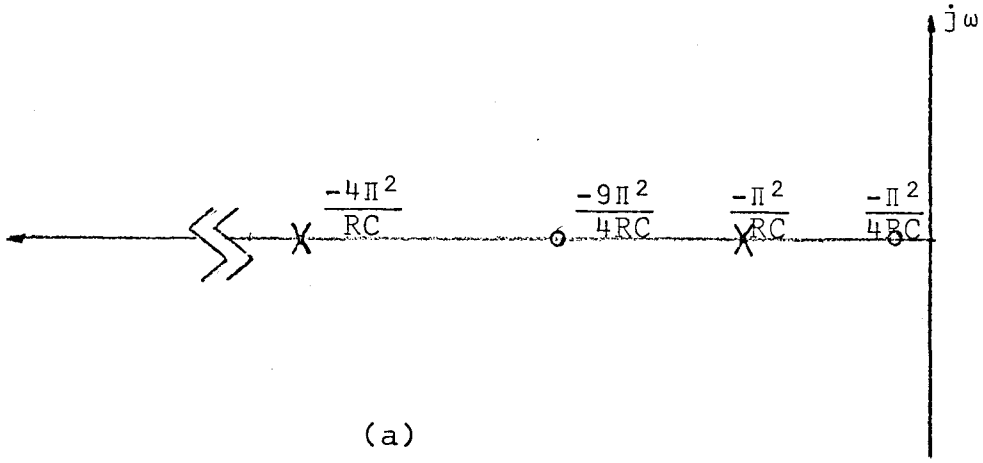
jω
$\frac{-4\Pi^2}{RC}$
$\frac{-9\Pi^2}{4RC}$
$\frac{-\Pi^2}{RC}$
$\frac{-\Pi^2}{4RC}$

(a)

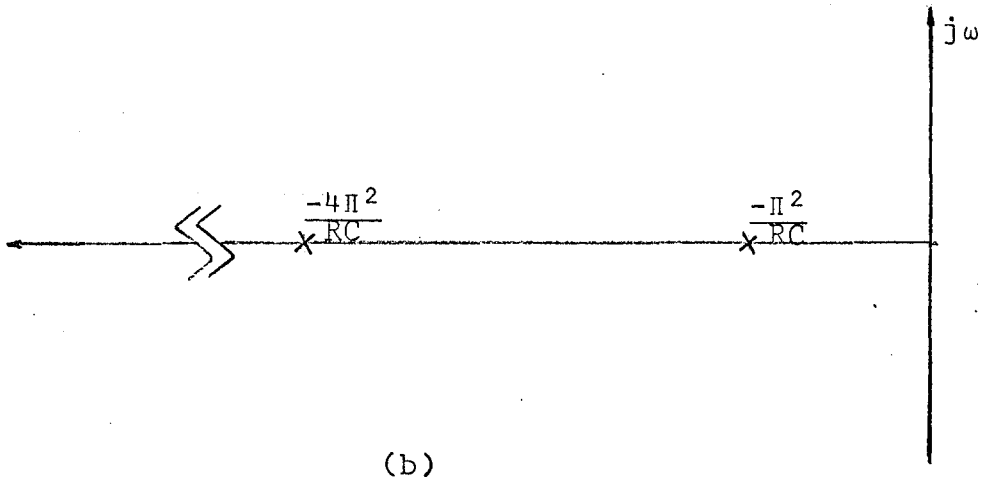
jω
$\frac{-4\Pi^2}{RC}$
$\frac{-\Pi^2}{RC}$

(b)

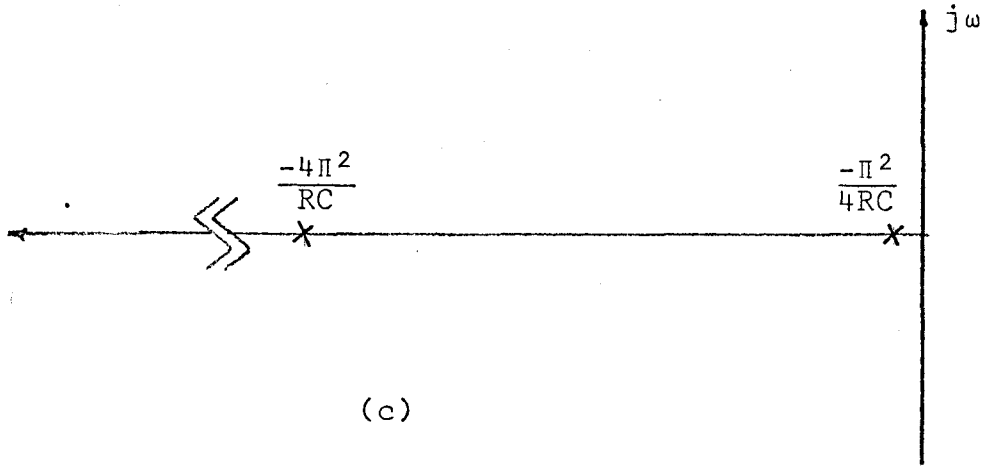
jω
$\frac{-4\Pi^2}{RC}$
$\frac{-\Pi^2}{4RC}$

(c)

The magnitude and phase angle of the short circuit input admittance and the transfer admittance can be determined using equations 2.25 and normalizing with respect to R. We then get

$$Ry_{11}(j\omega) = Ry_{22}(j\omega) = \sqrt{j\frac{\omega}{\omega_o}}\ \frac{\cosh\sqrt{j\frac{\omega}{\omega_o}}}{\sinh\sqrt{j\frac{\omega}{\omega_o}}} \qquad .....2.29$$

$$Ry_{12}(j\omega) = Ry_{21}(j\omega) = -\sqrt{j\frac{\omega}{\omega_o}}\ \frac{1}{\sinh\sqrt{j\frac{\omega}{\omega_o}}}$$

where $\omega_o = \frac{1}{RC}$

The magnitude and phase of the driving point admittances and transfer admittance are shown in Figures 2:5 and 2:6 respectively. By considering Figure 2:5, one can see that at high frequencies the magnitude has a slope of 3 dbs/ octave while the phase approaches 45° as a limit. Both these characteristics are half of those for a lumped network consisting of R and C in parallel. The magnitude and phase of the transfer admittance are ever decreasing functions with respect to an increase in frequency, which is to be expected since the function is composed only of poles.

The voltage transfer function (V_2/V_1) of the filter under no-load conditions can be determined by considering the y-parameter equations

$$I_1 = V_1 y_{11} + V_2 y_{12}$$

FIGURE 2:5

Magnitude and phase of the driving point admittance of a $\overline{URC}$ low pass filter.

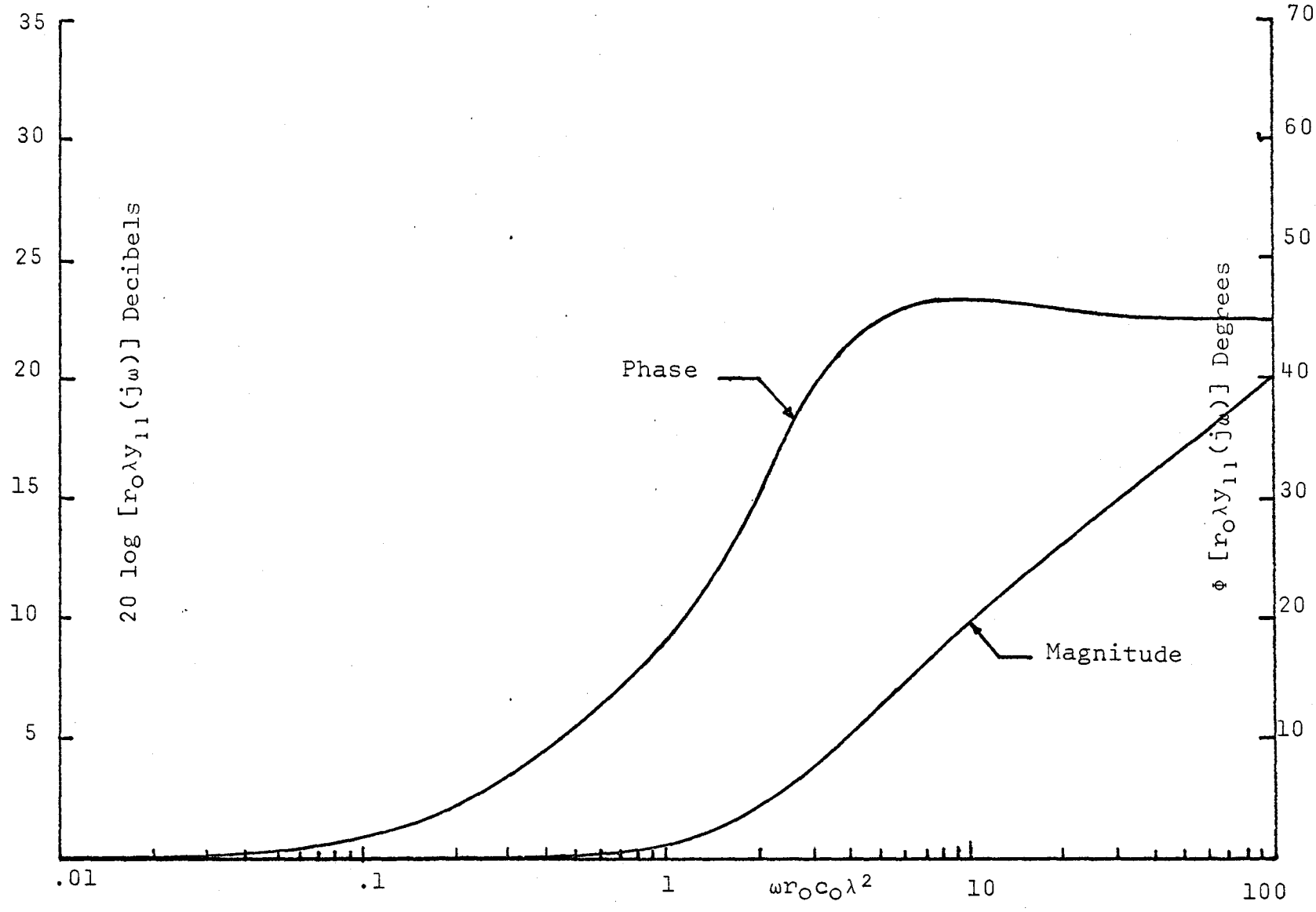
35
30
25
20
15
10
5
20 log [$r_o\lambda y_{11}(j\omega)$] Decibels
70
60
50
40
30
20
10
ϕ [$r_o\lambda y_{11}(j\omega)$] Degrees
Phase
Magnitude
.01
.1
1
10
100
$\omega r_o c_o \lambda^2$

FIGURE 2:6

Magnitude and phase of the transfer admittance of a $\overline{URC}$ low pass filter.

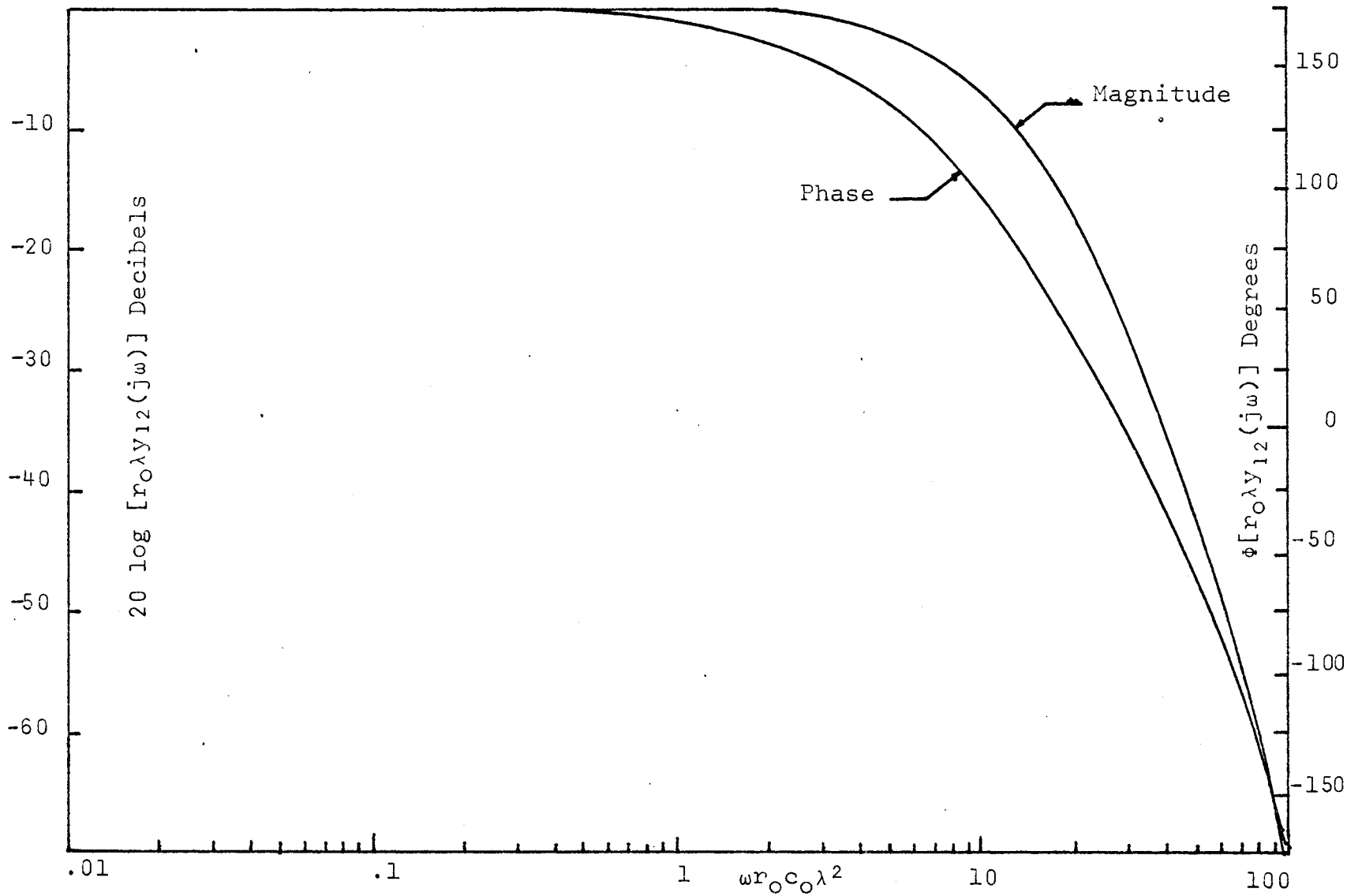
Magnitude
Phase
-10
-20
-30
-40
-50
-60
20 log [r_o λ y_12(jω)] Decibels
150
100
50
0
-50
-100
-150
φ[r_o λ y_12(jω)] Degrees
.01
.1
1
10
100
ωr_o c_o λ^2

FIGURE 2:7

Magnitude and phase of the voltage transfer function of a $\overline{URC}$ low pass filter.

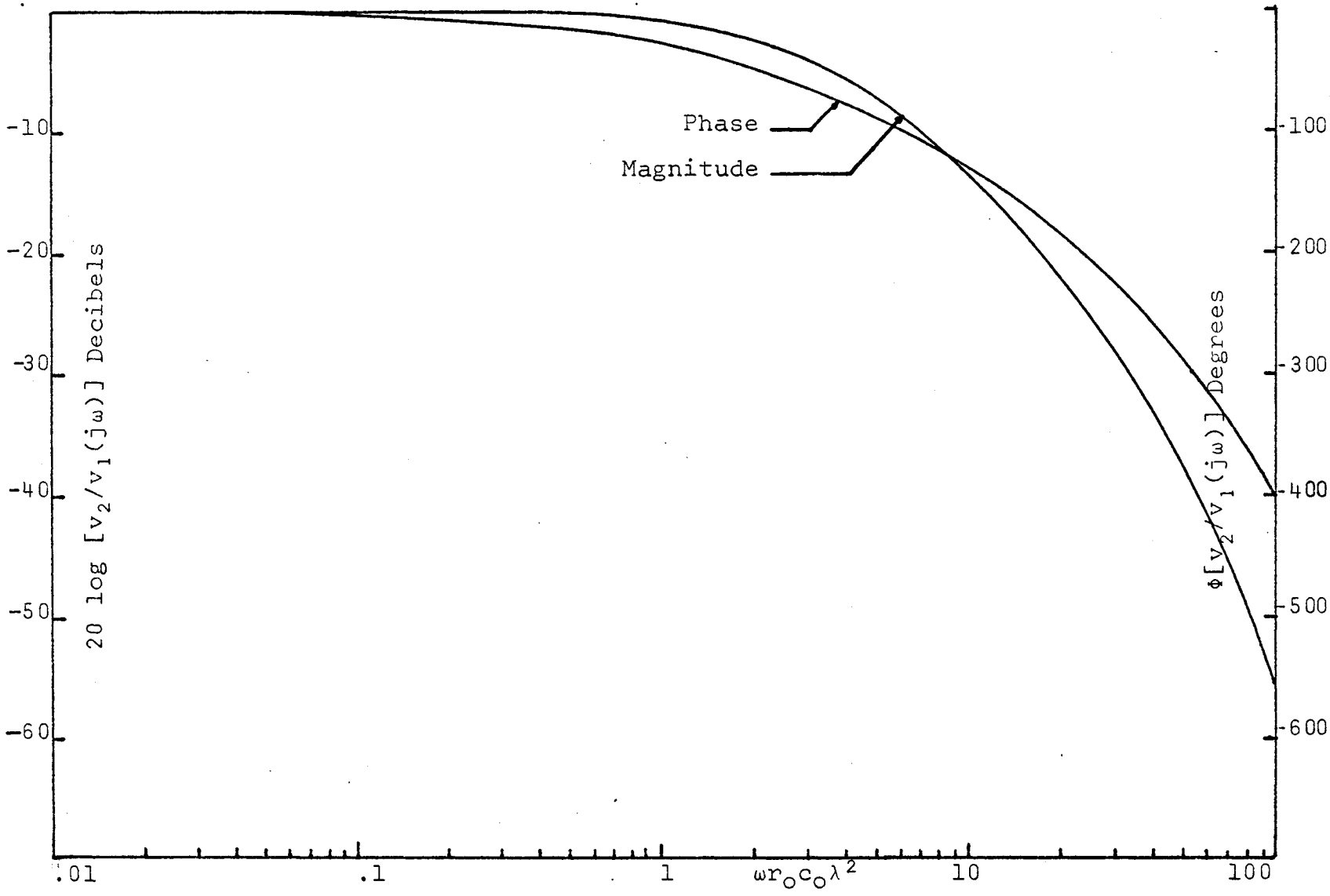
Phase
Magnitude
-10
-20
-30
-40
-50
-60
20 log [v2/v1(jω)] Decibels
-100
-200
-300
-400
-500
-600
Φ[v2/v1(jω)] Degrees
.01
.1
1
ωr0c0λ2
10
100

$$I_2 = V_1 y_{21} + V_2 y_{22} \qquad \text{.....2.30}$$

Under no-load conditions, $I_2 = 0$ and

$$\frac{V_2}{V_1} = \frac{-y_{21}}{y_{22}} = \frac{1}{\cosh\sqrt{j\frac{\omega}{\omega_o}}} \qquad \text{.....2.31}$$

The pole-zero diagram of the voltage transfer function is shown in Figure 2:4(c) and it can be seen that the function is composed entirely of poles. Therefore, the magnitude and phase will be ever decreasing functions with respect to an increase in frequency as shown in Figure 2:7.

It is interesting to note that, theoretically, the 3db frequency point of a $\overline{URC}$ filter is 2.44 times the cut-off point of a lumped parameter RC network for the same values of R and C. This can be shown as follows

$$\text{Let } T(s) = \frac{V_2(s)}{V_1(s)} = \frac{1}{\cosh\sqrt{jx}}$$

where $x = \omega RC$

$$|T(j\omega)|^2 = \frac{1}{\prod_{n=1}^{\infty}[1 + \frac{16R^2C^2\omega^2}{(2n-1)^4\pi^4}]} \qquad \text{.....2.31}$$

To determine the 3db frequency (half power point) we let

$$|T(j\omega)|^2_{\omega=\omega_{3db}} = \frac{1}{2}$$

We then have

$$\prod_{n=1}^{\infty}\left[1 + \frac{16R^2C^2\omega_{3db}^2}{(2n-1)^4\Pi^4}\right] = 2 \qquad .....2.32$$

$$2 = \left[1 + \left(\frac{\omega 3db}{P_1}\right)^2\right]\left[1 + \left(\frac{\omega 3db}{P_2}\right)^2\right]\left[1 + \left(\frac{\omega 3db}{P_3}\right)^2\right] \qquad .....2.33$$

We can let

$$P_n = \frac{(2n-1)^2\Pi^2}{4RC} \qquad .....2.34$$

where $P_1 < P_2 < P_3$

Equation 2.33 can be written in the following form

$$2 = 1 + \omega_{3db}^2\left[\frac{1}{P_1^2} + \frac{1}{P_2^2} + \frac{1}{P_3^2} + \ldots\right] + \omega_{3db}^4\left[\frac{1}{P_1^2P_2^2} + \frac{1}{P_1^2P_3^2} + \ldots\right] \qquad .....2.35$$

If we assume that

$$\omega_{3db} < P_1 < P_2 < P_3 \ldots\ldots\ldots\ldots$$

we can then write equation 2.35 as follows

$$\frac{1}{\omega_{3db}} = \left[\frac{1}{P_1^2} + \frac{1}{P_2^2} + \frac{1}{P_3^2} + \ldots.\right]^{\frac{1}{2}} \qquad .....2.36$$

$$\omega_{3db} = \frac{1}{\left[\sum_{n=1}^{\infty} \frac{1}{(Pn)^2}\right]^{\frac{1}{2}}}$$

$$= \frac{1}{\left[\sum_{n=1}^{\infty} \frac{16R^2C^2}{(2n-1)^4\Pi^4}\right]^{\frac{1}{2}}}$$

$$= \frac{\Pi^2}{4RC} \frac{1}{\left[\sum_{n=1}^{\infty} \frac{1}{(2n-1)^4}\right]^{\frac{1}{2}}}$$

Let us choose n=3 since values greater than this are insignificant. We then have

$$\omega_{3db} = \frac{\Pi^2}{4RC} \frac{1}{(1 + \frac{1}{81} + \frac{1}{625} + \ldots]^{\frac{1}{2}}}$$

$$= \frac{\Pi^2}{4(1.01)RC} = \frac{2.44}{RC}$$

By checking Figure 2:7, we see that the 3db point is indeed 2.44 times ω_o and we can conclude that our assumption of $\omega_{3db} < P_1 < P_2 < P_3 \ldots$ is correct.

2.2 URC Notch Filter[4,5]

The notch filter is also considered in this thesis because of its importance in frequency selectivity where it is used in a degenerative feedback loop around a high

FIGURE 2:8

(a) Physical structure of a $\overline{URC}$ notch filter

(b) Schematic representation of a $\overline{URC}$ notch filter

(c) Voltage vector diagram of a $\overline{URC}$ notch filter

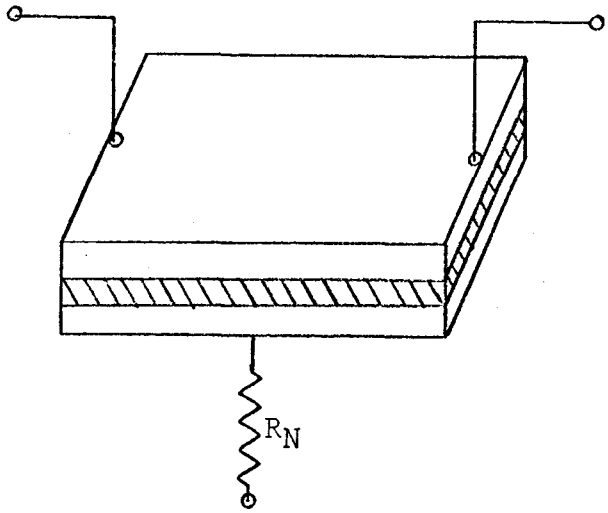

(a)

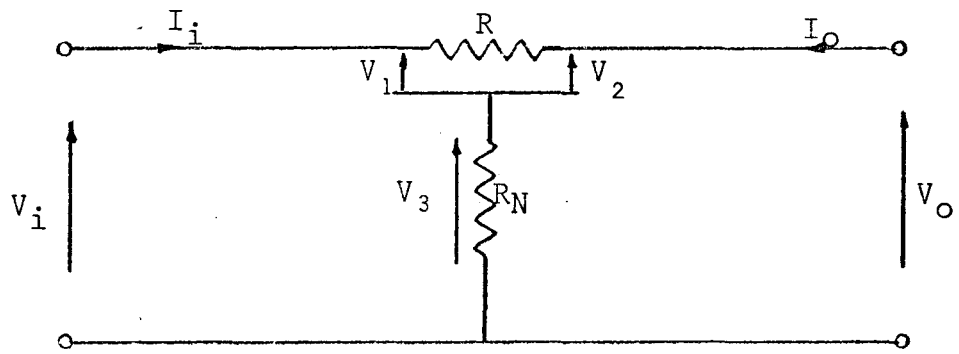

(b)

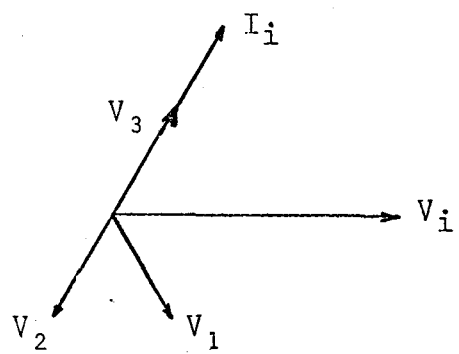

(c)

gain amplifier. The $\overline{URC}$ notch filter is identical to the $\overline{URC}$ low pass filter except for a lumped resistor connected between the highly conducting layer and ground as shown in Figure 2:8.

Referring to Figure 2:8(b), we can consider the $\overline{URC}$ notch filter under no-load conditions. When an input voltage V_i is applied, the input current flows through R_N producing a voltage V_3. Because the imaginary part of the input impedance of the distributed section is capacitive, the voltage across this section, V_1, lags V_i and the input current, hence V_3 leads V_i. Also, the distributed section can produce more than 90° of phase shift. Therefore, when the attenuated voltage, V_2, is equal and opposite to V_3, as shown in Figure 2:8(c), the output voltage V_o is equal to zero.

The transfer function of the $\overline{URC}$ notch filter can be determined by considering a series-series cascade configuration where the z-parameters can be added. We then have

$$z_{11d} = z_{22d} = \frac{R}{u}\frac{\cosh u}{\sinh u}$$

$$z_{12d} = z_{21d} = \frac{R}{u}\frac{1}{\sinh u} \qquad \text{.....2.37}$$

$$z_{11\ell} = z_{22\ell} = R_N$$

$$z_{12\ell} = z_{21\ell} = R_N$$

Where

$$u = \sqrt{j\frac{\omega}{\omega_o}}$$

d = distributed network

ℓ = lumped network

Taking the complete circuit into consideration we have

$$z_{11} = z_{22} = z_{11d} + z_{11\ell} = \frac{R}{u}\frac{\cosh u}{\sinh u} + R_N$$

$$z_{12} = z_{21} = z_{12d} + z_{21\ell} = \frac{R}{u}\frac{1}{\sinh u} + R_N \qquad \text{.....2.38}$$

We now consider the z-parameter equations to determine V_o/V_i under no load conditions.

$$V_1 = z_{11} I_1 + z_{12} I_2$$

$$V_2 = z_{21} I_1 + z_{22} I_2$$

$$V_o/V_i\Big|_{I_2 = 0} = \frac{z_{21}}{z_{11}} = \frac{\alpha + u\sinh u}{\alpha\cosh u + u\sinh u} \qquad \text{.....2.40}$$

Where $\alpha = R/R_N$

The notch effect is obtained if the numerator of equation 2.40 can contain a zero as a function of frequency. There is an infinite set of values for α which will allow a zero in the numerator for some frequency. The numbers of the set can be denoted by $\alpha_{o,n}$ where n can take on any odd integer. This can be shown by setting the numerator of the previous expression equal to zero.

$$\alpha + u \sinh u = 0 \qquad \text{.....2.41}$$

where $u = \sqrt{j\frac{\omega}{\omega_o}} = \sqrt{jx} = \frac{(1 + j)}{\sqrt{2}} x^{\frac{1}{2}}$

$$\therefore$$

$$\alpha + \frac{1 + j}{\sqrt{2}} x^{\frac{1}{2}} \sinh \frac{1 + j}{\sqrt{2}} x^{\frac{1}{2}} = 0 \qquad \text{.....2.42}$$

Making use of the identity

$$\sinh(a + jb) = \sinh a \cos b + j \cosh a \sin b \qquad \text{.....2.43}$$

we get

$$\alpha + y^{\frac{1}{2}}[\sinh y^{\frac{1}{2}} \cos y^{\frac{1}{2}} - \sin y^{\frac{1}{2}} \cosh y^{\frac{1}{2}}] + jy^{\frac{1}{2}}[\sinh y^{\frac{1}{2}} \cos y^{\frac{1}{2}} + \sin y^{\frac{1}{2}} \cosh y^{\frac{1}{2}}] = 0 \qquad \text{.....2.44}$$

where $y = \frac{x}{2}$

To find the frequency at which a null occurs we set the imaginary part of equation 2.44 equal to zero giving us

$$\sinh y^{\frac{1}{2}} \cos y^{\frac{1}{2}} = - \sin y^{\frac{1}{2}} \cosh y^{\frac{1}{2}} \qquad \text{.....2.45}$$

Dividing by $\cosh y^{\frac{1}{2}}$ and $\cos y^{\frac{1}{2}}$ gives

$$\tanh y^{\frac{1}{2}} = - \tan y^{\frac{1}{2}} \qquad \text{.....2.46}$$

Since $\tanh y^{\frac{1}{2}}$ is a transcendental function, the values for y which satisfy the above equation are found by plotting the curves for the two functions of $y^{\frac{1}{2}}$ as shown in Figure 2:9. However, we must keep in mind that $y = \frac{x}{2} = \frac{\omega}{2\omega_o}$

FIGURE 2:9

Curves of $\tanh y^{\frac{1}{2}}$ and $\tan y^{\frac{1}{2}}$

FIGURE 2:10

Polar plots of the voltage transfer function of a $\overline{\text{URC}}$ notch filter for α in the vicinity of $\alpha_{o,1}$.

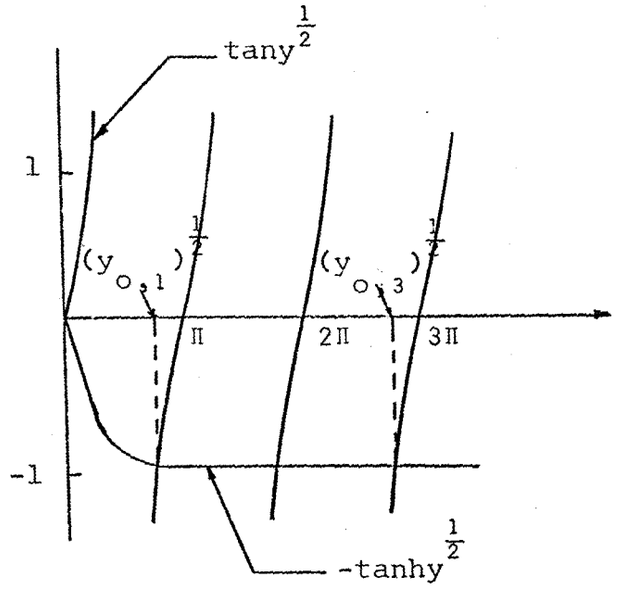

Figure 2:9

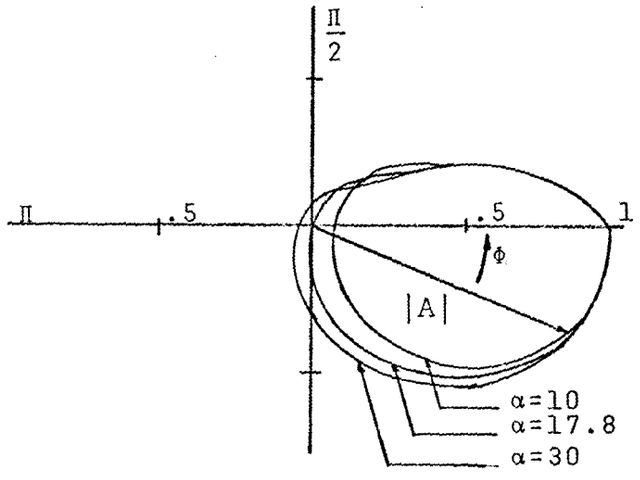

Figure 2:10

where $\omega_o = RC$. We can let $2\omega_o = \omega_1$ and the values of ω/ω_1 at which an intersection of the two curves occurs can be denoted by $\omega_{o,n}/\omega_1$.

The value of α corresponding to a given intersection is found by setting the real part of equation 2.44 equal to zero.

$$\alpha = - y^{\frac{1}{2}}[\sinh y^{\frac{1}{2}} \cos y^{\frac{1}{2}} - \sin y^{\frac{1}{2}} \cosh y^{\frac{1}{2}}] \qquad \ldots\ldots 2.47$$

$$= - y^{\frac{1}{2}} \sin y^{\frac{1}{2}} \cosh y^{\frac{1}{2}} [\tanh y^{\frac{1}{2}} \cot y^{\frac{1}{2}} - 1]$$

Now, from equation 2.41 we can obtain

$$\tanh y^{\frac{1}{2}} \cot y^{\frac{1}{2}} = - 1$$

to give us

$$\alpha = 2y^{\frac{1}{2}} \sin y^{\frac{1}{2}} \cosh y^{\frac{1}{2}} \qquad \ldots\ldots 2.48$$

The first intersection of the two curves in Figure 2:9 occurs at

$$\frac{\omega_{o,1}}{\omega_1} = 5.5951$$

or

$$\frac{\omega_{o,1}}{\omega_o} = 11.1902$$

The corresponding value of α is

$$\alpha_{o,1} = 17.786$$

The third and higher order intersections can be found by considering $y^{\frac{1}{2}}$ greater than one. We then have

$$\tanh y^{\frac{1}{2}} = \frac{e^{y^{\frac{1}{2}}} - e^{-y^{\frac{1}{2}}}}{e^{y^{\frac{1}{2}}} + e^{-y^{\frac{1}{2}}}} \simeq 1 \qquad \text{.....2.49}$$

From equation 2.46 we obtain

$$\tan y^{\frac{1}{2}} \simeq -1$$

and $$y^{\frac{1}{2}} = (\Pi - \Pi/4)$$

The intersections on the $y^{\frac{1}{2}}$ axis will occur every $(n\Pi-\Pi/4)$ times giving us

$$\frac{\omega_{o,n}}{\omega_1} = (n\Pi - \Pi/4)^2 \qquad \text{.....2.50}$$

If n is even, α is negative, so we are only interested in the case where n is an odd integer.

The behaviour of the transfer function for α near $\alpha_{o,1}$ can best be presented in the form of a polar plot of $V_o/V_i(jw)$. The polar plot is created by expressing the complex transfer function in the form of an amplitude "A" and a phase angle "Φ". Thus, the polar plot of the transfer function is the locus of points (A,Φ) for all frequencies ω as shown[5] in Figure 2.10. The magnitude and phase for the corresponding values of α is shown in Figures 2:11 and 2:12 respectively. For $\alpha < \alpha_{o,1}$, the polar plot does not encircle the origin and Φ is restricted to $-\Pi/2 < \Phi < \Pi/2$. However for

FIGURE 2:11

Magnitude of the voltage transfer function of a $\overline{URC}$ notch filter for α in the vicinity of $\alpha_{o,1}$.

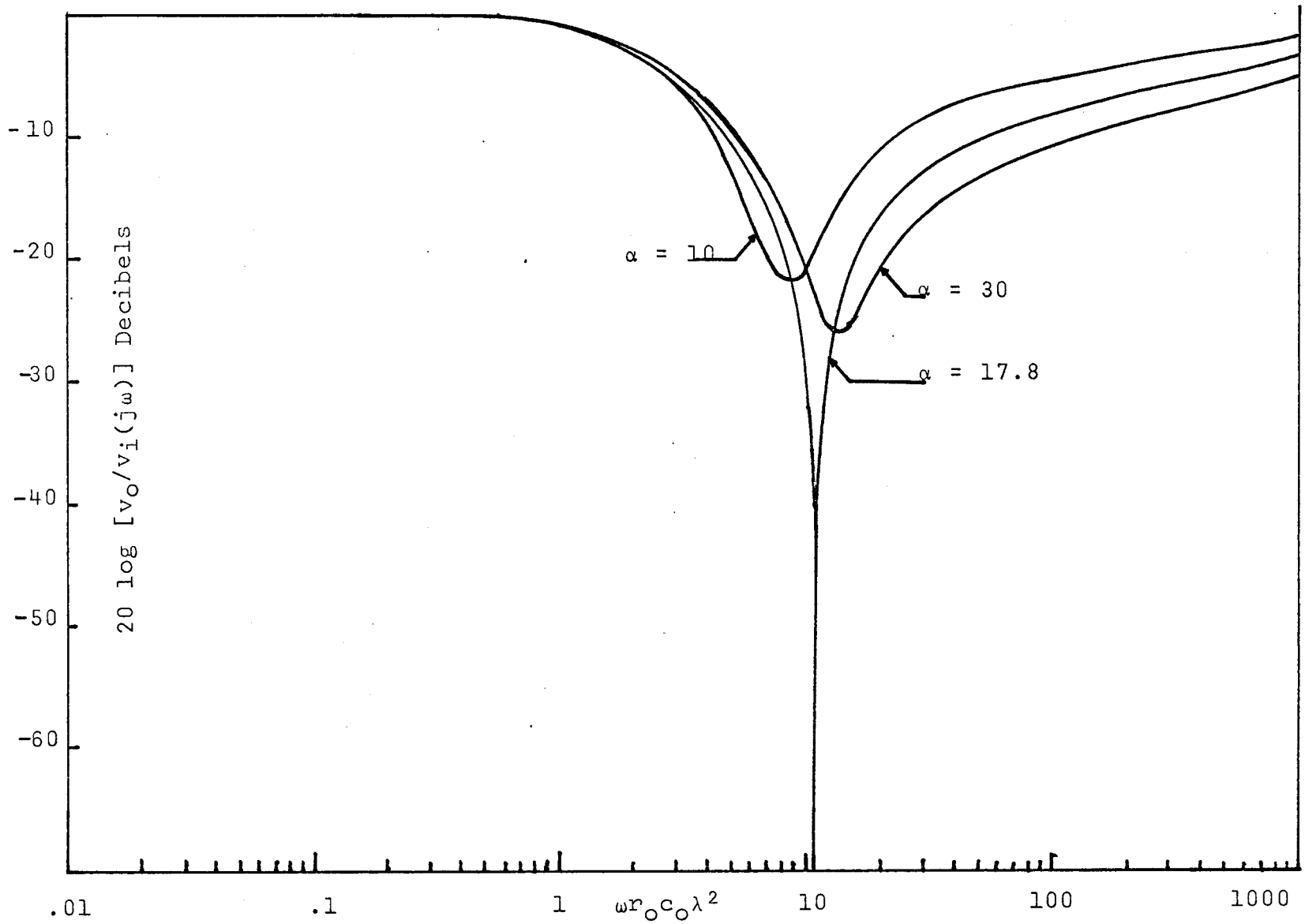
-10
-20
-30
-40
-50
-60
20 log [$v_o/v_i(j\omega)$] Decibels
α = 10
α = 30
α = 17.8
.01
.1
1
$\omega r_o c_o \lambda^2$
10
100
1000

FIGURE 2:12

Phase of the voltage transfer function of a $\overline{URC}$ notch filter for α in the vicinity of $\alpha_{0,1}$.

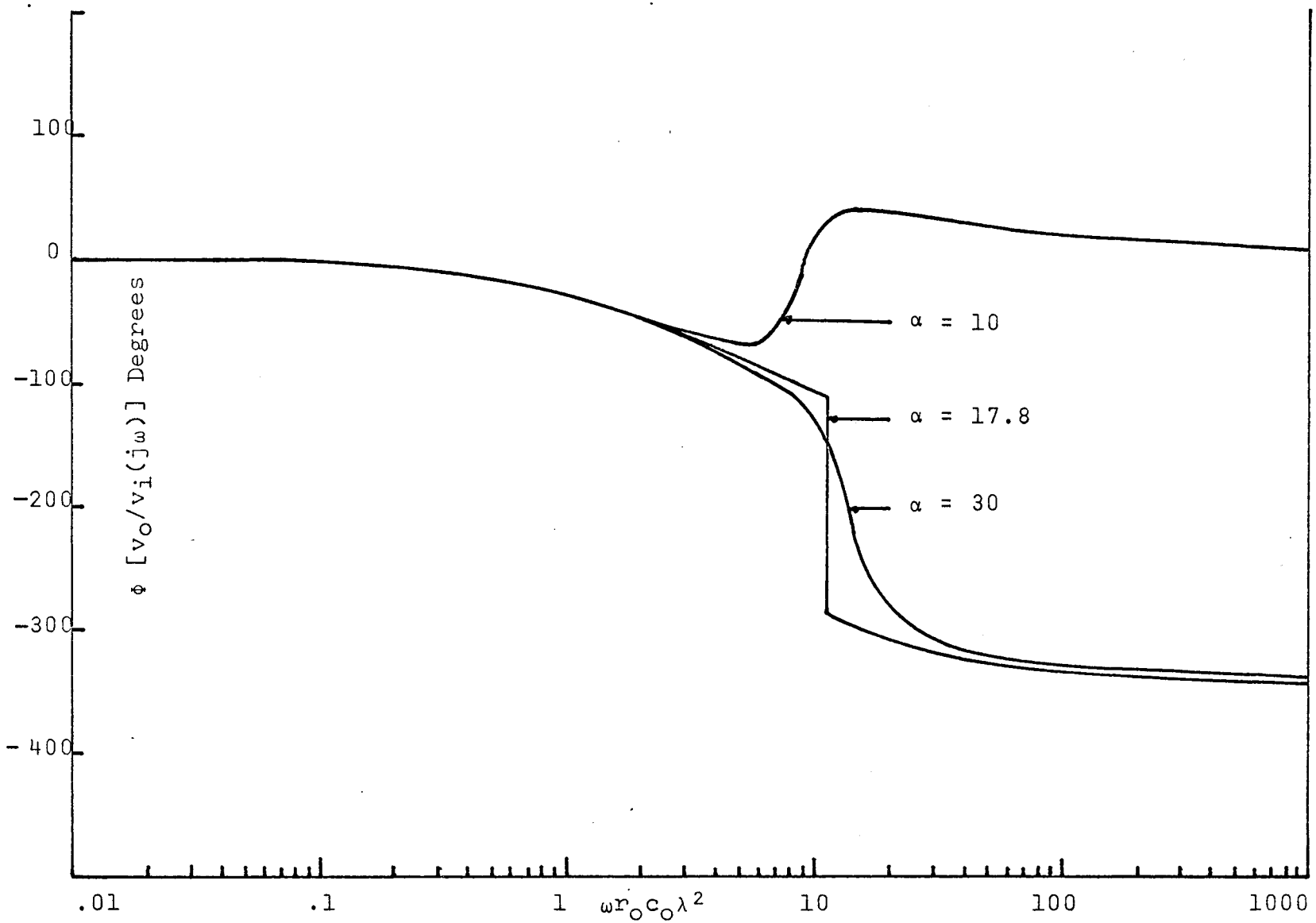
100
0
-100
-200
-300
-400
ϕ [$v_o/v_i(j\omega)$] Degrees
α = 10
α = 17.8
α = 30
.01
.1
1
$\omega r_o c_o \lambda^2$
10
100
1000

$\alpha_{o,1} < \alpha \leq 10{,}000$, the plot does encircle the origin and Φ goes from zero to -2Π. There is therefore a discontinuity in Φ for $\alpha = \alpha_{o,1}$ at $\omega = \omega_{o,1}$. Also for $\alpha_{o,1} << \alpha < \alpha_{o,3}$, we have $\frac{-3\Pi}{2} \leq \Phi \leq 0$. This case is applicable for the voltage transfer function of the $\overline{URC}$ low pass filter where the contact resistance gives a notch effect. For $\alpha_{o,3} < \alpha << \alpha_{o,5}$, Φ presumably goes from zero to -4Π and there is another discontinuity in Φ for $\alpha = \alpha_{o,3}$ where $\omega = \omega_{o,3}$. By considering equations 2.48 and 2.50 the values of $\frac{\omega_{o,n}}{\omega_o}$ and $\alpha_{o,n}$ can be solved for at different positions of optimum notch. Table I gives us these values for n = 1, 2 and 3.

TABLE I

n	$\frac{\omega_{o,n}}{\omega_o}$	$\alpha_{o,n}$
1	11.1902	17.786
2	60.451	- 949.161
3	149.278	3.451×10^4

2.3 $\overline{ERC}$ Low Pass Filter[1,2,5]

Exponentially tapered RC filters are worth consideration because they can be used to obtain an even sharper cutoff than the uniform RC filter. The $\overline{ERC}$ network can also produce more phase shift for a given attenuation than is obtainable with a uniform structure. Tapering can also be used to narrow the rejection band of a notch filter or to

FIGURE 2:13

(a) Physical structure of an $\overline{\text{ERC}}$ network

(b) Circuit model of an $\overline{\text{ERC}}$ low pass filter

(c) Circuit model of an $\overline{\text{ERC}}$ notch filter

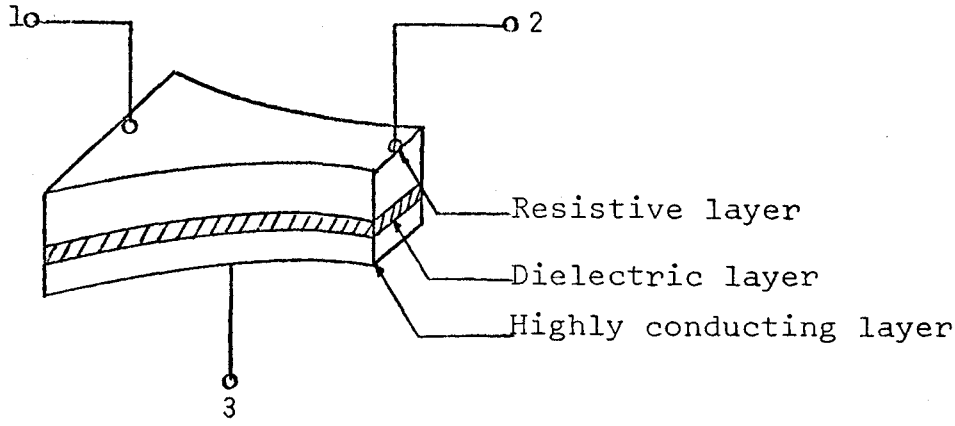
1
2
3
Resistive layer
Dielectric layer
Highly conducting layer

(a)

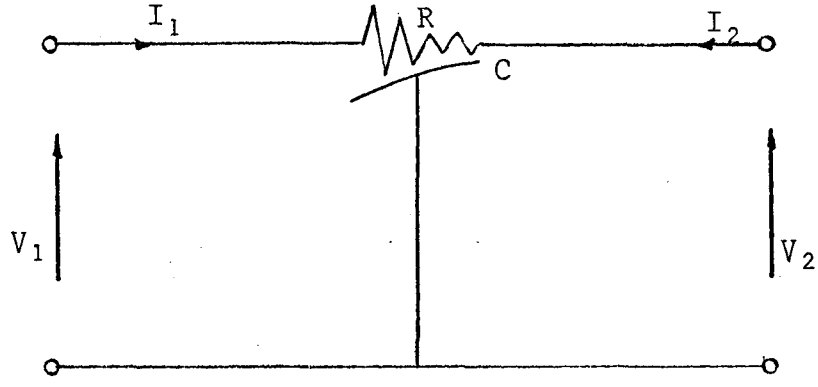
I_1
R
I_2
C
V_1
V_2

(b)

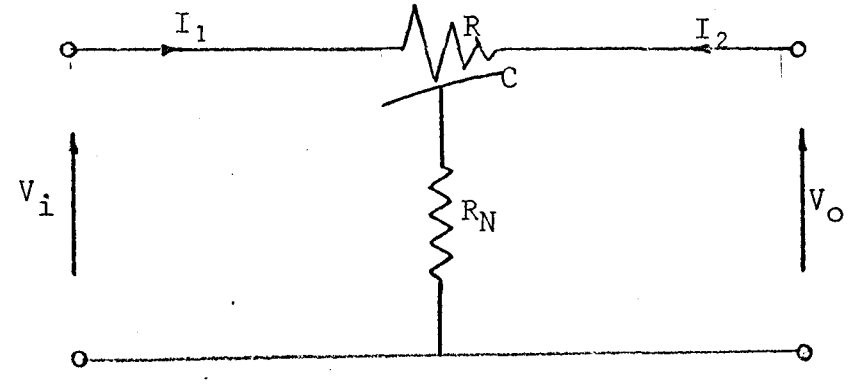
I_1
R
I_2
C
V_i
R_N
V_o

(c)

provide different input and output impedance levels for a distributed filter.

The $\overline{ERC}$ filter is physically similar to the $\overline{URC}$ filter except for the taper as shown in Figure 2:13. To describe the circuit, we consider the resistance r(x) per unit length and the capacitance c(x) per unit length to be a function of the distance x from the input end. Again considering the transmission line model and ignoring ℓ_o and g_o we may write

$$\frac{\partial v(t,x)}{\partial x} = - r(x)i(t,x) \qquad .....2.51$$

$$\frac{\partial i(t,x)}{\partial x} = - c(x)\frac{\partial v(t,x)}{\partial x} \qquad .....2.52$$

Substituting equation 2.52 into 2.51 gives

$$\frac{\partial}{\partial x}\left[- \frac{1}{r(x)} \frac{\partial v(t,x)}{\partial x}\right] = - c(x)\frac{\partial v(t,x)}{\partial t} \qquad .....2.53$$

The circuit can now be described if we consider r(x) and c(x) to be

$$r(x) = r_o e^{mx}$$
$$c(x) = c_o e^{-mx} \qquad .....2.54$$

Where $m = (\frac{1}{\lambda}) \ln[\frac{r(\lambda)}{r(o)}]$

and λ is the length of the structure. Equation 2.53 can be rewritten to give

$$\frac{\partial^2 v(t,x)}{\partial x^2} - \frac{1}{r(x)}\frac{dr(x)}{dx}\frac{\partial v(t,x)}{\partial x} = r(x)c(x)\frac{\partial v(t,x)}{\partial t} \qquad .....2.55$$

Equation 2.55 is a one-dimensional differential equation describing a distributed RC network and has been derived by several workers.[7] [8] This one-dimensional equation is only an approximation to the actual network description in the case of an exponentially tapered circuit. The one-dimensional equation is used because the general equation leads to formidable boundary value problems unless the network geometry is uniform.

Substituting the values for r(x) and c(x) in equation 2.55 gives

$$\frac{\partial^2 v(t,x)}{\partial x^2} - m\frac{\partial v(t,x)}{\partial x} = r_o c_o \frac{\partial v(t,x)}{\partial t} \qquad .....2.56$$

By transforming equation 2.56 into the s-domain and assuming zero initial conditions we obtain

$$\frac{d^2 V(s,x)}{dx^2} - m\frac{dV(s,x)}{dx} - sr_o c_o V(s,x) = 0 \qquad .....2.57$$

The solution to equation 2.57 is of the form

$$V(s,x) = e^{mx/2}\left[A\sinh\frac{\gamma x}{\lambda} + B\cosh\frac{\gamma x}{\lambda}\right] \qquad .....2.58$$

where A and B are constants and γ is defined as

$$\gamma = \sqrt{(\frac{m\lambda}{2})^2 + sr_o c_o \lambda^2} \qquad .....2.59$$

The current is found by transforming equation 2.51 into the s-domain and substituting for $\frac{dV(s,x)}{dx}$ to give us

$$I(s,x) = - \frac{e^{-mx/2}}{r_o} [(\frac{Am}{2} + \frac{B\gamma}{\lambda})\sinh\frac{\gamma x}{\lambda} + (\frac{A\gamma}{\lambda} + \frac{Bm}{2})\cosh\frac{\gamma x}{\lambda}] \qquad .....2.60$$

Using equation 2.60, the constants A and B can be evaluated in terms of the terminal currents (considering the circuit model as shown in Figure 2:13(b)).

$$I_1\Big|_{x=o} = - \frac{1}{r_o} (\frac{A\gamma}{\lambda} + \frac{Bm}{2}) \qquad .....2.61$$

$$I_2\Big|_{x=\lambda} = \frac{e^{\frac{-m\lambda}{2}}}{r_o} [(\frac{Am}{2} + \frac{B\gamma}{\lambda})\sinh\gamma + (\frac{A\gamma}{\lambda} + \frac{Bm}{2})\cosh\gamma] \qquad .....2.62$$

Using equation 2.58, the constants A and B can be evaluated in terms of the terminal voltages

$$V_1 = B \qquad .....2.63$$

$$V_2 = e^{\frac{m\lambda}{2}}[A\sinh\gamma + B\cosh\gamma] \qquad .....2.64$$

Using equations 2.61 and 2.62 to solve for A and B yields

$$A = \frac{e^{-m\lambda/2}}{\Delta}\left[\frac{\gamma}{\lambda}\sinh\gamma + \frac{m}{2}\cosh\gamma\right]I_1 + \frac{m}{2\Delta}I_2 \qquad \ldots\ldots 2.65$$

$$B = \frac{-e^{-m\lambda/2}}{\Delta}\left[\frac{m}{2}\sinh\gamma + \frac{\gamma}{\lambda}\cosh\gamma\right]I_1 + \frac{\gamma}{\Delta\lambda}I_2 \qquad \ldots\ldots 2.66$$

where

$$\Delta = \frac{e^{-m\lambda/2}}{r_o}\left(\frac{m^2}{4} - \frac{\gamma^2}{\lambda^2}\right)\sinh\gamma \qquad \ldots\ldots 2.67$$

We can now write the relationship between the terminal voltages and currents in the impedance parameter form

$$\begin{bmatrix} V_1 \\ \\ V_2 \end{bmatrix} = \begin{bmatrix} z_{11} & z_{12} \\ \\ z_{21} & z_{22} \end{bmatrix}\begin{bmatrix} I_1 \\ \\ I_2 \end{bmatrix} \qquad \ldots\ldots 2.68$$

where the z-parameters are obtained from equations 2.63 to 2.67 and are given by

$$z_{11} = \frac{1}{sc_o\lambda}\left(\frac{m\lambda}{2} + \frac{\gamma}{\tanh\gamma}\right)$$

$$z_{22} = \frac{e^{m\lambda}}{sc_o\lambda}\left(\frac{\gamma}{\tanh\gamma} - \frac{m\lambda}{2}\right) \qquad \ldots\ldots 2.69$$

$$z_{12} = z_{21} = \left(\frac{1}{sc_o\lambda}\,\frac{\gamma e^{m\lambda/2}}{\sinh\gamma}\right)$$

The impedance matrix can be converted to an admittance matrix by use of the conversion formulas to give us

$$y_{11} = \frac{1}{r_o\lambda \sinh\gamma}(\gamma\cosh\gamma - \frac{m\lambda}{2}\sinh\gamma)$$

$$y_{22} = \frac{e^{-m\lambda}}{r_o\lambda \sinh\gamma}(\gamma\cosh\gamma + \frac{m\lambda}{2}\sinh\gamma) \quad .....2.70$$

$$y_{12} = y_{21} = \frac{-1}{r_o\lambda}(\frac{\gamma e^{-m\lambda/2}}{\sinh\gamma})$$

In the limit as m approaches zero, we get $\gamma = \gamma_o$, and equations 2.70 describe a distributed RC network with no taper and are in agreement with the results obtained for a $\overline{URC}$ network.

The magnitude and phase of the y-parameters are shown in Figure 2:14 to 2:19. They are presented in normalized form with the normalized frequency being $\omega r_o c_o \lambda^2$. The amount of taper of the exponential networks is given by $D = \frac{m\lambda}{2}$ where $m\lambda = 0, \pm 2, \pm 4$.

If we consider the $\overline{ERC}$ network under no load conditions as shown in Figure 2:13(b) and also consider the y-parameter equations, it can be shown that the voltage transfer function is given by

$$\frac{V_2}{V_1} = \frac{-y_{12}}{y_{22}} = \frac{\gamma e^{m\lambda}}{\gamma\cosh\gamma + \frac{m\lambda}{2}\sinh\gamma} \quad .....2.71$$

The magnitude and phase of the voltage transfer function are shown in Figures 2:20 and 2:21 respectively. Once again, the frequency is normalized with respect to $\omega r_o c_o \lambda^2$ and the amount of taper is given by $D = \frac{m\lambda}{2}$ where $m\lambda = 0, \pm 2, \pm 4$.

FIGURE 2:14

Magnitude of the input admittance of an $\overline{\text{ERC}}$ low pass filter with different degrees of taper.

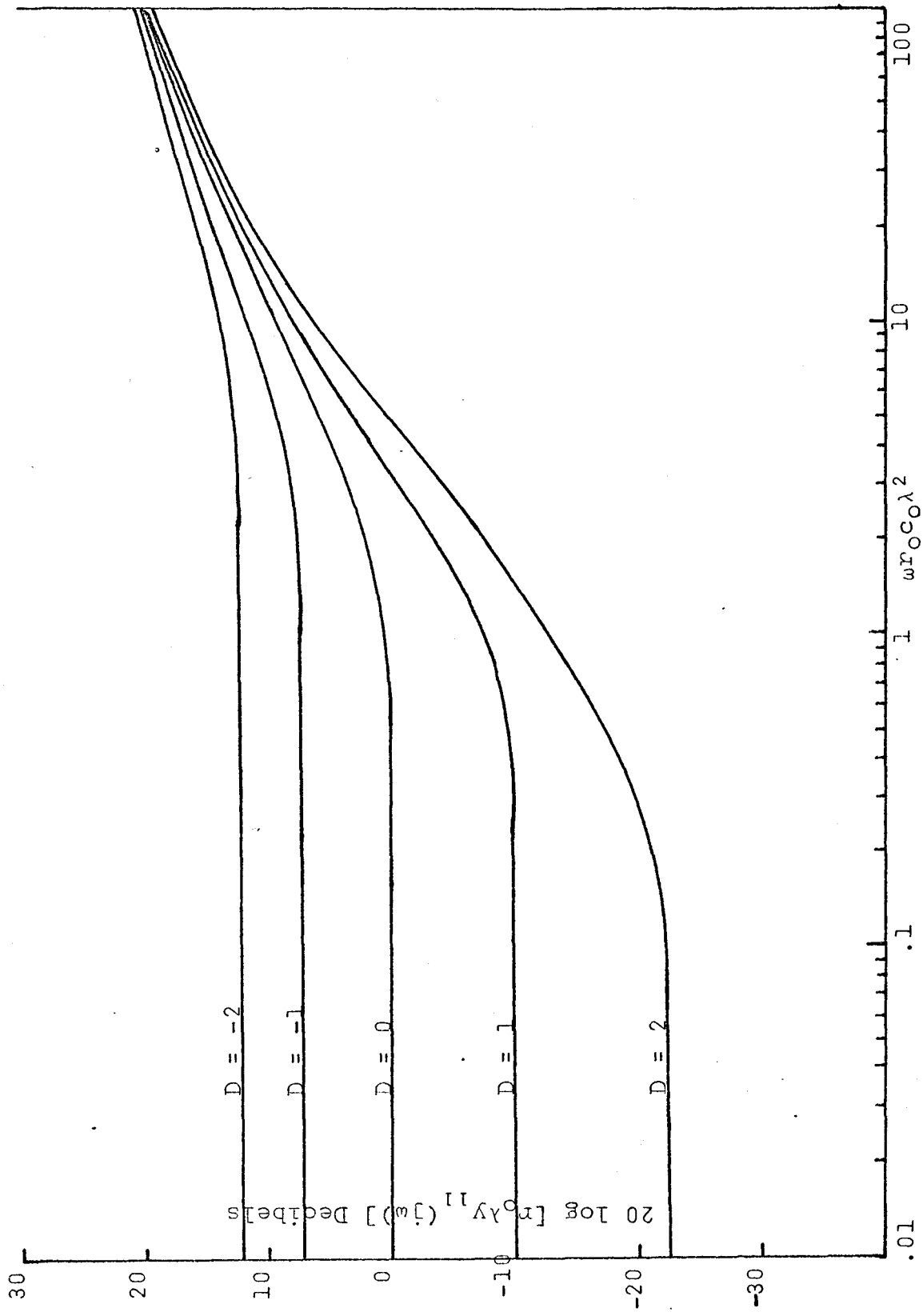
30
20
10
0
-10
-20
-30
.01
.1
1
10
100
$\omega r_o c_o \lambda^2$
$20 \log [r_o \lambda y_{11}(j\omega)]$ Decibels
D = -2
D = -1
D = 0
D = 1
D = 2

FIGURE 2:15

Phase of the input admittance of an $\overline{\text{ERC}}$ low pass filter with different degrees of taper.

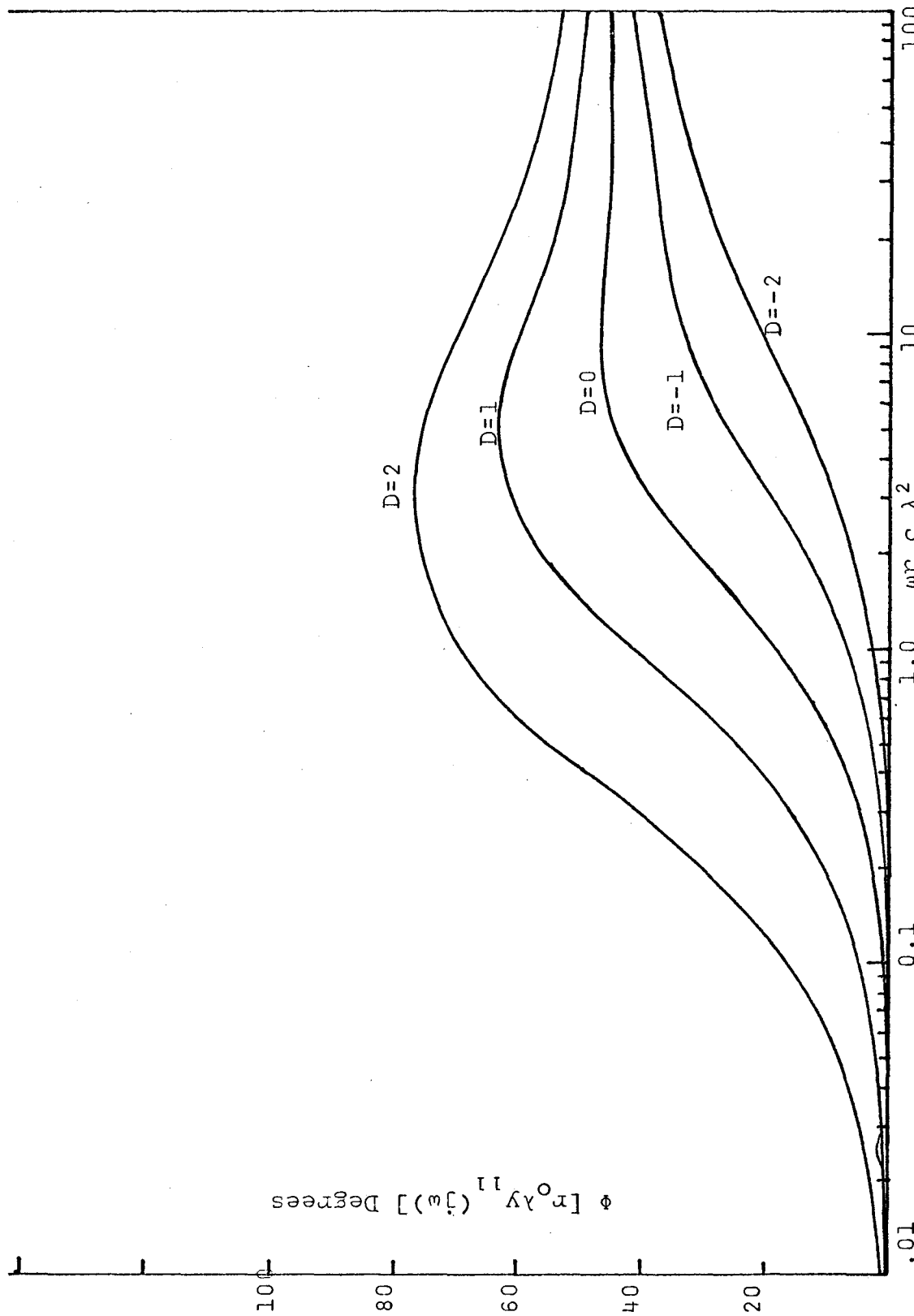
D=2
D=1
D=0
D=-1
D=-2
$\omega r_o c_o \lambda^2$
.01
0.1
1.0
10
100
Φ [$r_o \lambda y_{11}(j\omega)$] Degrees
20
40
60
80
100

FIGURE 2:16

Magnitude of the output admittance of an $\overline{\text{ERC}}$ low pass filter with different degrees of taper.

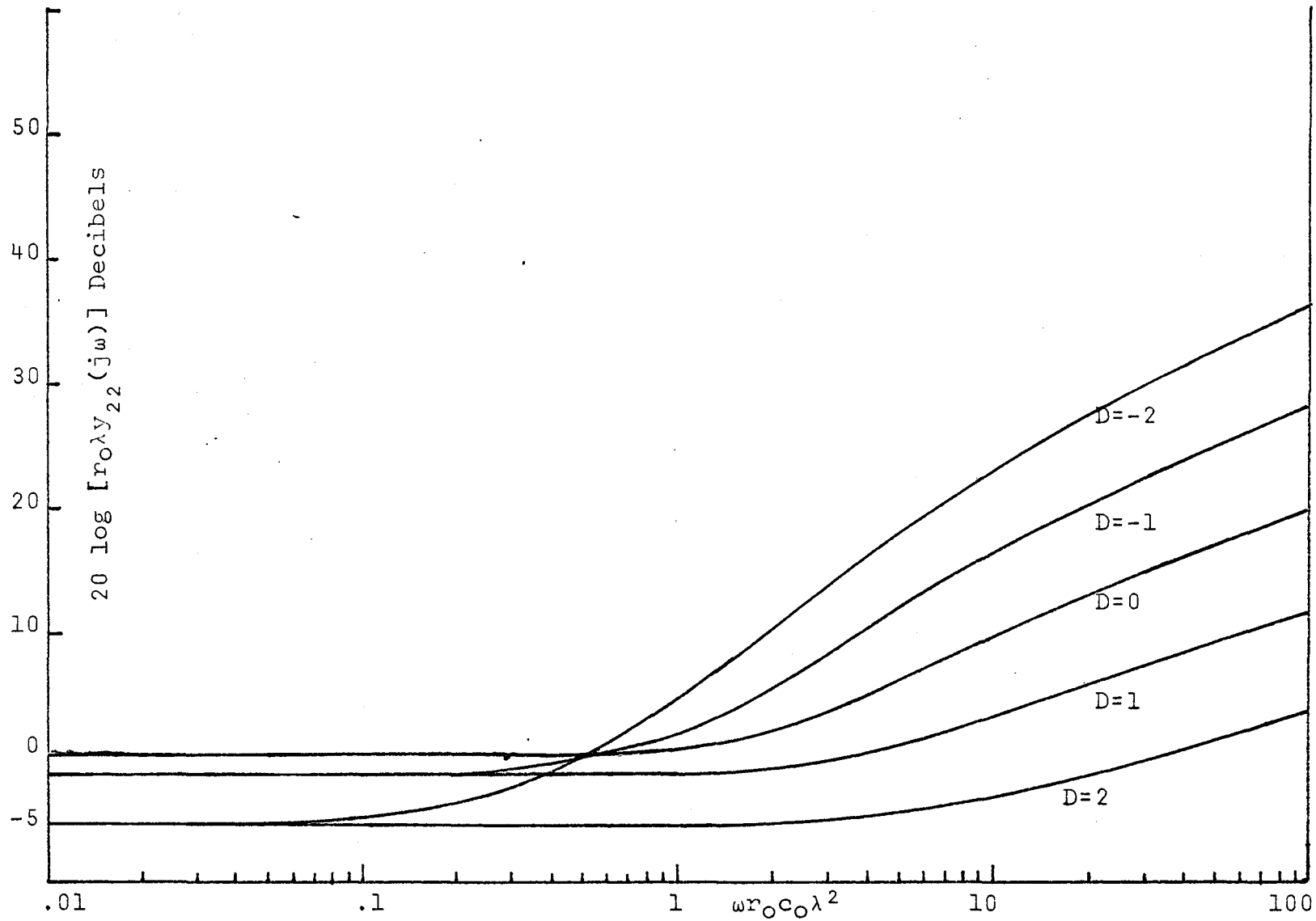
50
40
30
20
10
0
-5
20 log [$r_o \lambda y_{22}(j\omega)$] Decibels
D=-2
D=-1
D=0
D=1
D=2
.01
.1
1
$\omega r_o c_o \lambda^2$
10
100

FIGURE 2:17

Phase of the output admittance of an $\overline{\text{ERC}}$ low pass filter with different degrees of taper.

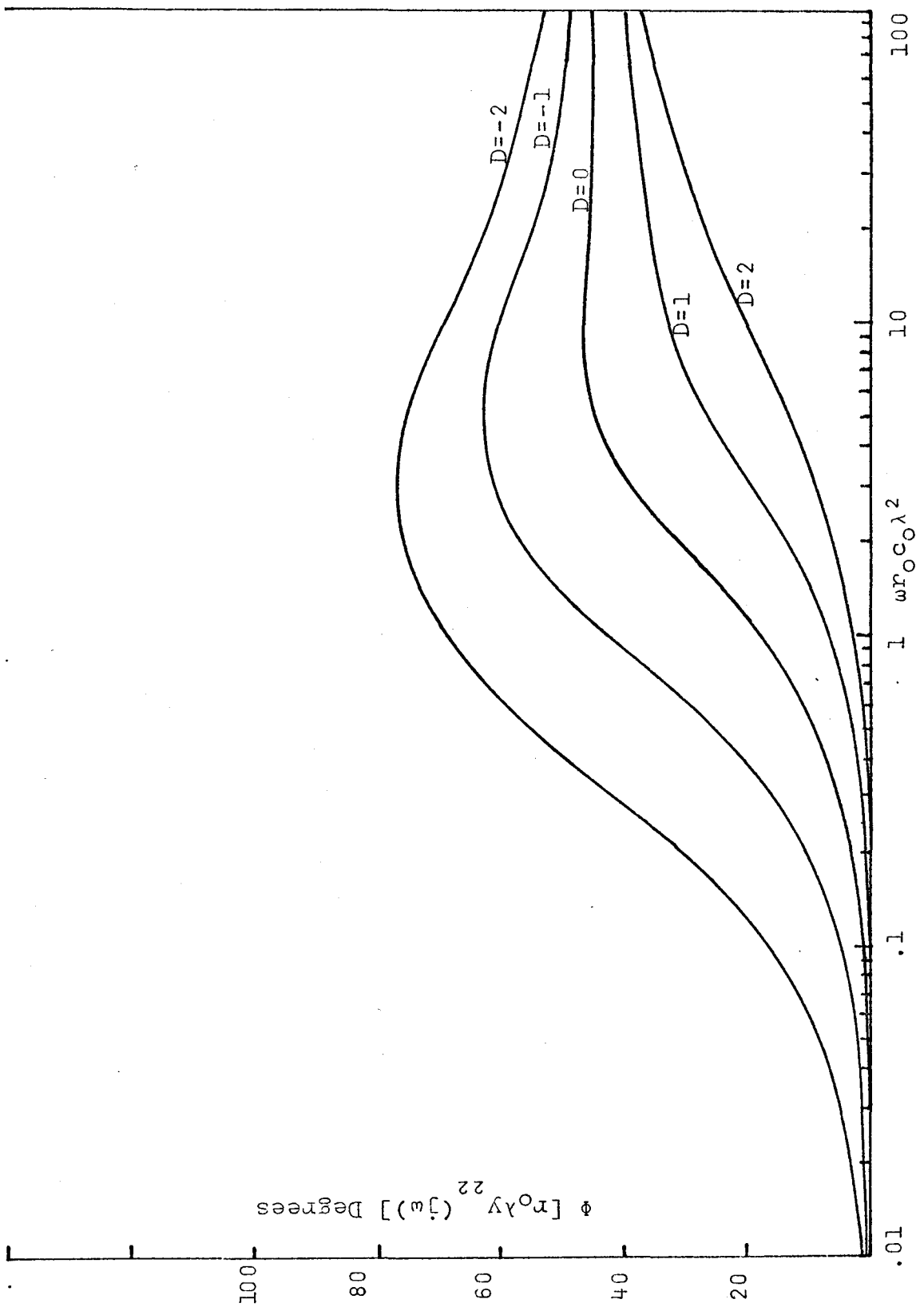
Φ [r_o λ y_22 (jω)] Degrees
100
80
60
40
20
.01
.1
1
10
100
ωr_o c_o λ^2
D=-2
D=-1
D=0
D=1
D=2

FIGURE 2:18

Magnitude of the transfer admittance of an $\overline{\text{ERC}}$ low pass filter with different degrees of taper.

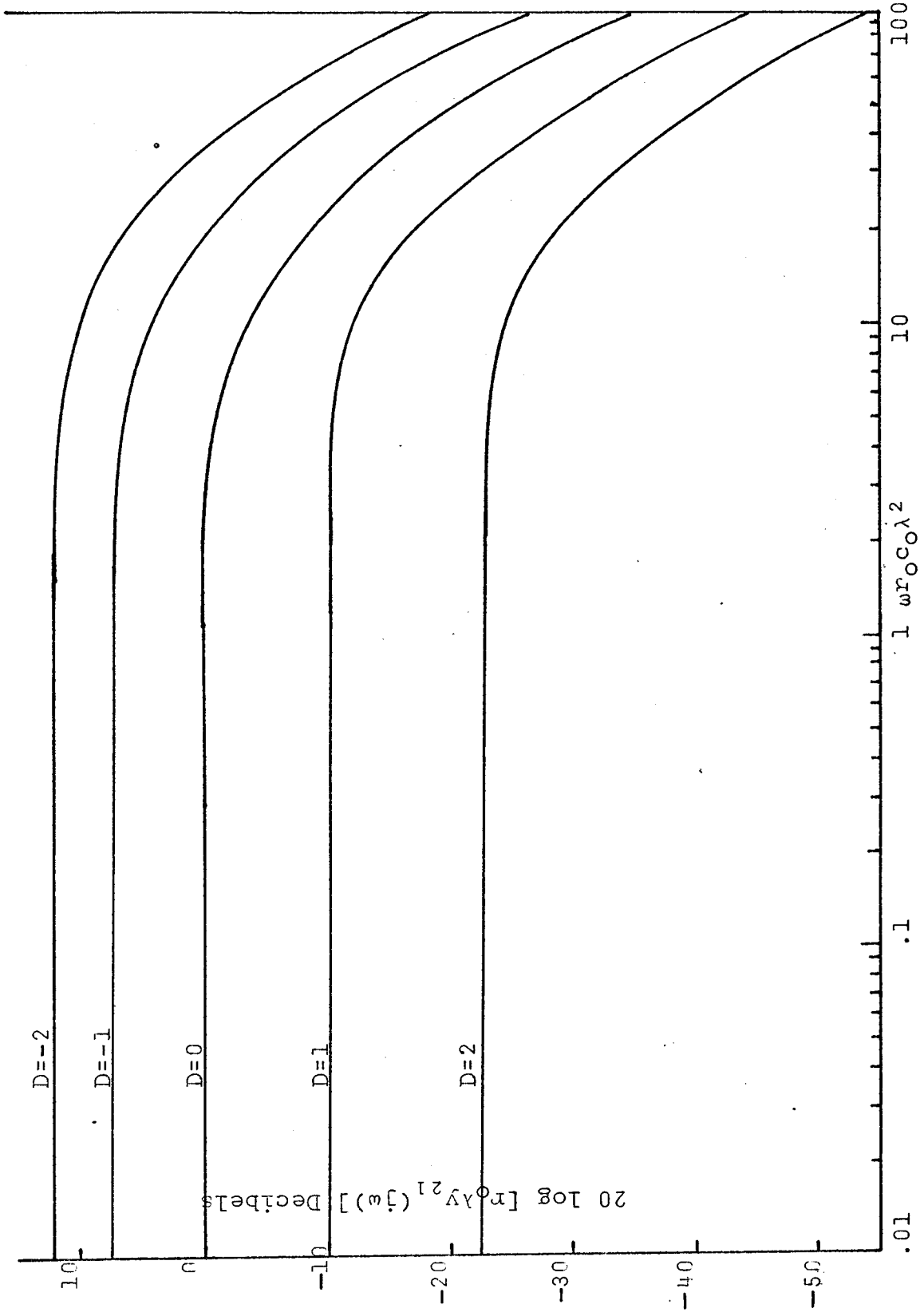
D=-2
D=-1
D=0
D=1
D=2
10
0
-10
-20
-30
-40
-50
20 log [r$_o\lambda y_{21}(j\omega)$] Decibels
.01
.1
1
10
100
1 $\omega r_o c_o \lambda^2$

FIGURE 2:19

Phase of the transfer admittance of an $\overline{\text{ERC}}$ low pass filter with different degrees of taper.

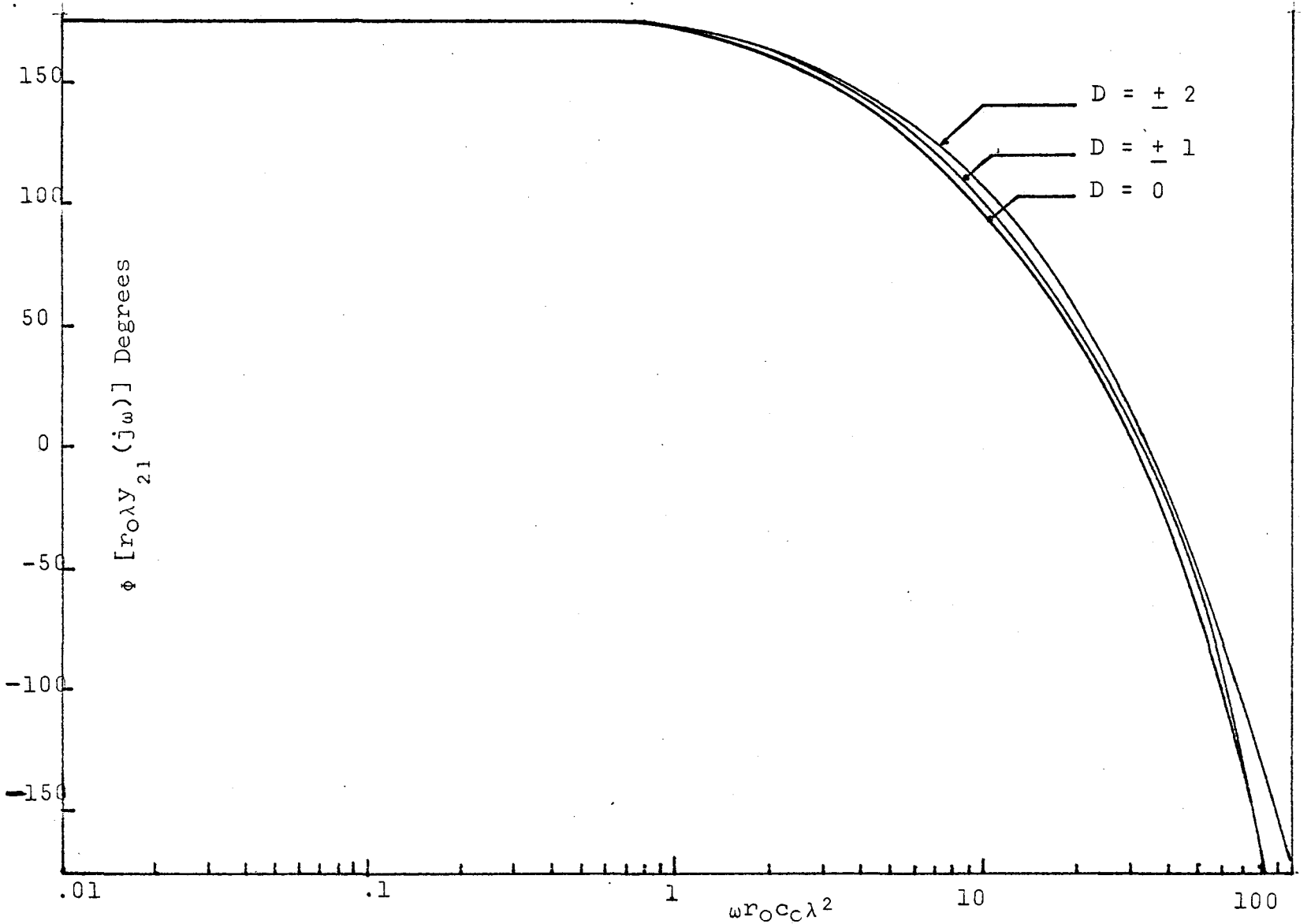
150
100
50
0
-50
-100
-150
ϕ [$r_o\lambda y_{21}(j\omega)$] Degrees
D = ± 2
D = ± 1
D = 0
.01
.1
1
10
100
$\omega r_o c_c \lambda^2$

42

FIGURE 2:20

Magnitude of the voltage transfer function of an $\overline{\text{ERC}}$ low pass filter with different degrees of taper.

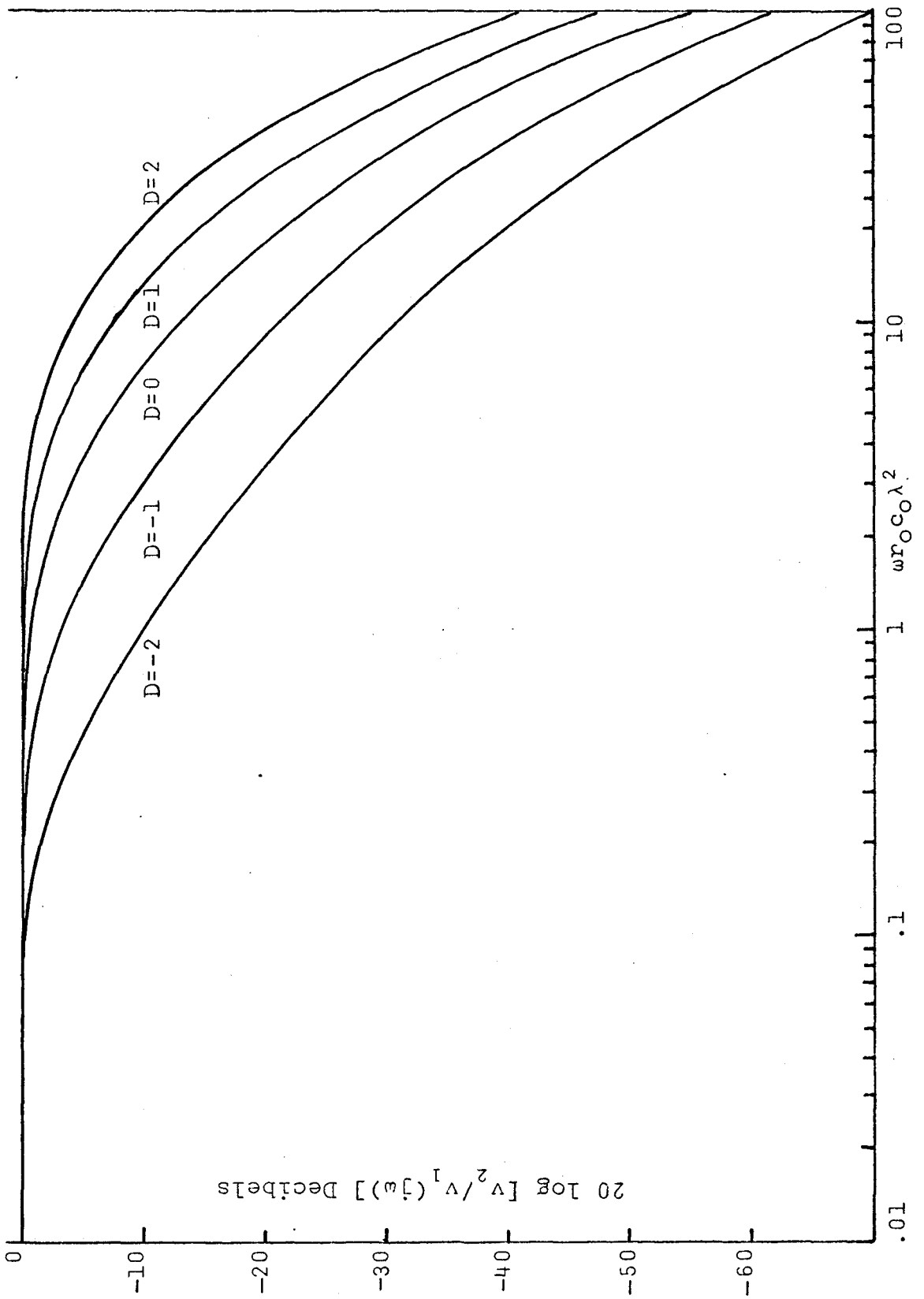
0
-10
-20
-30
-40
-50
-60
20 log [V2/V1(jω)] Decibels
.01
.1
1
10
100
ωr0c0λ2
D=2
D=1
D=0
D=-1
D=-2

FIGURE 2:21

Phase of the voltage transfer function of an $\overline{\text{ERC}}$ low pass filter with different degrees of taper.

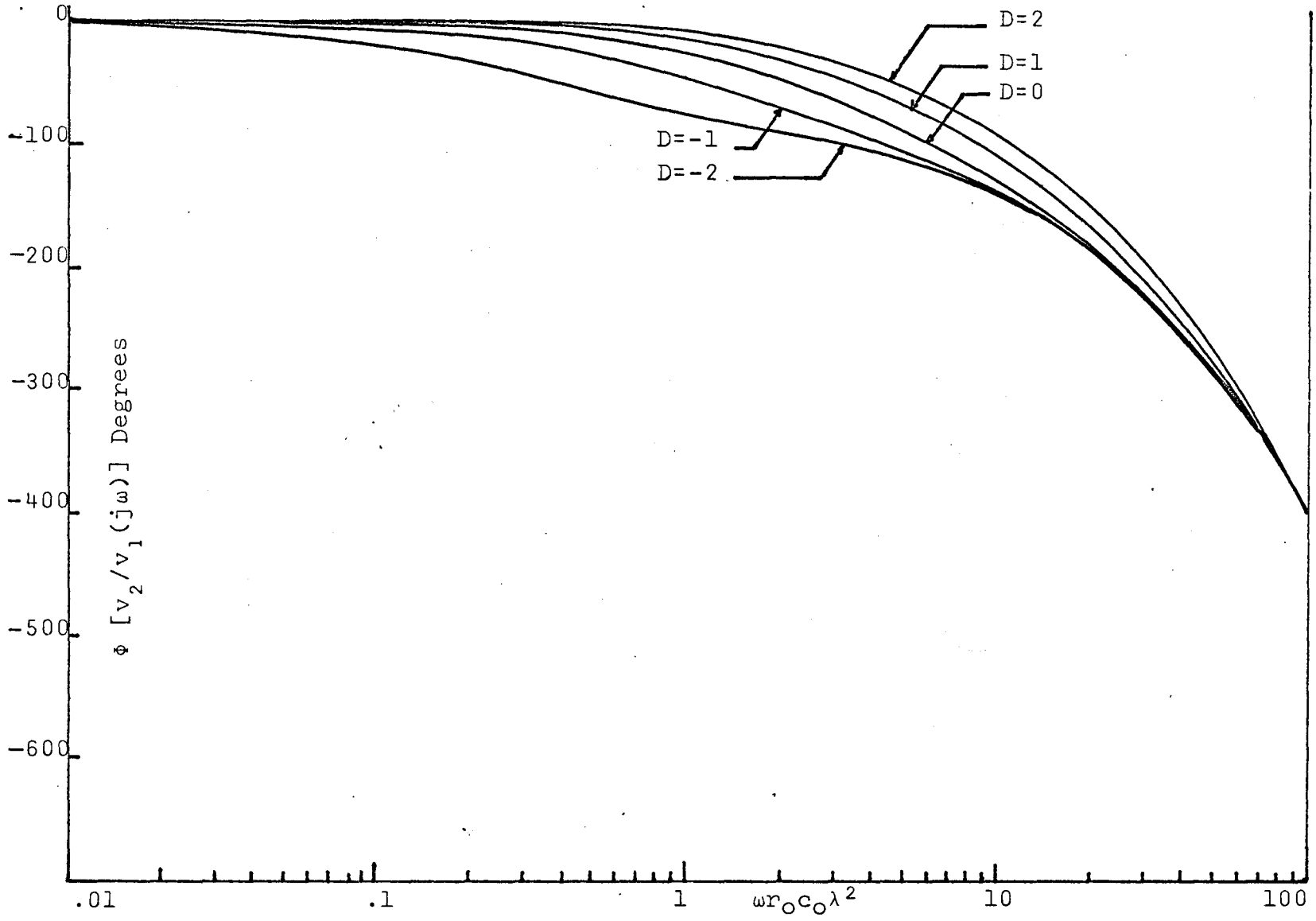
0
-100
-200
-300
-400
-500
-600
D=2
D=1
D=0
D=-1
D=-2
$\Phi\ [v_2/v_1(j\omega)]$ Degrees
.01
.1
1
10
100
$\omega r_o c_o \lambda^2$

Comparison of the curve for D equal to zero ($\overline{URC}$ network) with the curve for D = 2 shows us that the tapered network has a sharper cut-off and also a greater phase shift for a given attenuation.

2.4 $\overline{ERC}$ Notch Filter.[8]

As was mentioned in Section 2.3, the $\overline{ERC}$ notch filter is important since it has a narrower rejection band than the $\overline{URC}$ notch filter.

The configuration shown in Figure 2:13(c) shows the distributed network connected with a lumped resistor (R_N) to form a notch filter. The unloaded transfer function of the network is given by

$$\frac{V_o}{V_i} = \frac{z_{21} + R_N}{z_{11} + R_N}$$

$$= \frac{R_N + \dfrac{\gamma e^{m\lambda/2}}{j\omega c_o \lambda \sinh\gamma}}{R_N + \dfrac{1}{j\omega c_o \lambda}\left(\dfrac{m\lambda}{2} + \dfrac{\gamma\cosh\gamma}{\sinh\gamma}\right)} \qquad \ldots\ldots 2.72$$

Equation 2.72 may be simplified to give us

$$\frac{V_o}{V_i} = \frac{\dfrac{r_o\lambda}{R_N}\gamma e^{m\lambda/2} + j\omega c_o r_c \lambda^2 \sinh\gamma}{\left(\dfrac{r_o\lambda}{R_N}\dfrac{m\lambda}{2} + j\omega r_o c_o \lambda^2\right)\sinh\gamma + \dfrac{r_o\lambda}{R_N}\gamma\cosh\gamma}$$

If we let

$$A = \frac{r_o \lambda}{R_N}$$

$$D = \frac{m\lambda}{2}$$

$$W = \omega r_o c_o \lambda^2$$

and

$$\gamma = \sqrt{\left(\frac{m\lambda}{2}\right)^2 + j\omega r_o c_o \lambda^2}$$

we get

$$\frac{V_o}{V_i} = \frac{A\gamma e^D + jW\sinh\gamma}{(AD + jW)\sinh\gamma + A\gamma\cosh\gamma}$$

By following the same procedure as was outlined for the $\overline{URC}$ notch filter, we can determine the position of the null frequency for different values of D and the value of $\frac{R \text{ series}}{R_N}$ required to give a maximum notch at each null frequency position. We can find the value of R series as follows:

$$R_s = \int_o^\lambda r_o e^{mx} dx = \frac{r_o}{m}(e^{m\lambda} - 1)$$

Therefore $\frac{R_s}{R_N} = \frac{r_o \lambda}{R_N} \left(\frac{e^{m\lambda} - 1}{m\lambda}\right)$

Table II gives values of the notch frequency (ω_o) and R_S/R_N for $m\lambda = 0, \pm 2, \pm 4$.

FIGURE 2:22

Magnitude of the voltage transfer function of an $\overline{\text{ERC}}$ notch filter with different degrees of taper.

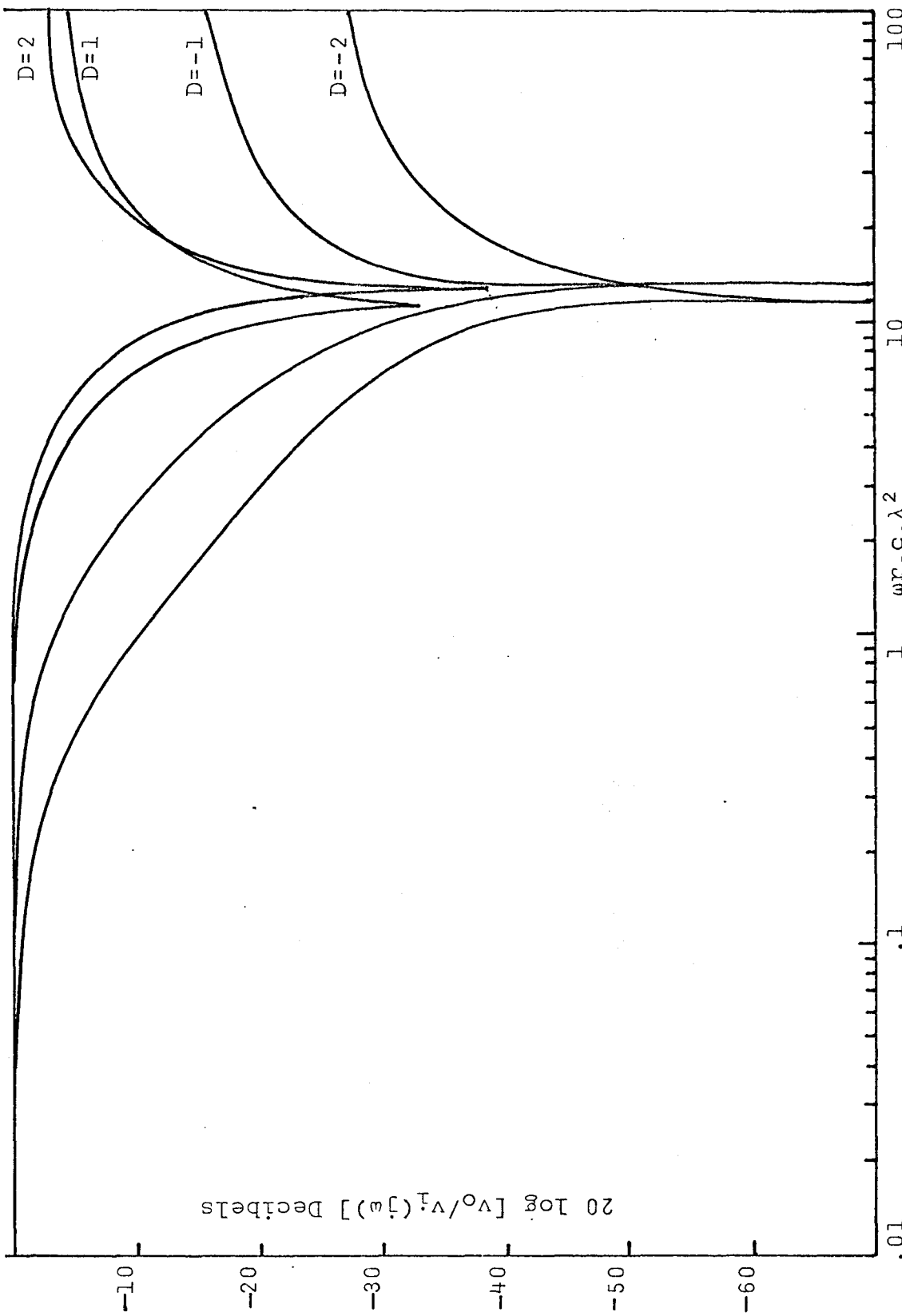
D=2
D=1
D=-1
D=-2
-10
-20
-30
-40
-50
-60
20 log [v_o/v_i(jω)] Decibels
.01
.1
1
10
100
ωr_oc_oλ^2

FIGURE 2:23

Phase of the voltage transfer function of an $\overline{\text{ERC}}$ notch filter with different degrees of taper.

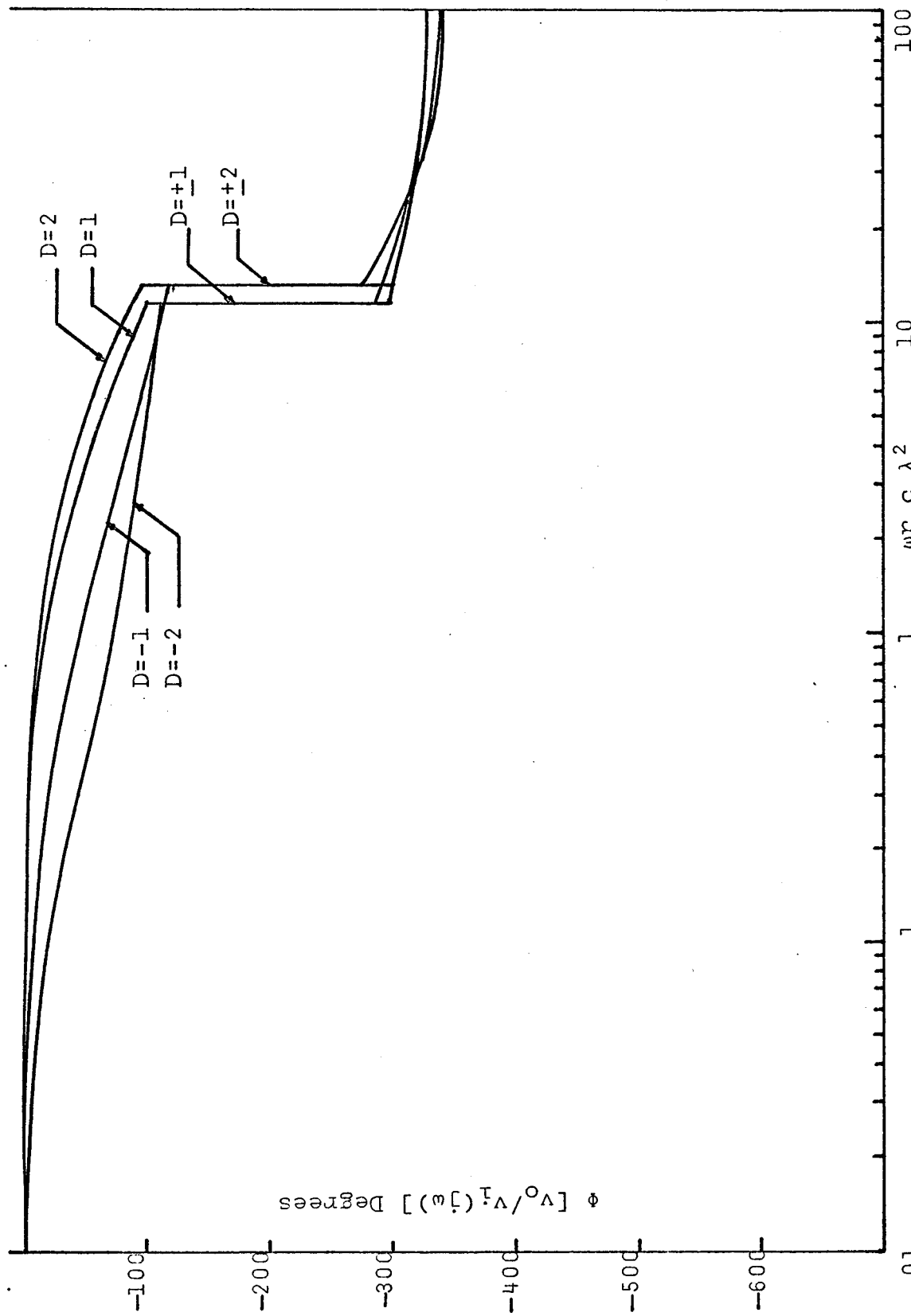
D=2
D=1
D=±1
D=±2
D=-1
D=-2
-100
-200
-300
-400
-500
-600
Φ [V_o/V_i(jω)] Degrees
.01
.1
1
10
100
ωr_o c_o λ^2

TABLE II

Degree of Taper $D = \frac{m\lambda}{2}$	Notch Frequency ω_o	$\frac{R_S}{R_N} = \frac{r_o\lambda}{R_N}\left(\frac{e^{m\lambda} - 1}{m\lambda}\right)$
0	$\frac{11.1902}{r_o c_o \lambda^2}$	17.786
± 1	$\frac{11.7216}{r_o c_o \lambda^2}$	25.129
± 2	$\frac{13.188}{r_o c_o \lambda^2}$	63.568

The magnitude and phase of the $\overline{ERC}$ notch filter are as shown in Figures 2:22 and 2:23. By observing Figure 2:22, one can see that the width of the rejection band decreases as the taper becomes more positive. By comparing Figures 2:24 and 2:11 ($\overline{URC}$ notch filter) it is obvious that an $\overline{ERC}$ notch filter with a positive taper has a narrower rejection band than the $\overline{URC}$ notch filter.

CHAPTER III

THEORETICAL ANALYSIS OF A $\overline{URC}$ AND AN $\overline{ERC}$ NETWORK INCLUDING DIELECTRIC LOSS

3.0 General

The theory in Chapter II was derived under the assumption that there was no loss in the dielectric material of the distributed parameter networks. It is therefore necessary to derive the responses of the $\overline{URC}$ and $\overline{ERC}$ network taking dielectric loss into consideration.

3.1 Effect of Dielectric Loss on a $\overline{URC}$ Low Pass Filter

A representative model of a capacitor which will take leakage conductance and dielectric loss into consideration is shown in Figure 3:1 where

G_o = leakage conductance

$R_s(\omega)$ = frequency dependent series resistance representing dielectric dissipation.

C_s = equivalent series capacitance

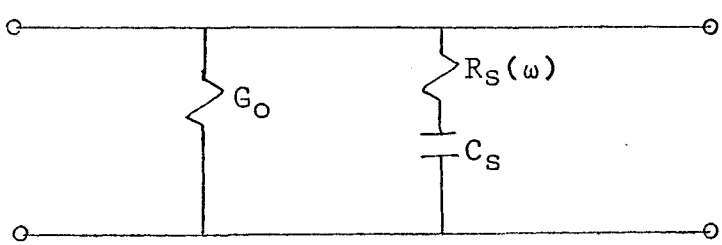

Figure 3:1 Capacitor Model

It would perhaps be beneficial at this time if the basis[15] of the simulated dielectric dissipation in the capacitor model were explained.* If one applies an alternating sinusoidal potential to a capacitor, the capacitor is alternately charged and discharged every half cycle. If the potential is of the form

$$V = V_o \sin\omega t \qquad .....3.1$$

then the charge on the electrodes is

$$q = CV = CV_o \sin\omega t \qquad .....3.2$$

and is in phase with the potential. The current which is the time rate of change of the charge also alternates sinusoidally but is 90° out of phase with the potential.

$$I = dq/dt = \omega CV_o \cos\omega t = \omega CV_o \sin(\omega t + \Pi/2) \qquad .....3.3$$

Dielectric absorption is a result of two effects. The finite time involved in moving charges results in a decrease in measured capacitance (quite small) with increasing frequency and also results in a slight shift in phase

---

* For a more detailed discussion of dielectric loss please refer to S. Wong, "Solid State Electronics", pp.391-417, McGraw-Hill Book Co., New York, N.Y., 1966.

difference between current and voltage. The magnitude of this shift in phase is the loss angle, δ. The tangent of the loss angle can be used to express the phase relationship and the a.c. losses in the capacitor and is commonly referred to as "tan δ" or "dissipation factor." The loss can be expressed in terms of a hypothetical resistance, which due to the physical properties of the dielectric, is a function of frequency. The resistance is placed in series with the capacitor and since G_o is usually small we may obtain

$$\tan\delta = \omega C_s R_s(\omega) \qquad .....3.4$$

The capacitor model shown in Figure 3:1 was used in the transmission line analogy for a distributed RC network in place of the ideal capacitor. The effect of leakage conductance on the network was first analyzed and then the effect of dielectric dissipation on the network was analyzed.

The network model used to determine the effect of leakage conductance on the $\overline{URC}$ network is as shown in Figure 3:2. Consider an incremental portion of the network at a distance x from the input end as shown in Figure 3:2(b). We may write

$$i(t,x) = c_o\Delta x\frac{\partial v(t,x)}{\partial t} + g_o\Delta x v(t,x) + i(t,x+\Delta x) .....3.5$$

$$v(t,x) = r_o\Delta x i(t,x+\Delta x) + v(t,x+\Delta x) \qquad .....3.6$$

FIGURE 3:2

(a) Network model of a $\overline{\text{URC}}$ network taking leakage conductance into consideration.

(b) Incremental network model of a $\overline{\text{URC}}$ network taking leakage conductance into consideration

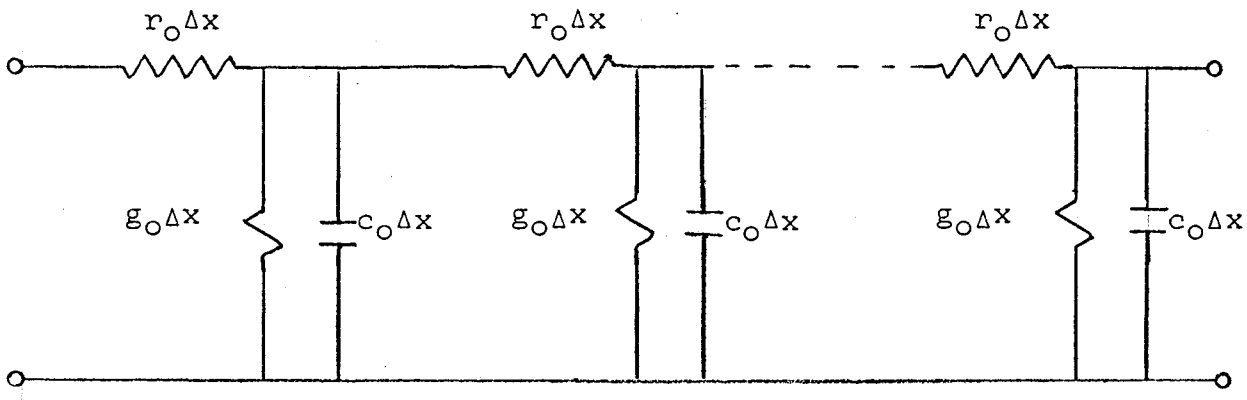
$r_o\Delta x$
$r_o\Delta x$
$r_o\Delta x$
$g_o\Delta x$
$c_o\Delta x$
$g_o\Delta x$
$c_o\Delta x$
$g_o\Delta x$
$c_o\Delta x$

(a)

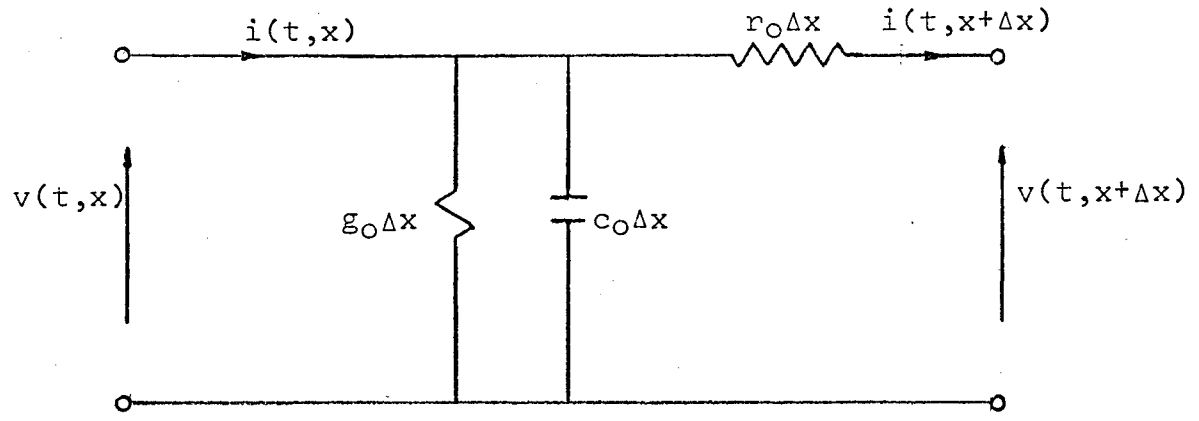
i(t,x)
$r_o\Delta x$
i(t,x+Δx)
v(t,x)
$g_o\Delta x$
$c_o\Delta x$
v(t,x+Δx)

(b)

where

g_o is conductance/unit length

r_o is resistance/unit length

c_o is capacitance/unit length

As $\Delta x \to 0$, equations 3.5 and 3.6 take on the form of a pair of partial differential equations as shown by

$$\frac{\partial i(t,x)}{\partial x} = - c_o \frac{\partial v(t,x)}{\partial t} - g_o v(t,x) \qquad .....3.7$$

$$\frac{\partial v(t,x)}{\partial x} = - r_o i(t,x) \qquad .....3.8$$

From equations 3.7 and 3.8 we may obtain

$$\frac{\partial^2 v(t,x)}{\partial x^2} = r_o c_o \frac{\partial v(t,x)}{\partial t} + r_o g_o v(t,x) \qquad .....3.9$$

Taking the Laplace transform of both sides and assuming zero initial conditions gives us

$$\frac{d^2 V(s,x)}{dx^2} - r_o(sc_o+g_o)V(s,x) = 0 \qquad .....3.10$$

This equation is of the same form as equation 2.15 and can be similarly solved to give

$$y_{11} = y_{22} = \frac{\cosh\gamma}{Z_o \sinh\gamma} \qquad .....3.11$$

$$y_{12} = y_{21} = - \frac{1}{Z_o \sinh\gamma} \qquad .....3.12$$

$$\frac{V_2}{V_1} = \frac{1}{\cosh\gamma} \qquad .....3.13$$

where

$$\gamma = \sqrt{RG + SCR} = \sqrt{A + SCR}$$

$$Z_o = \sqrt{\frac{R}{SC + G}} = \frac{R}{\sqrt{A + SCR}}$$

and

$$R = r_o\lambda$$

$$C = c_o\lambda$$

$$G = g_o\lambda$$

The driving point admittance and voltage transfer function were determined using A = 1,0.1,0.0 and are as shown in Figures 3:3 to 3:6. For $A \leq 0.1$, it is obvious that the leakage conductance has no significant effect on the response. Since all distributed RC networks which were fabricated in this thesis had a negligible leakage conductance ($A << 0.1$), it was assumed that the leakage conductance could be ignored from here on.

The next step was to consider the effect of dielectric dissipation on the $\overline{URC}$ network using the circuit model shown in Figure 3:7. Once again we consider an incremental portion of the network at a distance x from the input end as shown in Figure 3:7(b). We may write

$$v(t,x) = r_o\Delta x i(t,x+\Delta x) + v(t,x+\Delta x) \qquad .....3.14$$

FIGURE 3:3

Effect of leakage conductance on the magnitude of the driving point admittance of a $\overline{URC}$ low pass filter.

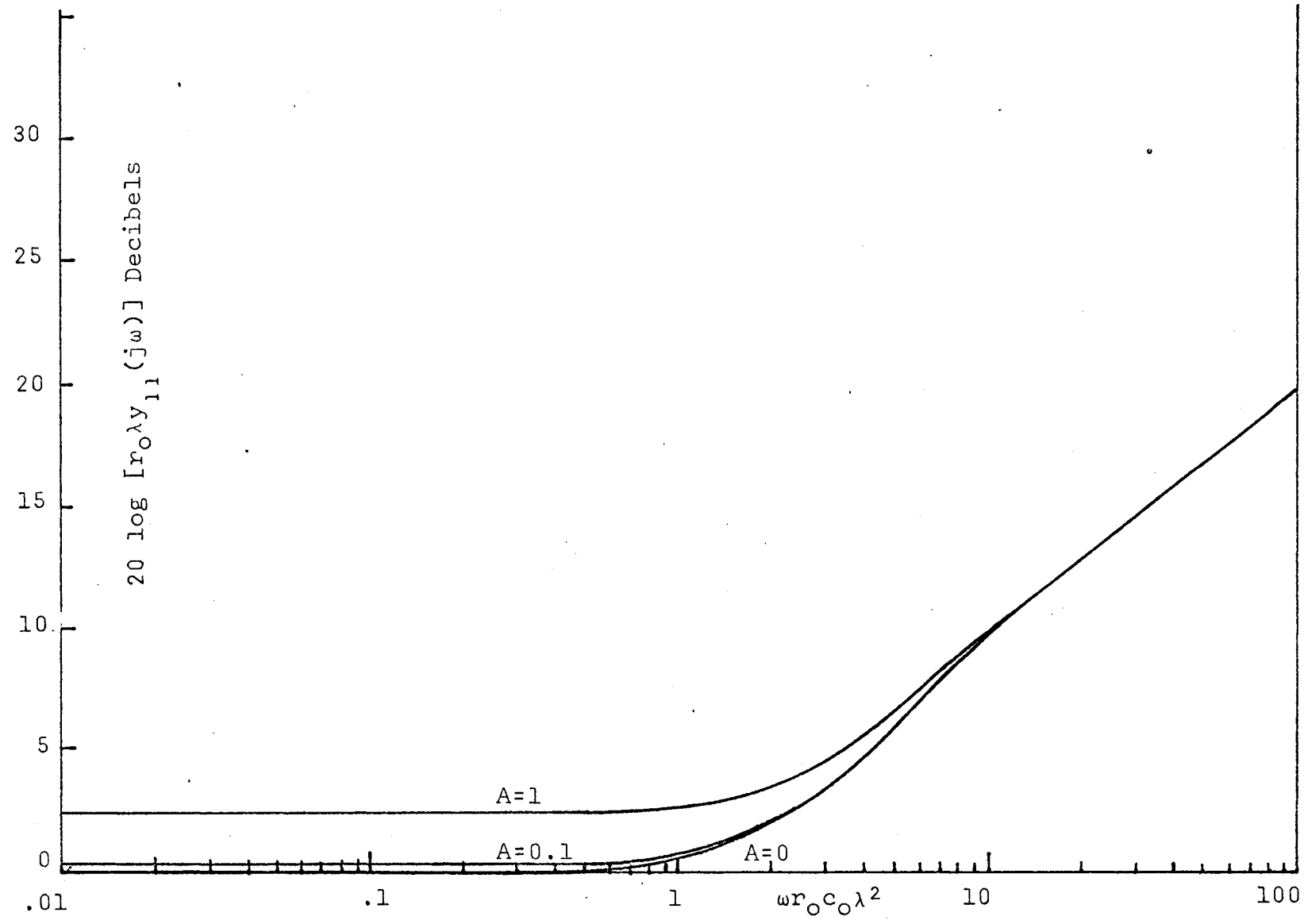
30
25
20
15
10
5
0
20 log [$r_o\lambda y_{11}(j\omega)$] Decibels
A=1
A=0.1
A=0
.01
.1
1
$\omega r_o c_o \lambda^2$
10
100

FIGURE 3:4

Effect of leakage conductance on the phase of the driving point admittance of a $\overline{URC}$ low pass filter.

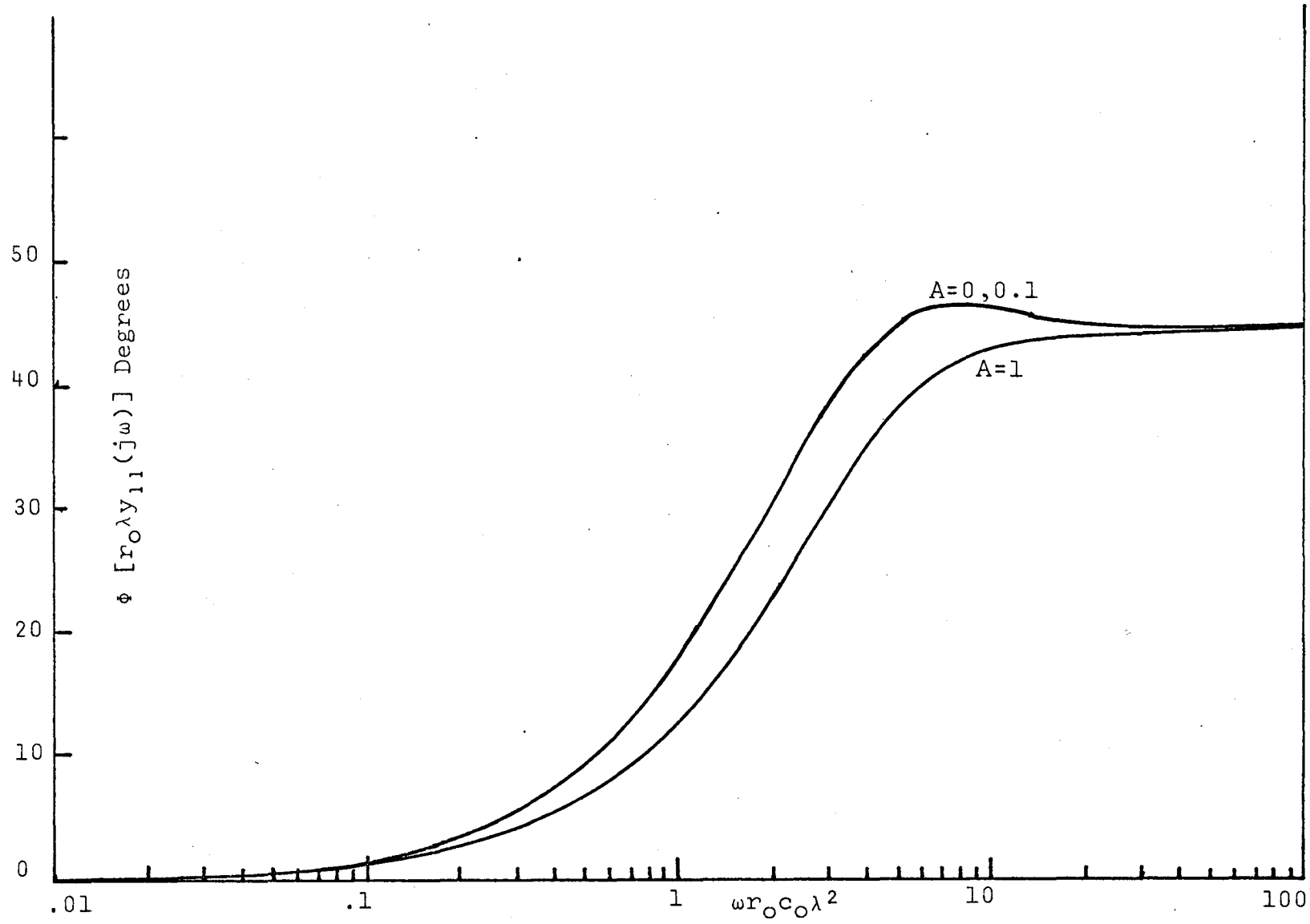
50
40
30
20
10
0
$\Phi\ [r_o\lambda y_{11}(j\omega)]$ Degrees
A=0,0.1
A=1
.01
.1
1
10
100
$\omega r_o c_o \lambda^2$

FIGURE 3:5

Effect of leakage conductance on the magnitude of the voltage transfer function of a $\overline{URC}$ low pass filter.

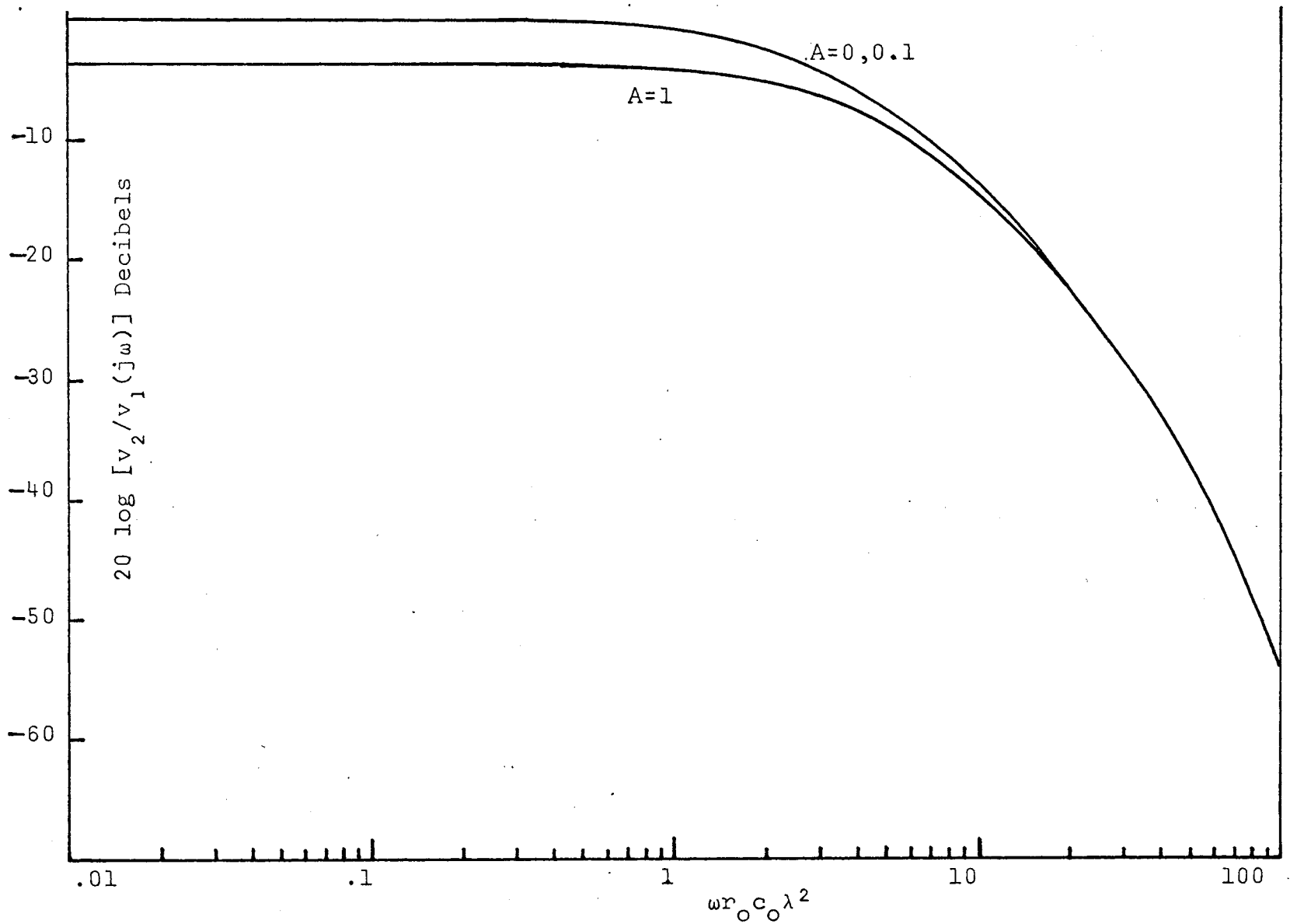
A=0,0.1
A=1
-10
-20
-30
-40
-50
-60
20 log [v2/v1(jω)] Decibels
.01
.1
1
10
100
ωr0c0λ2

FIGURE 3:6

Effect of leakage conductance on the phase of the voltage transfer function of a $\overline{URC}$ low pass filter.

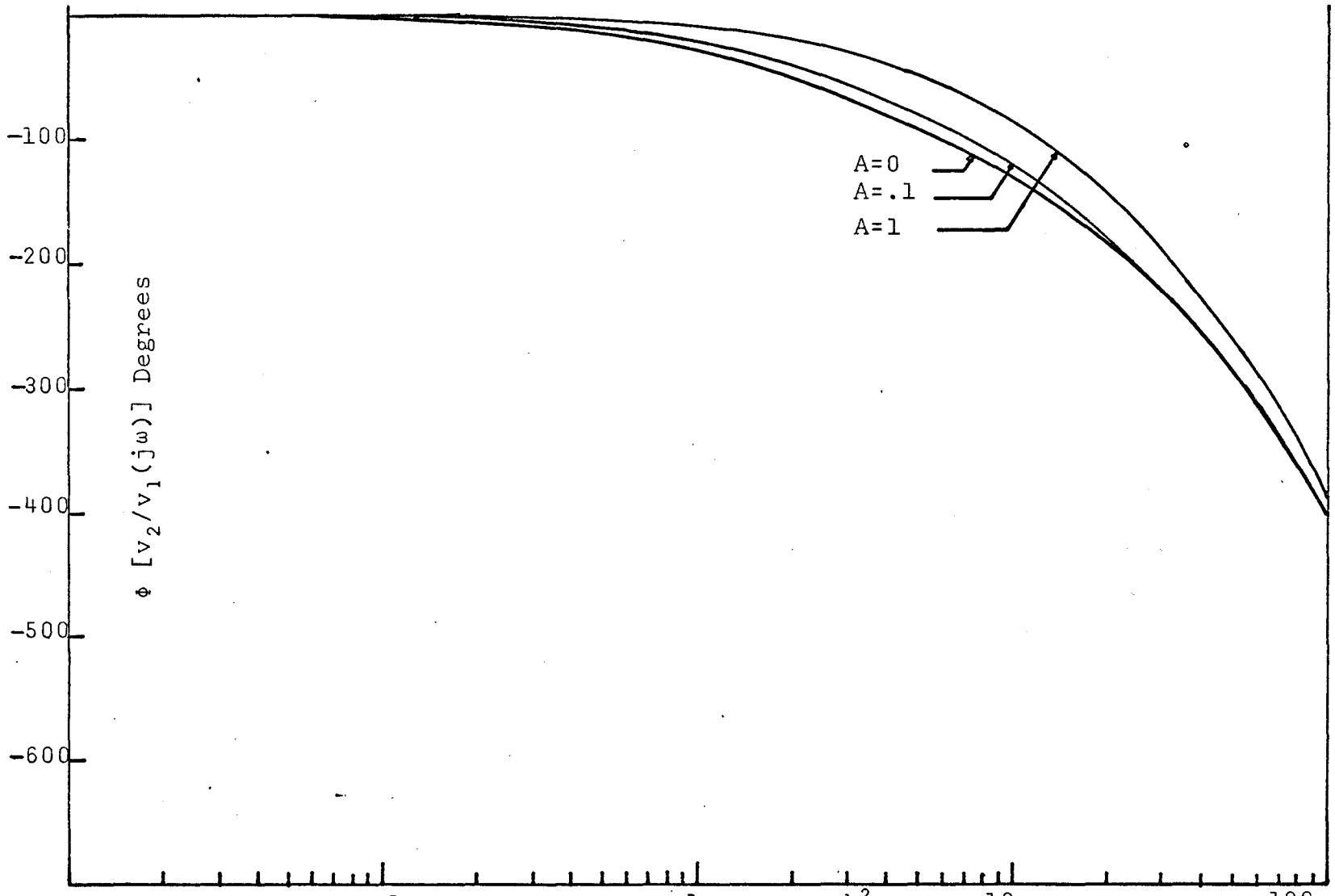
-100
-200
-300
-400
-500
-600
$\phi [v_2/v_1(j\omega)]$ Degrees
A=0
A=.1
A=1
.01
.1
1
$\omega r_o c_o \lambda^2$
10
100

FIGURE 3:7

(a) Network model of a $\overline{URC}$ network taking dielectric dissipation into consideration

(b) Incremental network model of a $\overline{URC}$ network taking dielectric dissipation into consideration

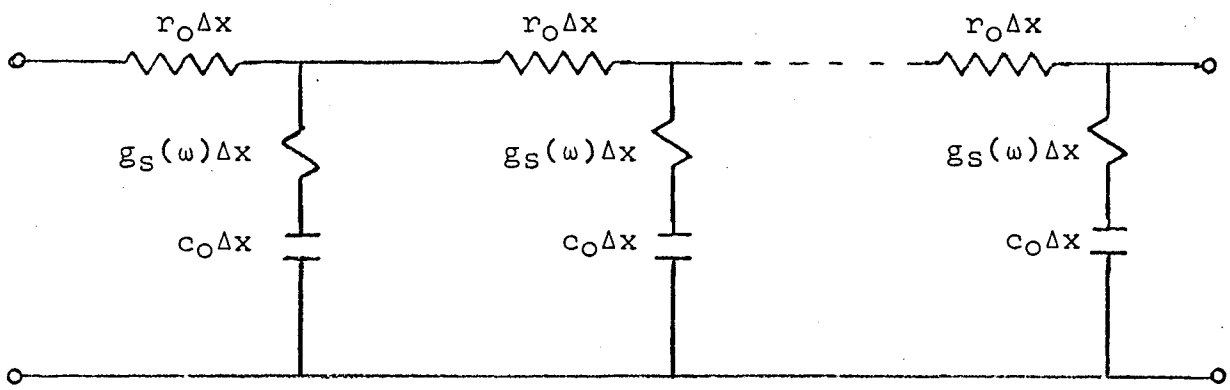
$r_o\Delta x$
$r_o\Delta x$
$r_o\Delta x$
$g_s(\omega)\Delta x$
$g_s(\omega)\Delta x$
$g_s(\omega)\Delta x$
$c_o\Delta x$
$c_o\Delta x$
$c_o\Delta x$

(a)

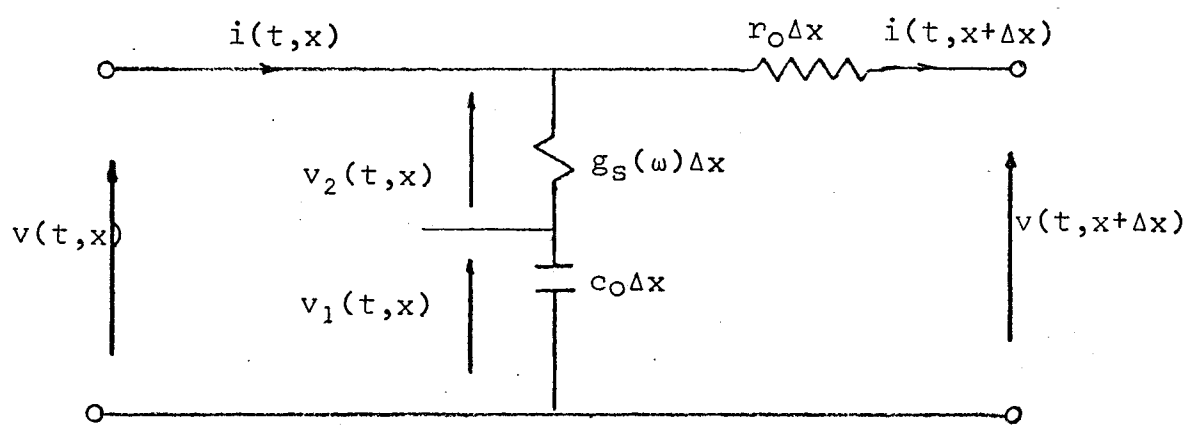
$i(t,x)$
$r_o\Delta x$
$i(t,x+\Delta x)$
$v_2(t,x)$
$g_s(\omega)\Delta x$
$v(t,x)$
$v(t,x+\Delta x)$
$c_o\Delta x$
$v_1(t,x)$

(b)

$$i(t,\Delta x) = - c_o \Delta x \frac{\partial v_1(t,x)}{\partial t} \qquad .....3.15$$

$$v_1(t,x) = v(t,x) + \frac{i(t,\Delta x)}{g_s(\omega)\Delta x} \qquad .....3.16$$

By allowing $\Delta x \to 0$, equations 3.14, 3.15 and 3.16 take on the form of partial differential equations as shown by

$$\frac{\partial v(t,x)}{\partial x} = -r_o i(t,x) \qquad .....3.17$$

$$\frac{\partial i(t,x)}{\partial x} = - c_o \frac{\partial v_1(t,x)}{\partial t} \qquad .....3.18$$

$$v_1(t,x) = v(t,x) + \frac{\partial i(t,x)}{\partial x} \frac{1}{g_s(\omega)} \qquad .....3.19$$

We can then show that

$$\frac{\partial i(t,x)}{\partial x} = - c_o \frac{\partial}{\partial t}\left[v(t,x) + \frac{1}{g_s(\omega)} \frac{\partial i(t,x)}{\partial x}\right] \qquad .....3.20$$

Taking the Laplace transform of both sides of equations 3.17 and 3.20 and assuming zero initial conditions gives us

$$\frac{dV(s,x)}{dx} = - r_o I(s,x) \qquad .....3.21$$

$$\frac{dI(s,x)}{dx} = - sc_o\left[V(s,x) + \frac{1}{g_s(\omega)} \frac{dI(s,x)}{dx}\right]$$

$$= - \frac{sc_o V(s,x)}{1 + sc_o r_s(\omega)} \qquad .....3.22$$

where $r_s(\omega) = 1/g_s(\omega)$

By differentiating equation 3.21 with respect to x we may obtain

$$\frac{d^2V(s,x)}{dx^2} = -r_o\frac{dI(s,x)}{dx} \qquad .....3.23$$

Upon substitution of equation 3.22 into 3.23 we obtain

$$\frac{d^2V(s,x)}{dx^2} - \frac{sc_or_o}{1 + sc_or_o(\frac{r_s(\omega)}{r_o})}V(s,x) = 0 \qquad .....3.24$$

This equation is of the same form as equation 2.15 and may be similarly solved to give us

$$y_{11} = y_{21} = \frac{\cosh\gamma}{Z_o\sinh\gamma} \qquad .....3.25$$

$$y_{12} = y_{21} = -\frac{1}{Z_o\sinh\gamma} \qquad .....3.26$$

$$\frac{V_2}{V_1}\Big|_{I_2=0} = \frac{1}{\cosh\gamma} \qquad .....3.27$$

where

$$\gamma = \sqrt{\frac{SCR}{1 + SCRB(\omega)}} \quad ,B(\omega) = \frac{R_s(\omega)}{R}$$

$$Z_o = R\sqrt{\frac{1 + SCRB(\omega)}{SCR}}$$

and

$$R = r_o\lambda$$

$$C = c_o\lambda$$

$$R_s(\omega) = \frac{r_s(\omega)}{\lambda}$$

In order to determine the dielectric dissipation as a function of frequency, it was necessary to build a capacitor with the same dimensions as the $\overline{URC}$ network and measure the dissipation factor and capacitance as functions of frequency. $R_s(\omega)$ can then be determined from equation 3.4. The results are shown in Chapter V.

3.2 Effect of Dielectric Loss on a $\overline{URC}$ Notch Filter

The $\overline{URC}$ notch filter is identical to the $\overline{URC}$ low pass filter except for a lumped resistor connected between the highly conducting layer and ground as shown in Figure 2:8. However, as opposed to the ideal case in Section 2.2, we must now contend with the dielectric loss and see what effect it has on the position of normalized notch frequency and the value of α required for an optimum notch.

The voltage transfer function for the notch filter including dielectric loss is

$$\frac{v_o}{v_i} = \frac{\alpha + \gamma \sinh\gamma}{\alpha\cosh\gamma + \gamma\sinh\gamma} \qquad .....3.28$$

where $$\gamma = \sqrt{\frac{jx}{1 + jxB}}$$

$$x = \omega r_o c_o \lambda^2$$

$$B = B(\omega)$$

$$\alpha = R/R_N$$

We get an optimum notch when the numerator of equation 3.28 contains a zero on the imaginary axis of the complex frequency plane.

We therefore have

$$\alpha + \sqrt{\frac{jx(1 - jxB)}{1 + x^2B^2}} \quad \sinh \sqrt{\frac{jx(1 - jxB)}{1 + x^2B^2}} = 0 \qquad .....3.29$$

If we let

$$\sqrt{\frac{x^2B}{1 + x^2B^2} + \frac{jx}{1 + x^2B^2}} = f(x) + jg(x) \qquad .....3.30$$

we can then write

$$\sinh[f(x) + jg(x)] = \sinh f(x)\cos g(x) + j\cosh f(x)\sin g(x)$$

By setting the numerator of equation 3.28 equal to zero we obtain

$$\alpha + [f(x) + jg(x)]\,[\sinh f(x)\cos g(x) + j\cosh f(x)\sin g(x)] = 0 \qquad .....3.31$$

We can rewrite equation 3.31 separating the real and imaginary parts to obtain

$$\alpha + [f(x)\sinh f(x)\cos g(x) - g(x)\cosh f(x)\sin g(x)] + j[f(x)\cosh f(x)\sin g(x) + g(x)\sinh f(x)\cos g(x)] = 0 \qquad .....3.32$$

To find the frequency at which an optimum notch occurs we set the imaginary part of equation 3.32 equal to zero.

$$f(x)\cosh f(x)\sin g(x) + g(x)\sinh f(x)\cos g(x) = 0 \qquad .....3.33$$

To find the corresponding value for α to give an optimum notch we set

$$\alpha = -[f(x)\sinh f(x)\cos g(x) - g(x)\cosh f(x)\sin g(x)] \qquad .....3.34$$

We now have two equations, 3.33 and 3.34, which will give us the normalized frequency at which an optimum notch occurs and the value of α required for an optimum notch when dielectric loss is considered. A program was written for the Hewlett-Packard Calculator Model 9100A (refer to Appendix A for program) which will solve equations 3.33 and 3.34 for different values of B. A general explanation for the program steps will be given at this point.

1. Choose a value for $B(\omega) = B$
2. Choose a value for x in the region of optimum notch and calculate f(x) and g(x).
3. Substitute the values for f(x) and g(x) into the imaginary part of the numerator

and allow the program to iterate until the imaginary part is equal to a small value ε where $\varepsilon \leq 10^{-6}$.

4. Substitute the respective value of x into the real part of the numerator and solve for α.

The following table gives an indication of the effect of dielectric loss on the position of normalized frequency, $\frac{\omega_{o,n}}{\omega_o}$, and the value of $\alpha_{o,n}$ for an optimum notch where n=1. One can see that the dielectric loss has a significant effect on the value of α required for optimum notch and the position of the normalized notch frequency.

TABLE III

B	$\frac{\omega_{o,1}}{\omega_o}$	$\alpha_{o,1}$
0	11.1902	17.786
10^{-4}	11.20	17.865
10^{-3}	11.365	18.525
10^{-2}	13.7906	29.9629
1.5×10^{-2}	16.8	48.686

3.3 Effect of Dielectric Loss on an $\overline{ERC}$ Low Pass Filter

The effect of dielectric loss on the $\overline{ERC}$ low pass filter can be determined in the same manner as it was for the $\overline{URC}$ network. We may consider an incremental model for the network as shown in Figure 3:7(b) where the parameters r_o, $g_s(\omega)$ and c_o are now functions of x and may be replaced by r(x), $g_s(\omega,x)$ and c(x) respectively. We may then write

$$v(t,x) = r(x)\Delta x i(t,x+\Delta x) + v(t,x+\Delta x) \qquad .....3.35$$

$$i(t,\Delta x) = - c(x)\Delta x \frac{\partial v_1(t,x)}{\partial t} \qquad .....3.36$$

$$v_1(t,x) = v(t,x) + \frac{i(t,\Delta x)}{g_s(\omega,x)\Delta x} \qquad .....3.37$$

By allowing $\Delta x \to 0$, equations 3.35, 3.36 and 3.37 take on the form of partial differential equations as shown by

$$\frac{\partial v(t,x)}{\partial x} = - r(x)i(t,x) \qquad .....3.38$$

$$\frac{\partial i(t,x)}{\partial x} = - c(x)\frac{\partial v_1(t,x)}{\partial t} \qquad .....3.39$$

$$v_1(t,x) = v(t,x) + \frac{\partial i(t,x)}{\partial x}\,\frac{1}{g_s(\omega,x)} \qquad .....3.40$$

We can then show that

$$\frac{\partial i(t,x)}{\partial x} = - c(x)\frac{\partial}{\partial t}\left[v(t,x) + \frac{1}{g_s(\omega,x)}\,\frac{\partial i(t,x)}{\partial x}\right] \qquad .....3.41$$

Taking the Laplace transform of both sides of equations 3.38 and 3.41 and assuming zero initial conditions we may obtain

$$\frac{dV(s,x)}{dx} = - r(x)I(s,x) \qquad .....3.42$$

$$\frac{dI(s,x)}{dx} = - sc(x)[V(s,x) + \frac{1}{g_s(\omega,x)} \frac{dI(s,x)}{dx}]$$

$$= - \frac{sc(x)V(s,x)}{1 + \frac{sc(x)}{g_s(\omega,x)}} \qquad .....3.43$$

By differentiating equation 3.42 with respect to x we may obtain

$$\frac{d^2V(s,x)}{dx^2} = - \frac{dI(s,x)}{dx} r(x) - I(s,x) \frac{dr(x)}{dx} \qquad .....3.44$$

By substitution of equation 3.43 into 3.44 we may obtain

$$\frac{d^2V(s,x)}{dx^2} - \frac{sc(x)r(x)V(s,x)}{1 + \frac{sc(x)}{g_s(\omega,x)}} - \frac{dV(s,x)}{dx} \frac{1}{r(x)} \frac{dr(x)}{dx} = 0 \qquad .....3.45$$

We may now set

$$c(x) = c_o e^{-mx}$$

$$r(x) = r_o e^{mx}$$

$$g_s(\omega,x) = g_{so}(\omega) e^{-mx}$$

where r_o = resistance/unit length at x = 0

c_o = capacitance/unit length at x = 0

$\frac{1}{g_{so}(\omega)}$ = dielectric dissipation/unit length at x = 0

We now have

$$r(x)c(x) = r_o c_o$$

and

$$\frac{dr(x)}{dx} = mr_o e^{mx} = mr(x)$$

Equation 3.45 may now be written as

$$\frac{d^2V(s,x)}{dx^2} - m\frac{dV(s,x)}{dx} - \frac{sc_o r_o}{1 + \frac{sc_o r_o}{g_{so}(\omega)\ r_o}} = 0 \qquad .....3.46$$

Equation 3.46 is of the same form as equation 2.57 and may be similarly solved to give us

$$y_{11} = \frac{1}{r_o \lambda \sinh\gamma}\left(\gamma\cosh\gamma - \frac{m\lambda}{2}\sinh\gamma\right) \qquad .....3.47$$

$$y_{12} = y_{21} = -\frac{\gamma e^{\frac{-m\lambda}{2}}}{r_o\lambda\ \sinh\gamma} \qquad .....3.48$$

$$y_{22} = \frac{e^{-m\lambda}}{r_o\lambda\ \sinh\gamma}\left(\gamma\cosh\gamma + \frac{m\lambda}{2}\sinh\gamma\right) \qquad .....3.49$$

$$\left.\frac{V_2}{V_1}\right|_{I_2 = 0} = \frac{\gamma e^{\frac{m\lambda}{2}}}{\gamma\cosh\gamma + \frac{m\lambda\sinh\gamma}{2}} \qquad .....3.50$$

where $$\gamma = \sqrt{\left(\frac{m\lambda}{2}\right)^2 + \frac{j\omega r_o c_{o\lambda}^{\ 2}}{1 + j\omega r_o c_o \lambda^2 B(\omega)}} \qquad .....3.51$$

and $$B(\omega) = \frac{1}{g_{so}(\omega)\ r_o\lambda^2}$$

Since the object is to determine the theoretical response when dielectric loss is taken into consideration, and $B(\omega)$ is a measured value which indicates the amount of dielectric loss, then the product $g_{so}(\omega)\lambda r_o\lambda$ is a measured value. However, the values of $g_{so}(\omega)\lambda$ and $r_o\lambda$ are determined at $x = 0$. We must therefore convert them to total values so they can be correlated with the total values which are measured.

If we let

R = total network resistance

and

$$R_s(\omega) = \frac{1}{G_s(\omega)} = \text{total dielectric dissipation}$$

we can then find these values as follows

$$R = \int_o^\lambda r_o e^{mx}\, dx = r_o\lambda\left(\frac{e^{m\lambda} - 1}{m\lambda}\right)$$

$$G_s(\omega) = \int_o^\lambda g_{so} e^{-mx}\, dx = \frac{g_{so}\lambda(1 - e^{-m\lambda})}{m\lambda}$$

We may now obtain

$$g_{so}(\omega)\lambda r_o\lambda = \frac{G_s(\omega)RD^2}{\sinh^2 D}$$

where

$$D = \frac{m\lambda}{2}$$

and $G_s(\omega)$ and R are measurable values.

We may now rewrite equation 3.51 as

$$\gamma = \sqrt{D^2 + \frac{j\omega r_o c_o \lambda^2}{1 + j\omega r_o c_o \lambda^2 (\frac{\sinh^2 D}{D^2})\frac{Rs(\omega)}{R}}}$$

The driving point admittances and voltage transfer function may now be determined and normalized with respect to $\omega r_o c_o \lambda^2$ when the measured value of the dielectric loss is taken into consideration. The results are shown in Chapter V.

3.4 Effect of Dielectric Loss on an $\overline{ERC}$ Notch Filter

The voltage transfer function for the $\overline{ERC}$ notch filter was derived in Section 2.4 and found to be

$$\frac{V_o}{V_i} = \frac{\frac{r_o\lambda}{R_N}\gamma e^{\frac{m\lambda}{2}} + j\omega c_o r_o \lambda^2 \sinh\gamma}{(\frac{r_o\lambda}{R_N}\frac{m\lambda}{2} + j\omega r_o c_o \lambda^2)\sinh\gamma + \frac{r_o\lambda}{R_N}\gamma\cosh\gamma} \quad .....3.52$$

Since $r_o\lambda$ is the resistance of the resistive layer at $x = 0$, we must once again convert it to the total measurable resistance R where

$$R = \frac{r_o\lambda(e^{m\lambda} - 1)}{m\lambda}$$

Equation 3.52 may now be rewritten to give us

$$\frac{v_o}{v_i} = \frac{\alpha\gamma e^{D} + \frac{e^{2D} - 1}{2D} jx\sinh\gamma}{(\alpha D + \frac{(e^{2D}-1)}{2D} jx)\sinh\gamma + \alpha\gamma\cosh\gamma} \qquad .....3.53$$

where $\alpha = \frac{R}{R_N} = \frac{r_o\lambda(e^{m\lambda} - 1)}{m\lambda}$

$$D = \frac{m\lambda}{2}$$

$$x = \omega r_o c_o \lambda^2$$

and

$$\gamma = \sqrt{D^2 + \frac{jx}{1 + jx\frac{(\sinh^2 D)B(\omega)}{D^2}}}$$

when dielectric loss is taken into consideration.

We get an optimum notch when the numerator of equation 3.53 contains a zero on the imaginary axis of the complex frequency plane.

We therefore have

$$\alpha\gamma e^{D} + \frac{e^{2D} - 1}{2D} jx\sinh\gamma = 0 \qquad .....3.54$$

If we let

$$\gamma = f(x) + jg(x)$$

we can then write

$$\sinh[f(x) + jg(x)] = \sinh f(x)\cos g(x) + j\cosh f(x)\sin g(x)$$

Equation 3.54 will now become

$$\alpha[f(x) + jg(x)]e^{D} + \frac{e^{2D} - 1}{2D}jx[\sinh f(x)\cos g(x) + j\cosh f(x)\sin g(x)] = 0 \quad .....3.55$$

By considering the real part of equation 3.55 we may obtain

$$\alpha f(x)e^{D} - \left(\frac{e^{2D} - 1}{2D}\right)x\cosh f(x)\sin g(x) = 0 \quad .....3.56$$

and by considering the imaginary part of equation 3.53 we may obtain

$$\alpha g(x)e^{D} + \left(\frac{e^{2D} - 1}{2D}\right)x\sinh f(x)\cos g(x) = 0 \quad .....3.57$$

By determining the value of α from equation 3.56 and substituting this value into equation 3.57 we obtain

$$\frac{g(x)}{f(x)}\frac{e^{2D} - 1}{2D}x\cosh f(x)\sin g(x) + \frac{e^{2D} - 1}{2D}x\sinh f(x)\cos g(x) = 0$$

This equation may be simplified to give us

$$g(x)\tan g(x) + f(x)\tanh f(x) = 0 \quad .....3.58$$

From equation 3.58, we may now find the normalized frequency at which an optimum notch occurs and from equation 3.56 we may find the corresponding value of α for an optimum notch when dielectric loss is considered. A program was written for the Hewlett-Packard Calculator Model 9100A (Refer to Appendix B for program)which will solve equations 3.58 and 3.56 for different values of B. The operation of this program is the same as that for the $\overline{URC}$ notch filter only the value of D (amount of taper) must now be entered

into the program.

The following table gives an indication of the effect of dielectric loss on the position of normalized frequency, $\frac{\omega_{o,n}}{\omega_o}$, and the value of $\alpha_{o,n}$ for an optimum notch where n=1. Since the $\overline{ERC}$ filters fabricated in this thesis had a taper of D=1, this will be the only value considered from here on. One can see from Table IV that the dielectric loss has a significant effect on the value of α required for optimum notch and the position of the normalized notch frequency.

TABLE IV

B	$\frac{\omega_{o,1}}{\omega_o}$	$\alpha_{o,1}$
0	11.72	25.129
10^{-5}	11.727	25.14
10^{-4}	11.73	25.2
10^{-3}	11.808	25.99
10^{-2}	13.331	38.64

CHAPTER IV

Fabrication Techniques

4.0 General

The techniques of evaporating thin films, the materials used, and the procedure followed in fabrication of the masks and devices are discussed in this Chapter.

4.1 Vacuum Coating Unit

The evaporation of the RC networks was carried out in a modified Edwards Type 12E3 vacuum coating unit. The pumping unit consists of a 7-inch oil diffusion pump backed by a 144 liter/min rotary pump. About 45 minutes is required for the system to pump down to a working vacuum of 3×10^{-5} torr. A schematic of the vacuum system is shown in Figure 4:1.

As is shown in Figure 4:1, there is a multi filament turret assembly which enables four materials to be evaporated in any desired order from the same location. The material is evaporated from a filament that is resistance heated. However, the system does not have a multi turret mask holder. It was therefore necessary to break vacuum each time a different mask was used which could have been the cause of

FIGURE 4:1

Schematic diagram of vacuum coating unit.

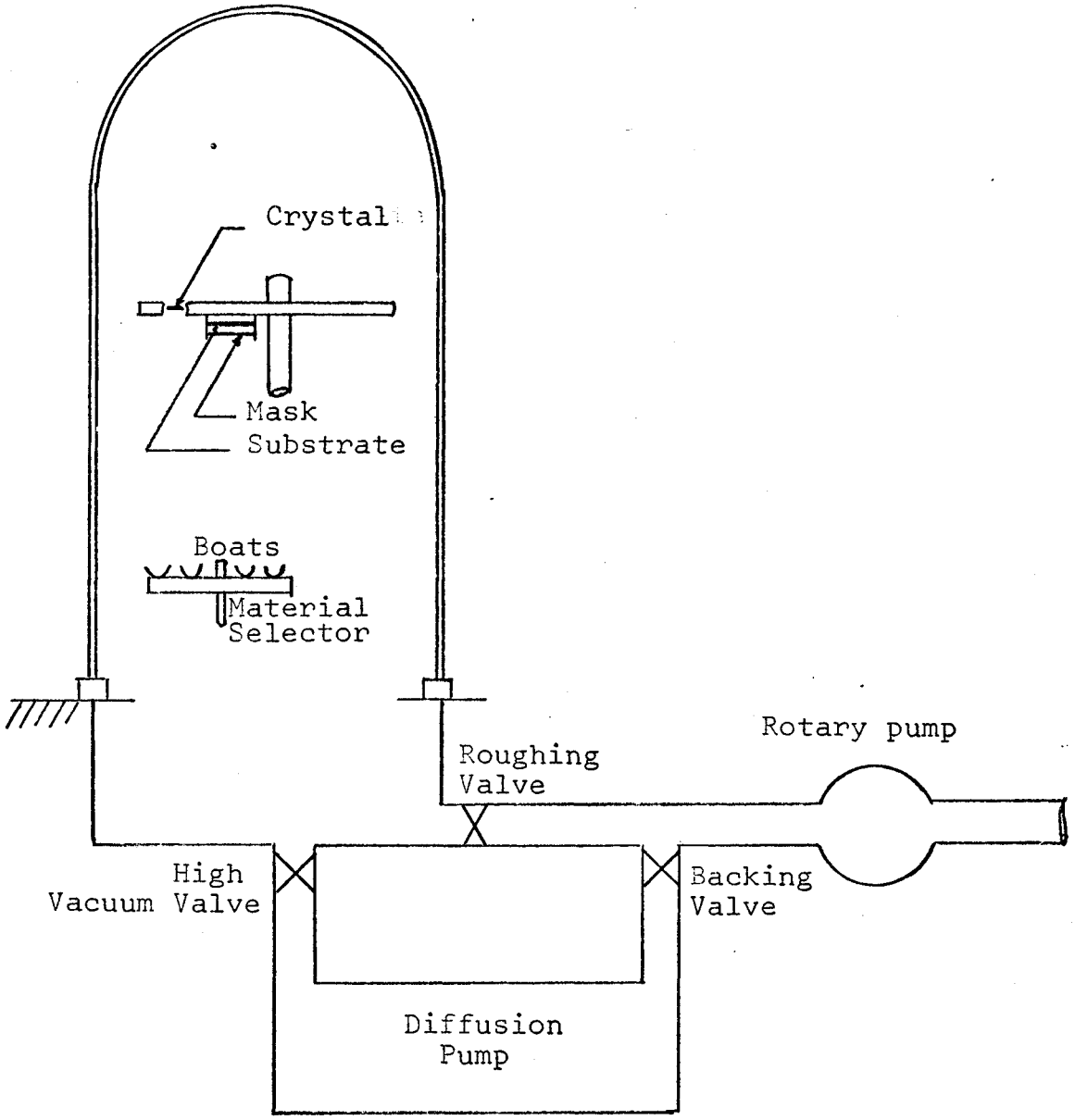
Crystal
Mask
Substrate
Boats
Material
Selector
Rotary pump
Roughing
Valve
High
Vacuum Valve
Backing
Valve
Diffusion
Pump

some materials problems such as a coating of oxide on the bottom Al. conductor and water vapor in the dielectric ($Si_x O_y$).

The system was modified to enable heating of the substrate. This was done by inserting a hollow copper block in the substrate holder and positioning it so that it would rest against the substrate. Nichrome wire wrapped around a piece of mica was inserted in the copper block and two pieces of mica were used to separate the wire from the copper block. A thermistor was inserted in the copper block and used to monitor the temperature.

The film thickness monitor consists of a quartz crystal mounted beside the substrate holder and the electronic circuitry (oscillator and emitter follower) is mounted outside the bell jar. As the film is deposited on the substrate, a film is also deposited on the quartz crystal. The increase in mass of the crystal due to the deposited film causes its natural oscillation frequency to decrease. The change of frequency is essentially linear with the change of mass provided the change of mass is small. The change of frequency was measured with a Hewlett Packard Model 3734A frequency counter.

The monitor is calibrated by preparing a special slide with a step in the deposited film. The frequency change is noted and the film thickness is measured with an

optical interferometer.[9] A number of such measurements is plotted on a graph. From the resulting curve, an empirical relationship is obtained relating film thickness to frequency change for a given material.

The monitor used in this thesis was calibrated by R.C. Dynes[10] and the resultant relationship was determined to be,

$$t = \frac{2.3\ \Delta f}{\rho m}$$

where t = film thickness in Å

Δf = frequency change in Hz

ρm = density [gm/cc]

The type of quartz crystal used is a 6 MHz AT cut crystal[11] and the maximum cumulative frequency change which may be measured accurately is 200 KH_z. Above this range, the change of frequency is no longer linear with change of mass and the crystal must be replaced or re-cleaned.

4.2 Substrate Preparation

Before a film can be deposited on the substrate, it is important that the substrate be properly cleaned. The type of substrates used for all experiments were Esco Microscope Slides No. 60-490.

Cleaning of the substrates took place in a Heat Systems Model HD-50 Ultra-sonic cleaner. The substrates were first placed in a solution of Cutscum detergent (mixed in the proportion 8 oz. of detergent to 160 gallons of distilled water) and emerged in the Ultra-sonic cleaner for 15 minutes. The substrates were then cleaned in distilled water for another 15 minutes and then in Isopropyl Alcohol for 5 minutes. Prior to using the substrates they were exposed to an Isopropyl "vapor degrease bath"[12] for 15 minutes. It was also important that the slides be handled with rubber gloves and tweezers at all stages of cleaning.

4.3 Mask Fabrication

Fabrication of masks for the $\overline{URC}$ network is quite straightforward. However, it would be beneficial if we consider a certain facet of the design theory before proceeding with the discussion on fabrication.

Let us consider the uniform RC network sections shown in Figure 4:2. The theory for a $\overline{URC}$ network is based on one dimensional current flow and abrupt transition at the contacts. It is therefore imperative that the resistive layer has a highly conducting strip down each side where the contacts join as shown in Figure 4:3(b). The actual masks were machined out of 1/16" brass and are

FIGURE 4:2

Two cascaded $\overline{URC}$ networks

(a) Without a conducting boundary

(b) With a conducting boundary

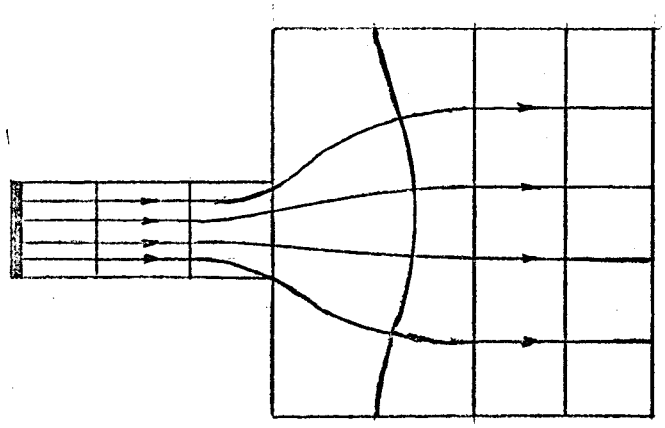

(a)

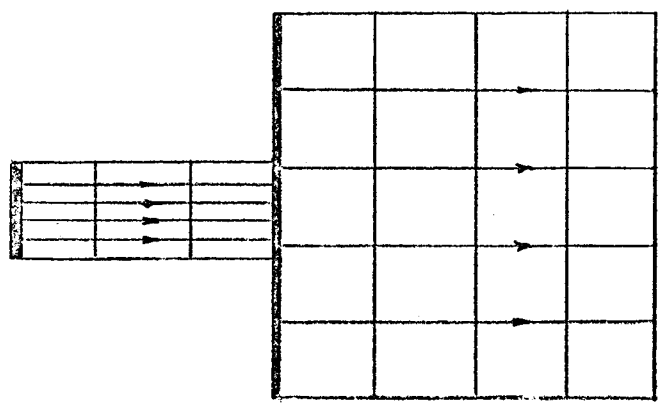

(b)

FIGURE 4:3

Photograph of masks that were used to fabricate a $\overline{URC}$ network

(a) Bottom conductor

(b) Dielectric layer and cover

(c) Resistive layer

(d) Contact pads for resistive layer

(a)

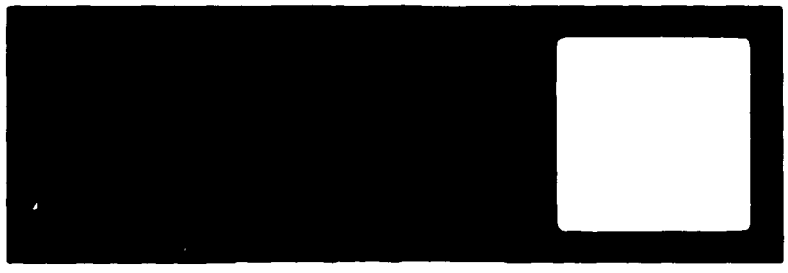

(b)

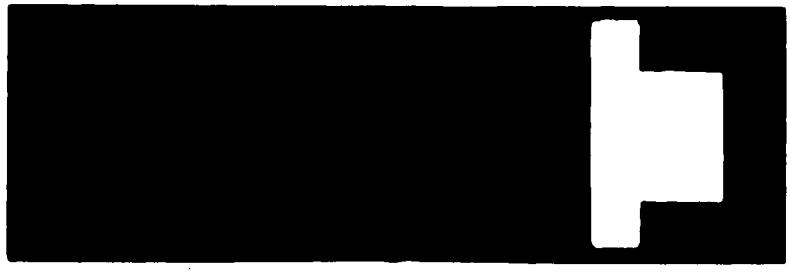

(c)

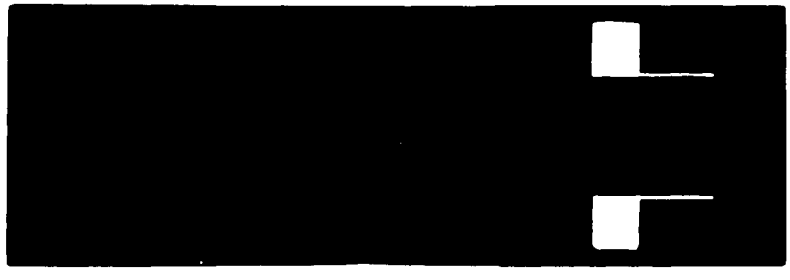

(d)

as shown in Figure 4:3.

Mask fabrication for the $\overline{ERC}$ network is somewhat more complicated. It has been shown in the literature[1] that uniform and linear electrical tapers can be realized exactly by two-dimensional geometrical shapes with continuous thickness. The same is true for parabolic and elliptic tapers because co-ordinate systems exist for these networks. For an exponentially tapered RC network, we must revert to a graphical method[1] whereby we can determine the geometrical shape that gives a good approximation to the desired electrical taper. This construction technique is described in detail by Ghausi & Kelly[1] and will therefore be only briefly covered here.

The construction technique is based on the use of curvilinear squares which enables one to obtain the proper shape of network to give a close approximation to one dimensional current flow and the desired electrical taper. A graphical technique for obtaining field patterns in curvilinear square form when the flow lines are known has been developed by Moore.[13] In Figure 4:4, abcd is assumed to be a true curvilinear square. When a circle is fitted tangent to three sides (ad, ab, bc) and a fourth side (d'c') tangent to the circle, the new figure (abc'd') is approximately a curvilinear square. The error as a f(θ) has been tabulated by Moore[13] and goes from .16% for $\theta = 10°$ to 7.52% for $\theta = 60°$.

FIGURE 4:4

True and approximate curvilinear squares

FIGURE 4:5

Illustration of the construction procedure used to obtain the geometric shape for an exponential taper.

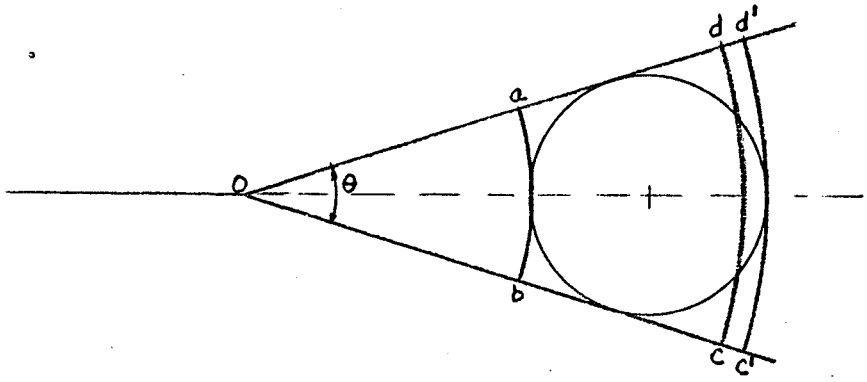

Figure 4:4

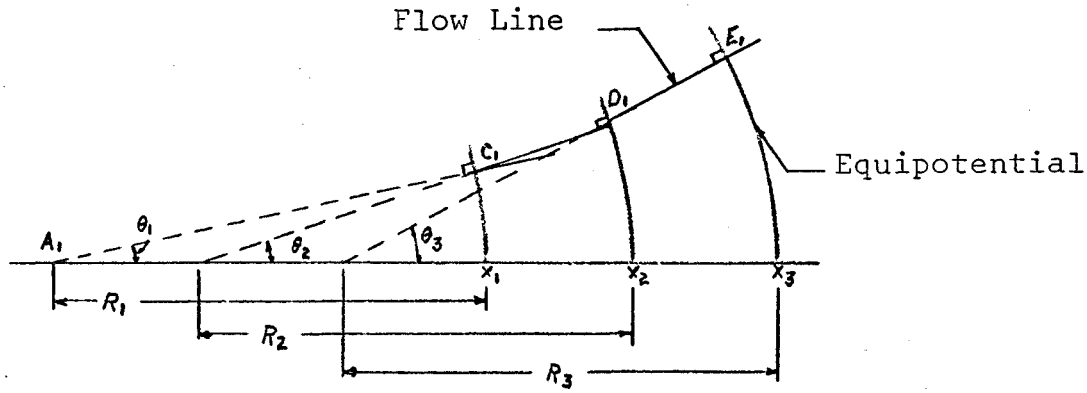

Figure 4:5

Also, the resistance and capacitance per unit length will be inversely proportional to each other only if the curvilinear squares have the same dimensions across the width of the network. This is equivalent to saying that the distance between equipotentials must be constant over the network length for the product $r(x)c(x) = T(x)$ to be a constant. A construction technique that produces orthogonal flow lines and equipotential lines is shown by Ghausi & Kelly[1] and briefly outlined here. We construct an electrical taper, $p(x)$, where $p(x)$ is the width measured along an equipotential from centerline to borderline. Interior flow lines are constructed separately. For four interior flow lines we have

$$P_1(x) = p(x)$$

$$P_{\frac{3}{4}}(x) = \tfrac{3}{4}\, p(x)$$

$$P_{\frac{1}{2}}(x) = \tfrac{1}{2}\, p(x)$$

$$P_{\frac{1}{4}}(x) = \tfrac{1}{4}\, p(x)$$

Referring to Figure 4:5, the construction procedure is as follows:

1. Calculate $P_1(x_1)$ at $x = x_1$

where $P_1(x_1) = e^{Kx_1}$

$$K = \frac{m}{2}$$

2. Calculate $p_1'(x_1)$ at $x = x_1$

3. Calculate $\theta_1 = \tan^{-1} P_1'(x_1)$ at $x = x_1$

4. Calculate $R_1 = P_1(x_1)/\theta_1$ at $x = x_1$

5. Lay off R_1 from x_1 to locate point A_1

6. At point A_1, lay off line A_1C_1 with angle θ_1 to the x-axis

7. From point A_1, draw an arc of radius R_1 from x_1 to intersect A_1C_1. This locates point C_1.

8. Repeat steps 1 through 7 to locate points D_1 and E_1 corresponding to $x = x_2$ and $x = x_3$.

9. Join points C_1, E_1 and D_1 to form a portion of a flow line.

10. Arcs C_1x_1, D_1x_2 and E_1x_3 represent equipotential lines.

11. Repeat the process for as many flow lines as desired.

In this thesis, an exponential RC network was constructed where

$$p(x) = 0.2\ e^{Kx}$$

$$K = 0.4$$

and 0.2 is a scaling factor. The resultant geometric structure is as shown in Figure 4:6. Since a configuration like this cannot be machine cut, it was necessary to use photo-resist techniques to fabricate the masks.

The final size of the masks was determined by the size of substrate which was used. The pattern for each mask was blacked out on a white piece of cardboard using a scale factor of 20 times the final desired size. Four masks were required; one for the bottom conducting layer of Al., one for the dielectric layer which was also used for the cover, one for the resistive layer and one for the contacts relevant to the resistive layer. The patterns were then photographed and reduced by a factor of 20.

A 1/16" thick brass mask blank was used with a square hole cut in one end. The mask blank was the same size as those used for the $\overline{\text{URC}}$ network so it would fit in the substrate holder. The actual mask patterns were etched out of copper foil and the copper foil was spot welded to the mask blank.

In preparation for etching, the copper foil was first cleaned thoroughly with Tripoli Powder, an abrasive which removes surface irregularities. This was followed by placing the copper foil in an Aquatone bath to remove contaminants. The foil was then rinsed in Acetone and

FIGURE 4:6

Geometric structure for an exponential taper

where $p(x) = 0.2e^{0.4x}$

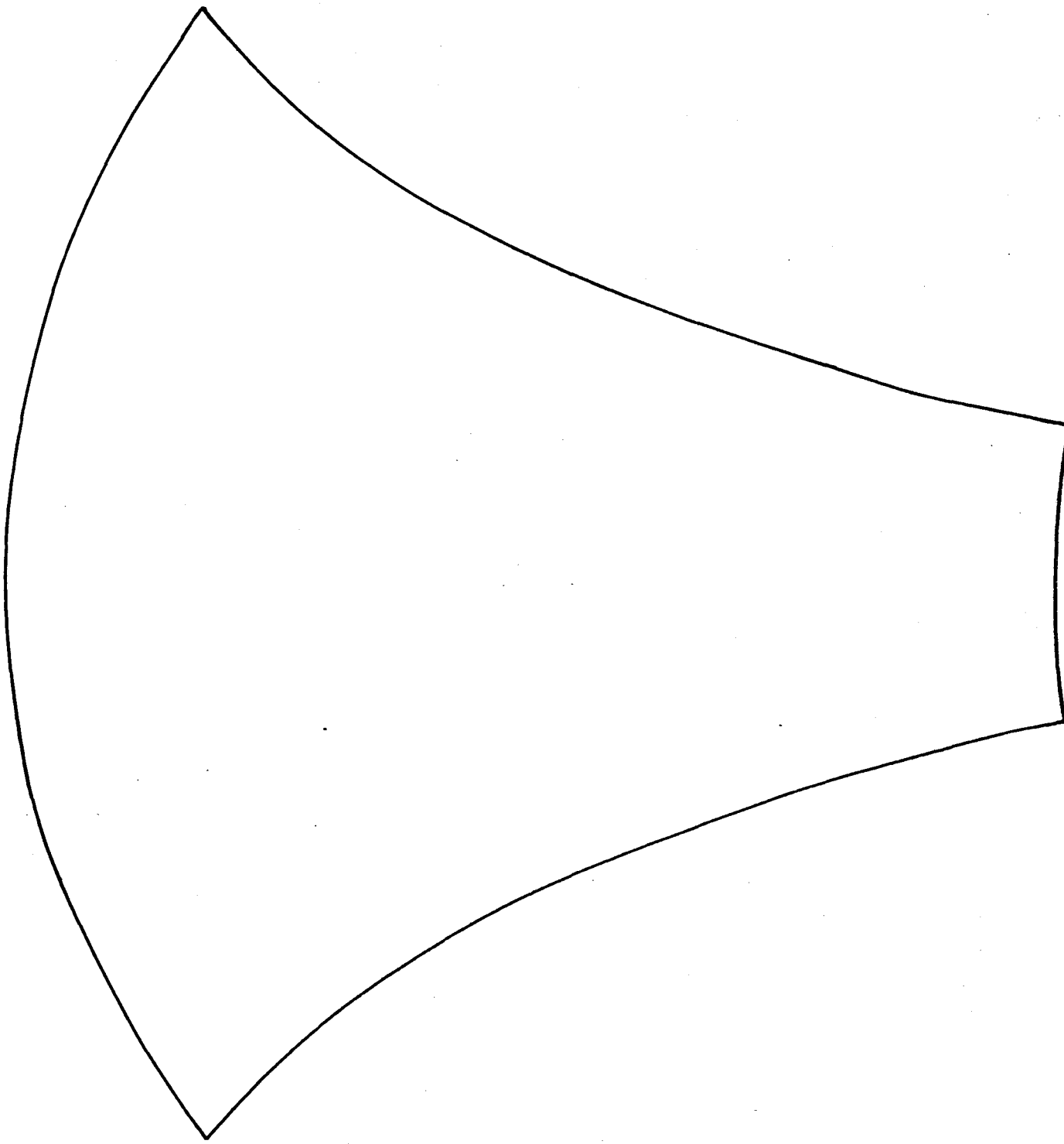

baked in an oven at 85°C. for 15 minutes.

Following this preparation the copper foil was then attached to a spinner. One cc. of Shipley AZ1350 photoresist was dripped on to the foil while it was being spun at 2000 r.p.m. The spinning was continued for 3 minutes to allow the photoresist to spread evenly and dry.

The next step was to place a negative of the desired pattern over the sensitized copper foil and expose it for 30 seconds. Where the photoresist has been exposed to the light, it can be removed in a developer. A satisfactory developer is 1% KOH and a development time of one minute was found to be sufficient. The mask was then baked at 120°C. for one hour to harden the photo-resist remaining on the copper foil.

Following this the back of the copper foil was coated with a solution of Apiezon Wax dissolved in Carbon Tetrachloride. After allowing the wax to harden, the foil was placed in a solution of $Fe_2\ Cl_3$. The copper was dissolved where the photoresist had been removed and the wax and remaining photo-resist were then removed with Chloroform. The copper foil with the desired pattern was then spot welded to the mask blank and the resultant masks are as shown in Figure 4:7.

FIGURE 4:7

Photograph of masks that were used to fabricate an $\overline{\text{ERC}}$ network.

(a) Bottom conductor

(b) Dielectric layer and cover

(c) Resistive layer

(d) Contact pads for resistive layer.

(a)

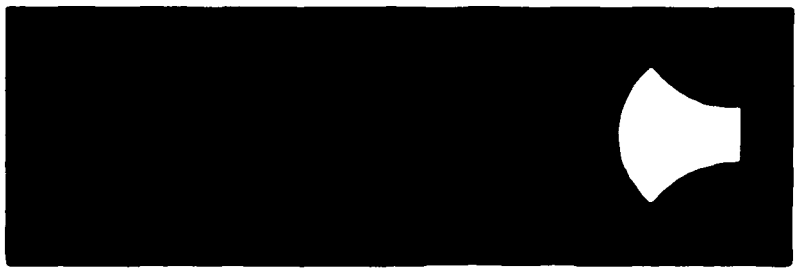

(b)

(c)

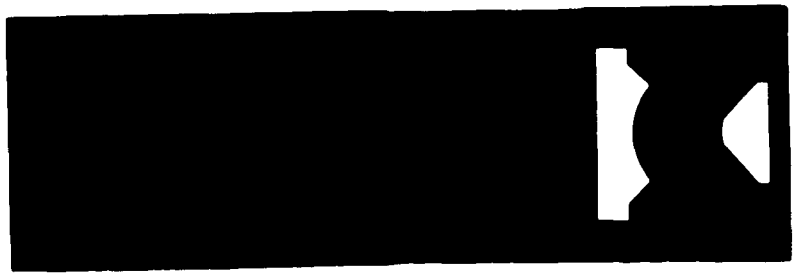

(d)

4.4 Device Fabrication

Prior to the first pump down, the substrate, the first mask to be used and the materials to be deposited were prepared and placed in the vacuum system. The system was then pumped down to approximately 3×10^{-5} torr.

The first material to be deposited was Al. for the highly conducting bottom layer. Good results were obtained with an evaporation rate of 10 Å/second from a tungsten basket. A layer of 5000 Å was evaporated which gave a theoretical resistance of 0.05 ohms. This made it possible to neglect the resistance of the bottom conductor since it is much less than the resistance of the resistive layer ($\sim \frac{1}{100,000}$).

Vacuum was then broken and the mask required for the dielectric layer was inserted. The system was evacuated and the substrate temperature raised to 250°C. Silicon Monoxide was evaporated from a Molybdenum boat at a rate of 4 Å/second in an atmosphere of oxygen at a pressure of 10^{-4} torr. If the substrate was not heated, a clear uncolored film resulted which was stable in vacuum but ruptured in air. By heating the substrate, a mechanically stable film resulted. The dielectric was deposited to a thickness of 3,000 Å in a series of three steps (i.e. 1000 Å/step). It has been shown by Miksic[14] et al that the dielectric

has an increase in breakdown strength when deposited in this manner. There was also a problem with pinholes in the dielectric causing a short circuit between the top and bottom conductors. It was found that the pinholes could be eliminated by discharging a capacitor across the network.[15] This discharge vaporizes the metal film around pinholes in the dielectric and thus averts shorts without allowing sufficient current to destroy the network.

After the insulator was deposited, vacuum was again broken and the resistive layer mask inserted. The system was evacuated and Nichrome was deposited from a tungsten boat at a rate of 10 Å/second. It was found that a Nichrome film thickness of approximately 100 Å resulted in a resistance of 15 KΩ.

Vacuum was again broken and the mask inserted which allowed deposition of the contacts for the resistive layer. The Al. contacts were deposited at a rate of 10 Å/second until a deposition thickness of 1000 Å was achieved.

After the contacts were deposited, vacuum was broken and the mask for the cover inserted. This was the same mask as that used for the dielectric layer. Silicon Monoxide was evaporated in the same manner as for the dielectric until a deposition thickness of 5000 Å was achieved.

After the complete RC network had been deposited, the device was removed from the vacuum coating unit and placed in a Delta-Design Model MK2300 oven. The device was annealed at 350°C. for a period of 1 hour. This procedure reduces dielectric losses and helps to prevent rupturing of the cover which resulted in a more stable device

The next step was to make contact to the Al. contact pads. This was accomplished by attaching small wires to the pads with Eccobond Solder 56C and then heating the device at 150°F. for 1/2 hour to anneal the solder.

CHAPTER V

EXPERIMENTAL ANALYSIS

5.0 General

Upon completion of device fabrication, the voltage transfer function and driving point admittances for the $\overline{URC}$ network and the voltage transfer function for the $\overline{ERC}$ network were measured. Twenty-four devices were fabricated before a satisfactory $\overline{URC}$ network was obtained. Measurements were then carried out on a number of $\overline{URC}$ and $\overline{ERC}$ networks with the result of similar responses for each set of measurements. Figure 5:1 is a photograph of the $\overline{URC}$ network and $\overline{ERC}$ network on which measurements were carried out to obtain the experimental results in this thesis. Before the experimental results could be compared to theory, it was necessary to determine the dielectric loss as a function of frequency.

5.1 Measured Effect of Dielectric Loss on a $\overline{URC}$ Network

As was shown in Chapter III, the dielectric material can be represented by an ideal capacitor in series with a frequency dependent resistor. To take leakage conductance into account, a conductance can be placed in parallel with these. Figures 3:3 to 3:6 show the effect of leakage conductance on the $\overline{URC}$ network responses and it was concluded

FIGURE 5:1

(a) Thin film $\overline{URC}$ network deposited on a glass substrate

(b) Thin film $\overline{ERC}$ network deposited on a glass substrate

(a)

(b)

that for $A \leq 0.1$, the leakage conductance could be ignored. The resistance of the $\overline{URC}$ network resistive layer was measured on a General Radio Type 1608A Impedance Bridge and found to be 17.6 KΩ. This means that G would have to be greater than 5.68×10^{-5} mhos to be effective. Since measured values for G were never greater than 10^{-7} mhos, leakage conductance is not taken into consideration from this point on.

To determine the dielectric dissipation as a function of frequency, it was necessary to build a capacitor with the same dimensions as the $\overline{URC}$ network. The dielectric layer of the capacitor will not have exactly the same properties as that of the $\overline{URC}$ network because evaporation conditions cannot be precisely duplicated. It will, however, be close enough to give a realistic indication of the effect of dielectric dissipation on the network responses.

The dissipation factor and capacitance were measured as functions of frequency on a General Radio Type 1608A Impedance Bridge which has a frequency range of $20H_z$ to 20 KH_z. $R_s(\omega)$ was determined using equation 3.4 and the results are as shown in Figure 5:2 where a method of Least Squares Fit was used to obtain the curve. Knowing the measured value of R, $B(\omega)$ could now be determined and hence the driving point admittance and voltage transfer function for the $\overline{URC}$ network could be determined when dielectric dissipation

FIGURE 5:2

Dielectric loss shown as a function of frequency as applied to a 3000Å evaporated thin film layer of Silicon Monoxide.

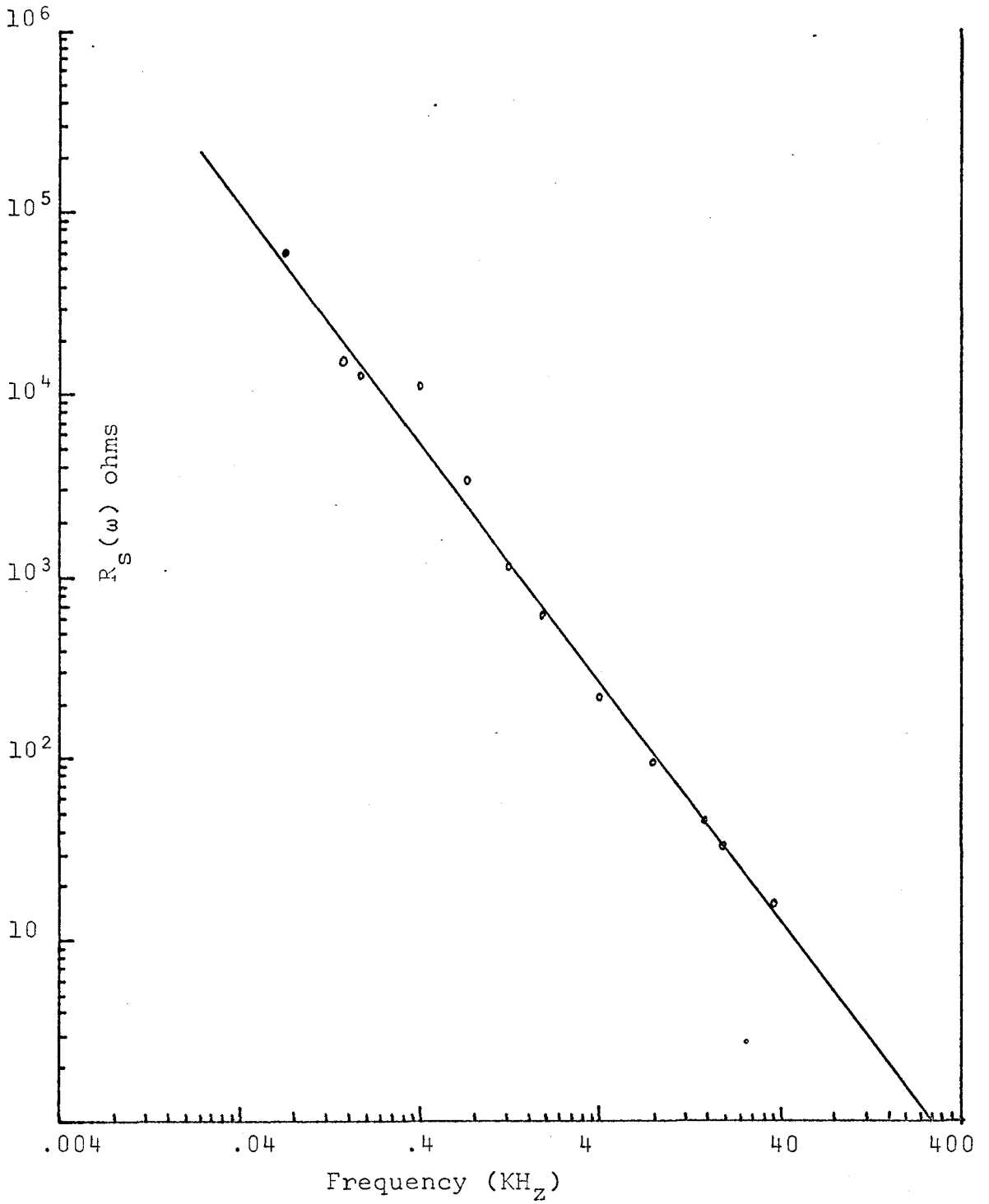
10^6
10^5
10^4
10^3
10^2
10
$R_s(\omega)$ ohms
.004
.04
.4
4
40
400
Frequency (KH_z)

FIGURE 5:3

Magnitude of the driving point admittance of a $\overline{\text{URC}}$ low pass filter taking dielectric loss into consideration.

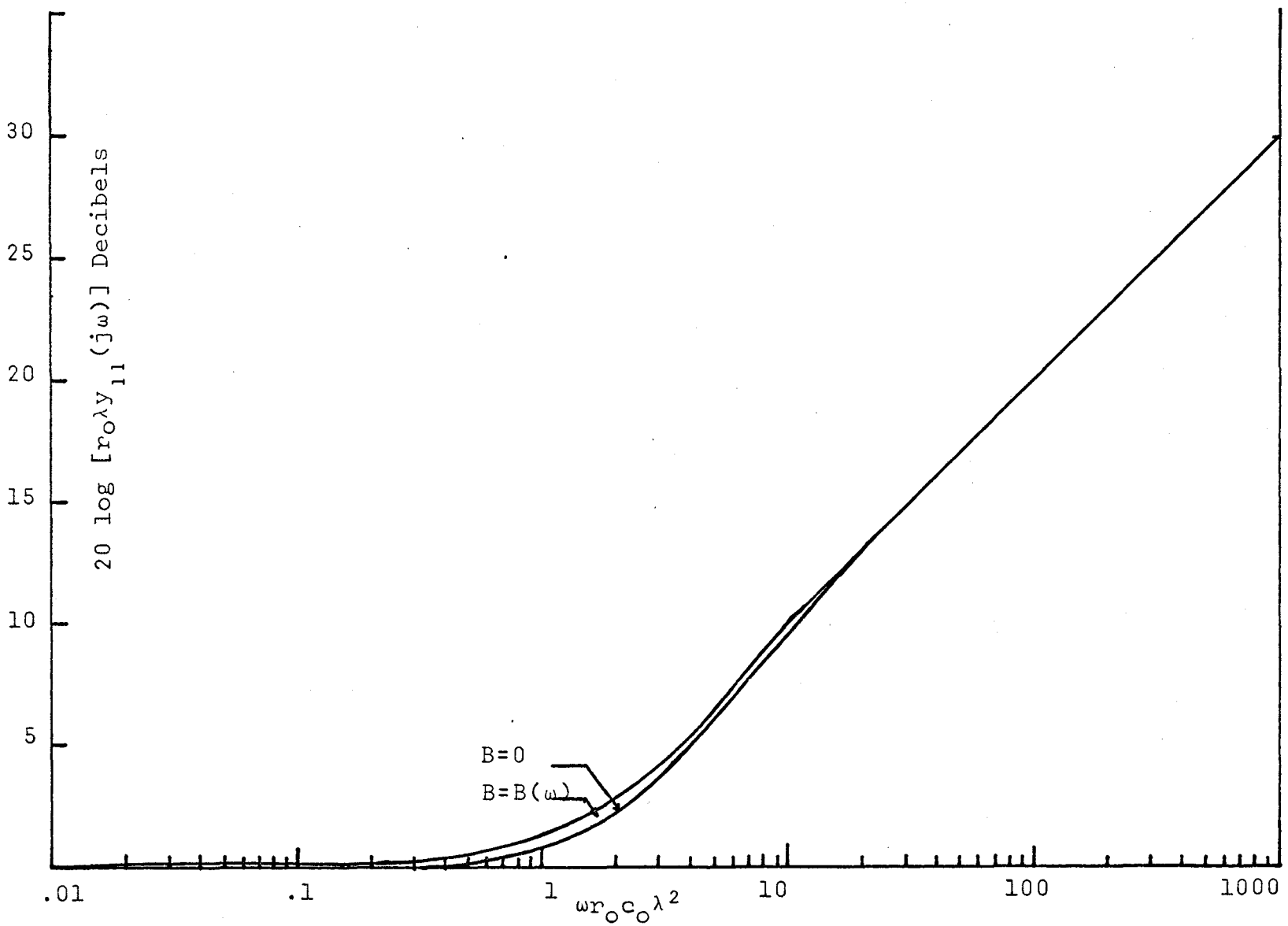
30
25
20
15
10
5
20 log [r_o λ y_11 (jω)] Decibels
B=0
B=B(ω)
.01
.1
1
10
100
1000
ωr_o c_o λ^2

FIGURE 5:4

Phase of the driving point admittance of a $\overline{\text{URC}}$ low pass filter taking dielectric loss into consideration.

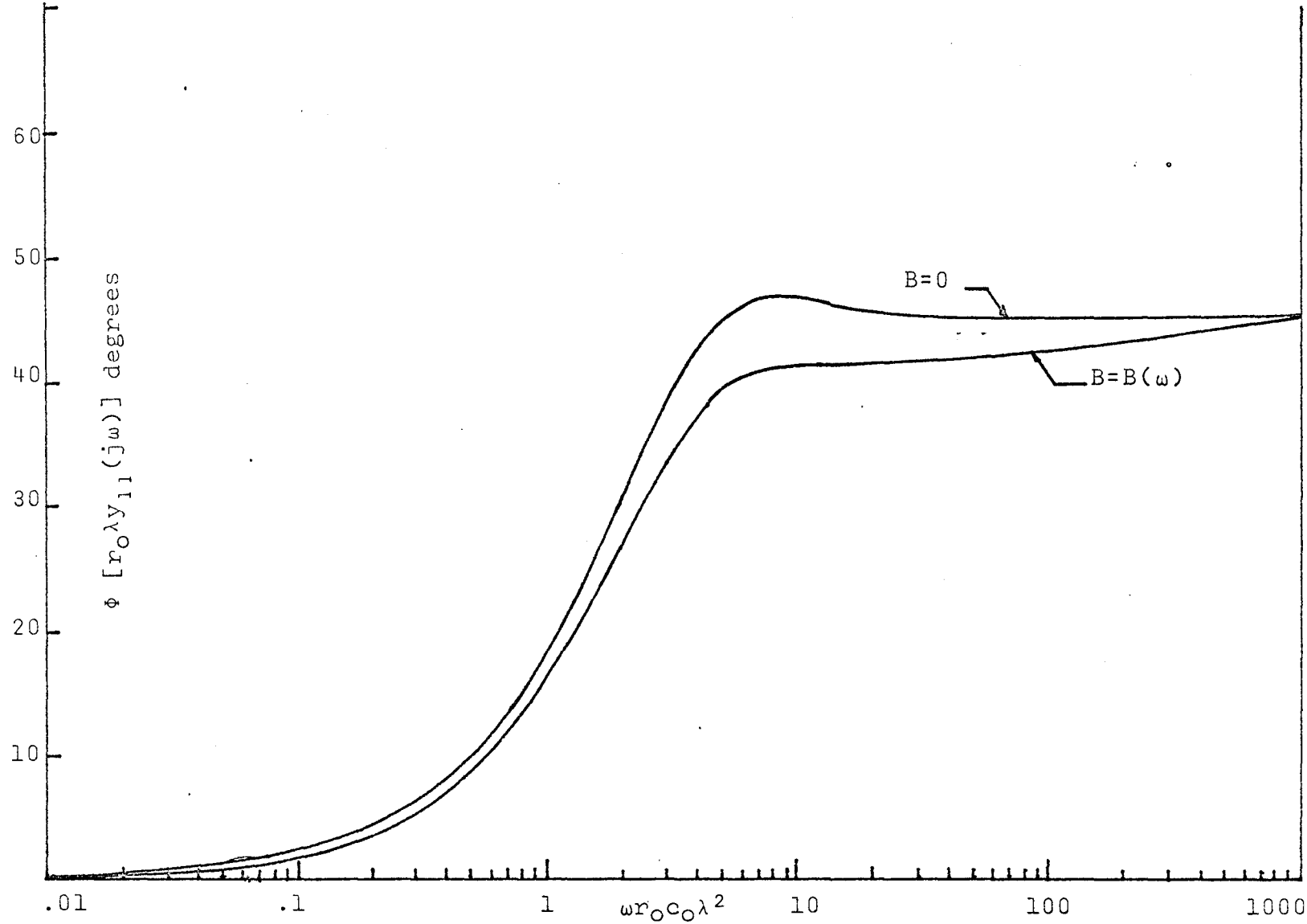
60
50
40
30
20
10
$\Phi\ [r_o\lambda y_{11}(j\omega)]$ degrees
B=0
B=B(ω)
.01
.1
1
$\omega r_o c_o \lambda^2$
10
100
1000

FIGURE 5:5

Magnitude of the voltage transfer function of a $\overline{\text{URC}}$ low pass filter taking dielectric loss into consideration.

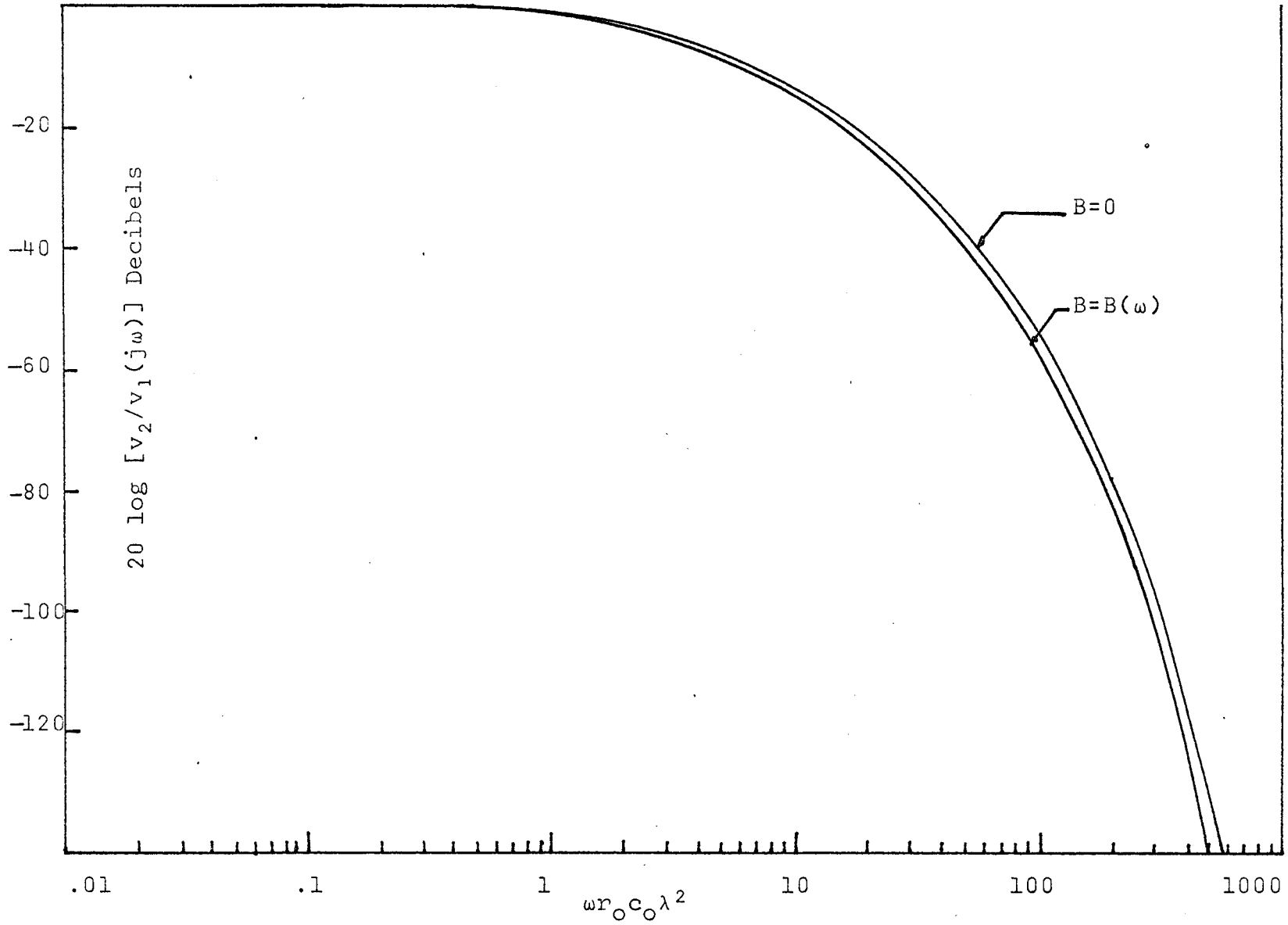
-20
-40
-60
-80
-100
-120
20 log [$v_2/v_1(j\omega)$] Decibels
B=0
B=B(ω)
.01
.1
1
10
100
1000
$\omega r_o c_o \lambda^2$

FIGURE 5:6

Phase of the voltage transfer function of a $\overline{URC}$ low pass filter taking dielectric loss into consideration.

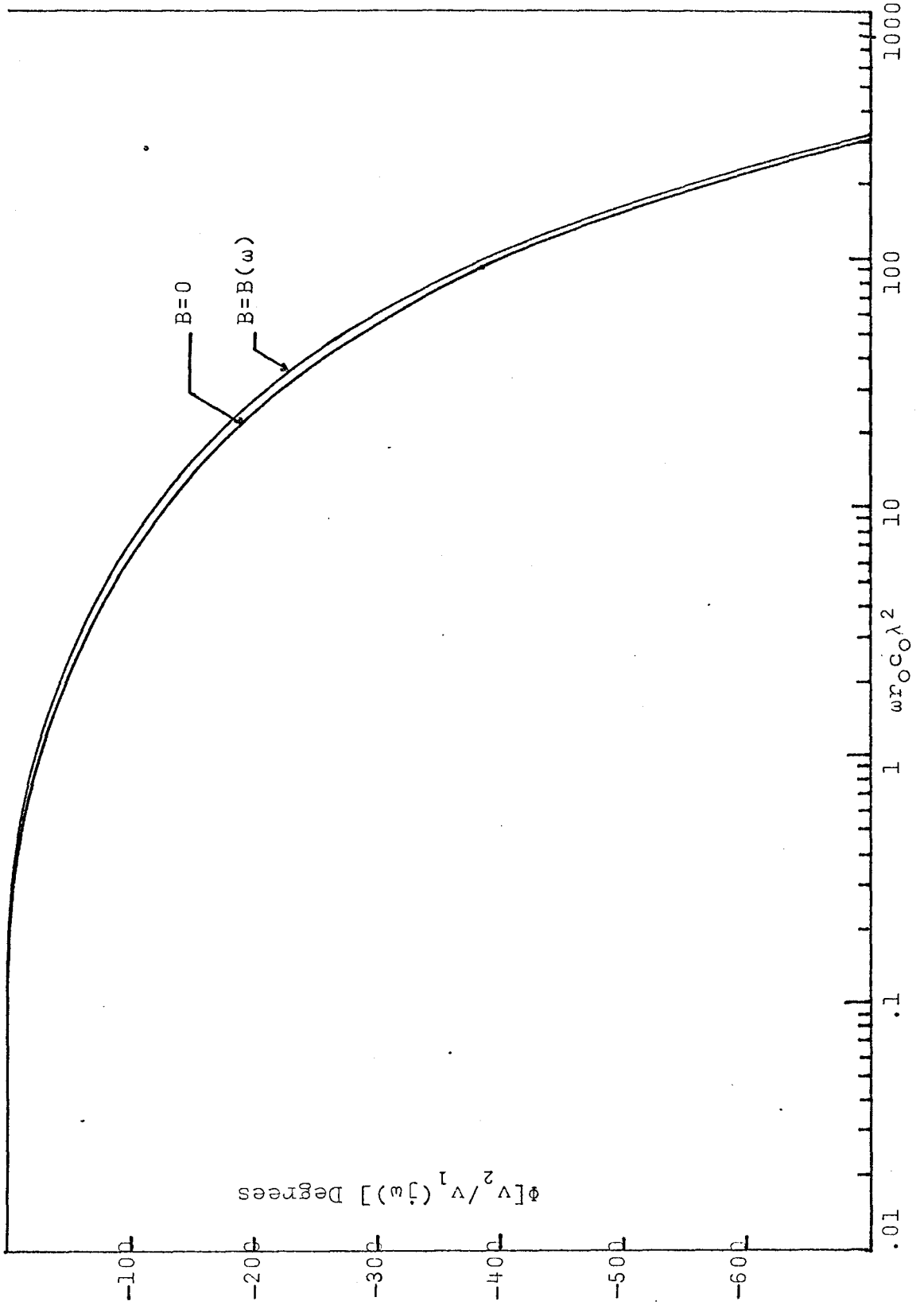

is taken into consideration.

The ideal (B=0) and non-ideal (B=B(ω)) magnitude and phase for the driving point admittance (short circuit on output) and open circuit voltage transfer function are shown in Figures 5:3 to 5:6. If we consider Figures 5:3 and 5:4, we see that the magnitude is slightly less and there is a significant decrease in phase shift when dielectric loss is considered. By considering Figures 5:5 and 5:6, we see that the magnitude and phase of the voltage transfer function have shifted down slightly due to dielectric loss. However, the only responses which appear to be significantly affected by dielectric loss are the phase and magnitude of the driving point admittance.

5.2 Notch Effect on the Voltage Transfer Function of a $\overline{URC}$ Low Pass Filter.

The notch effect which was present in the voltage transfer function was due to contact resistance of the bottom conductor. A block diagram of the equipment used to measure the voltage transfer function is shown in Figure 5:7. The equivalent circuit diagram is shown in Figure 5:8(b) where the notch effect is taken into consideration. The voltage transfer function for this circuit will be the same as that for the notch filter as given by equation 3.28.

The measured value of R was 17.6 KΩ and the measured

FIGURE 5:7

Block diagram of the test equipment used to measure the voltage transfer function.

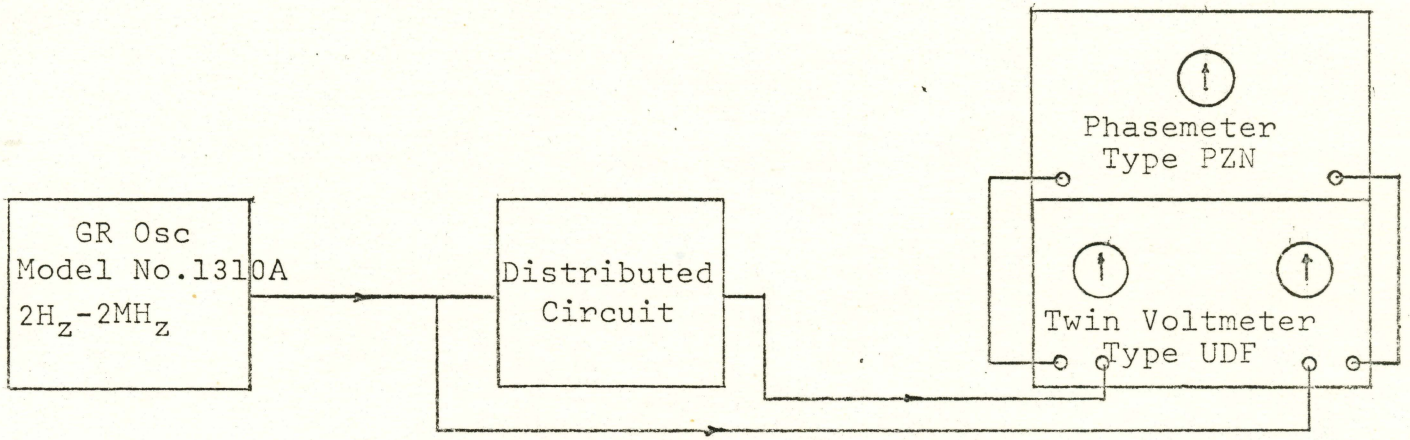
GR Osc
Model No.1310A
2Hz-2MHz
Distributed
Circuit
Phasemeter
Type PZN
Twin Voltmeter
Type UDF

FIGURE 5:8

(a) Test circuit used to measure the voltage transfer function of a $\overline{\text{URC}}$ network.

(b) Equivalent test circuit showing the notch effect.

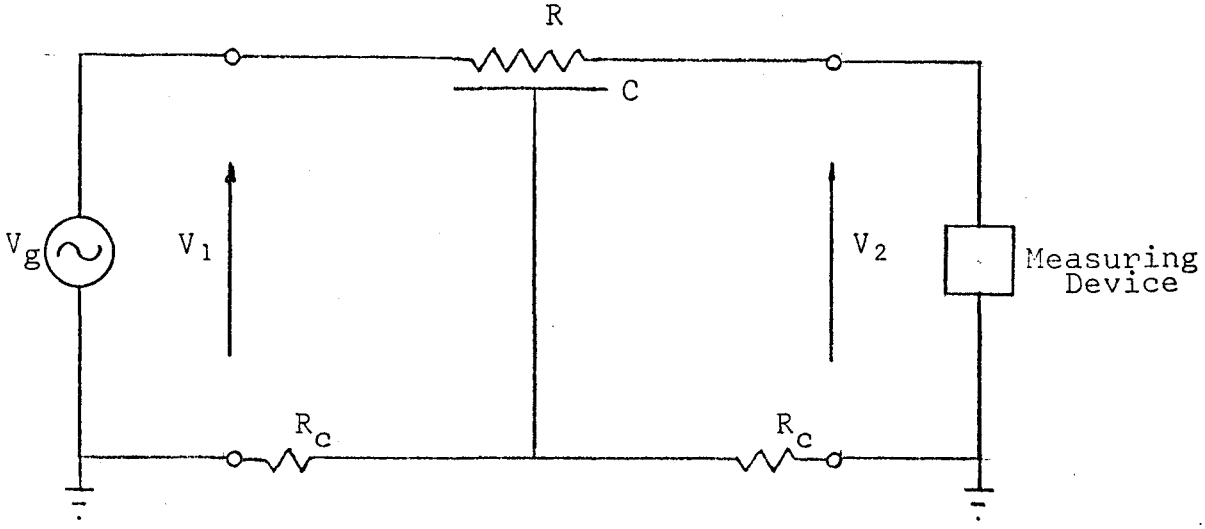
R
C
Vg
V1
V2
Measuring Device
Rc
Rc

(a)

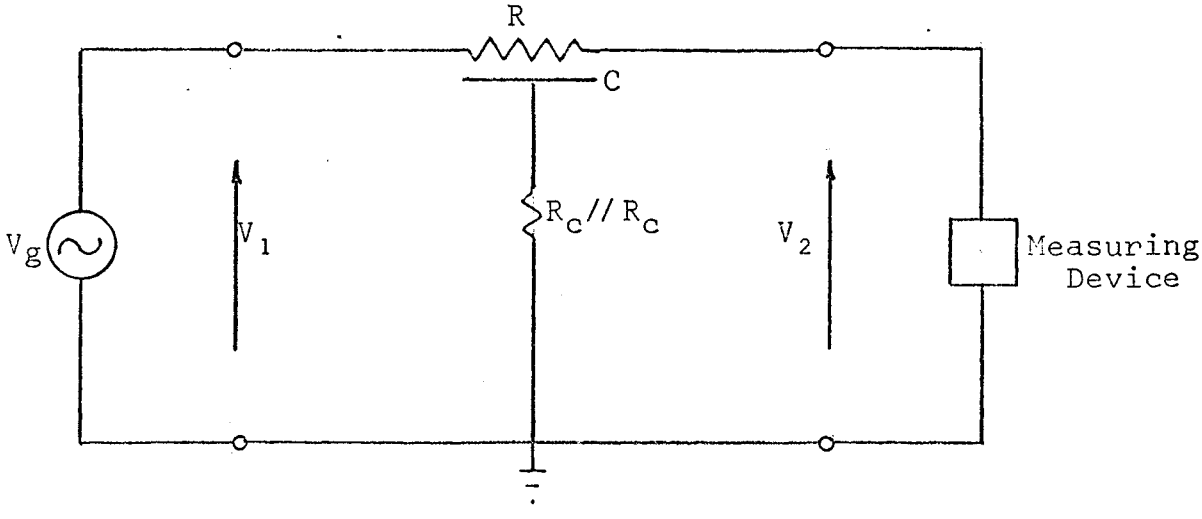
R
C
Vg
V1
Rc // Rc
V2
Measuring Device

(b)

value of Rc was 1.76 ohms for the $\overline{URC}$ low pass filter. Since the effective notch resistance is the equivalent of the parallel resistance of the two contacts, then the resultant value for α is 2×10^4. The voltage transfer function was determined taking the dielectric loss and notch effect into consideration. The magnitude and phase are shown in Figures 5:9 and 5:10. The disagreement between the ideal curves ($B=o$, $\alpha=o$) and the non-ideal curves ($B=B(\omega)$, $\alpha=2\times10^4$) at low frequencies is due to dielectric loss. At normalized frequencies greater than 100, the disagreement between ideal and non-ideal curves is mainly due to the notch effect. By using the program in Appendix A, it was found that a normalized optimum notch frequency occured at 160.4 for $B=3.8\times10^{-4}$ and the resultant value of α was 6.362×10^4. According to Section 2.2, the normalized optimum notch frequency, $\omega_{o,3}$, is 149.278 and the corresponding value of $\alpha_{o,3}$ is 3.451×10^4 when B is zero. The calculated values above ($\omega=160.4$, $\alpha=6.362\times10^4$) are therefore the corresponding values for an optimum notch when B is taken into consideration. However, by referring to Figure 5:9, we see that the measured value for α is 2×10^4 and the position of maximum notch is at a normalized frequency of 140. This means that the measured value of α is less than that required for optimum notch (i.e., $\alpha<\alpha_{o,3}$). It was also pointed out in Section 2.2 that for $\alpha_{o,1}<<\alpha<\alpha_{o,3}$ we have $-\frac{3\pi}{2} \leq \Phi \leq 0$. This is in agreement with the phase as shown in Figure 5:10.

FIGURE 5:9

Magnitude of the voltage transfer function of a $\overline{URC}$ low pass filter taking dielectric loss and notch effect into consideration.

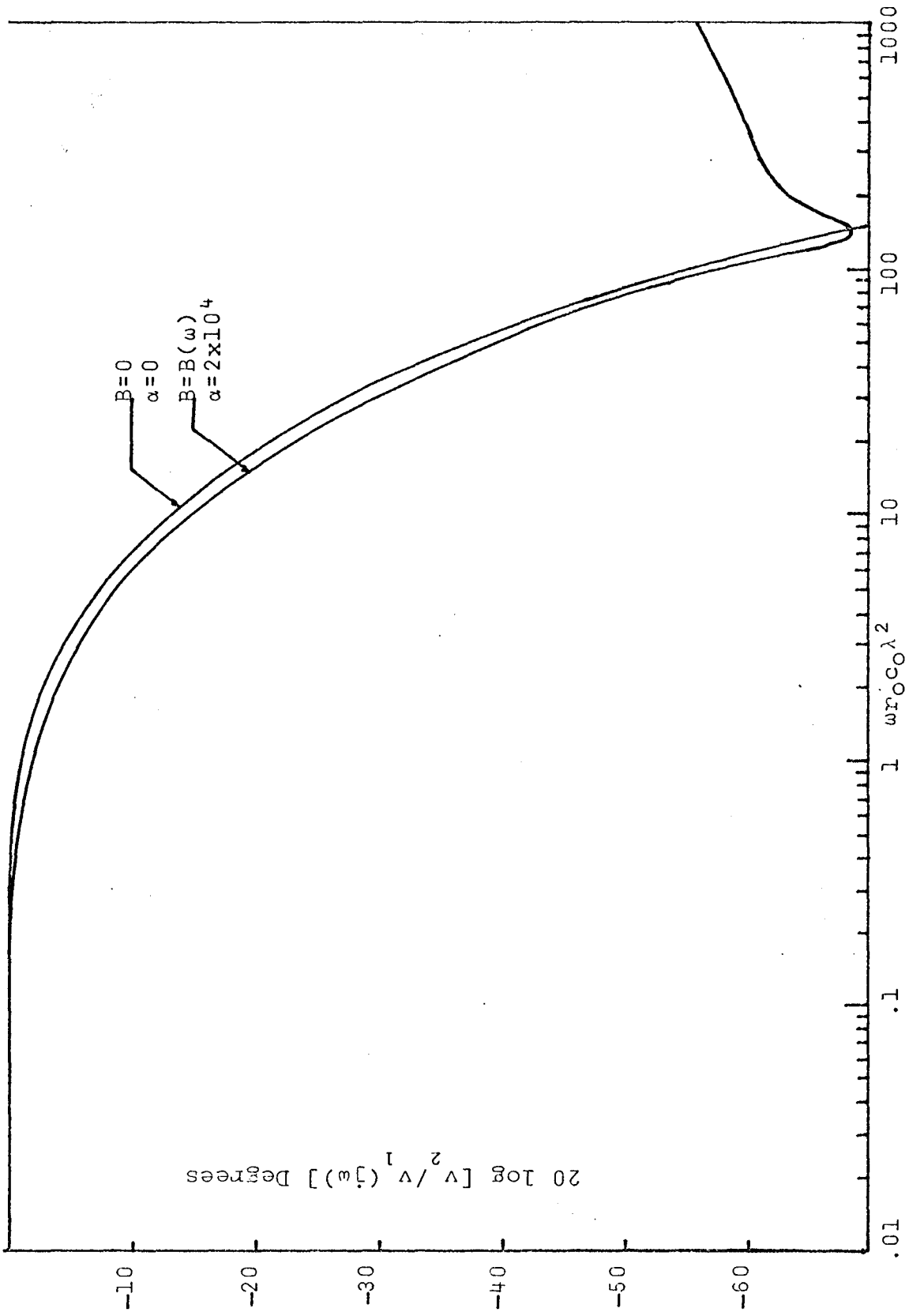
B=0
α=0
B=B(ω)
α=2x10^4
-10
-20
-30
-40
-50
-60
20 log [v2/v1(jω)] Degrees
.01
.1
1
10
100
1000
ωr0c0λ^2

FIGURE 5:10

Phase of the voltage transfer function of a $\overline{URC}$ low pass filter taking dielectric loss and notch effect into consideration.

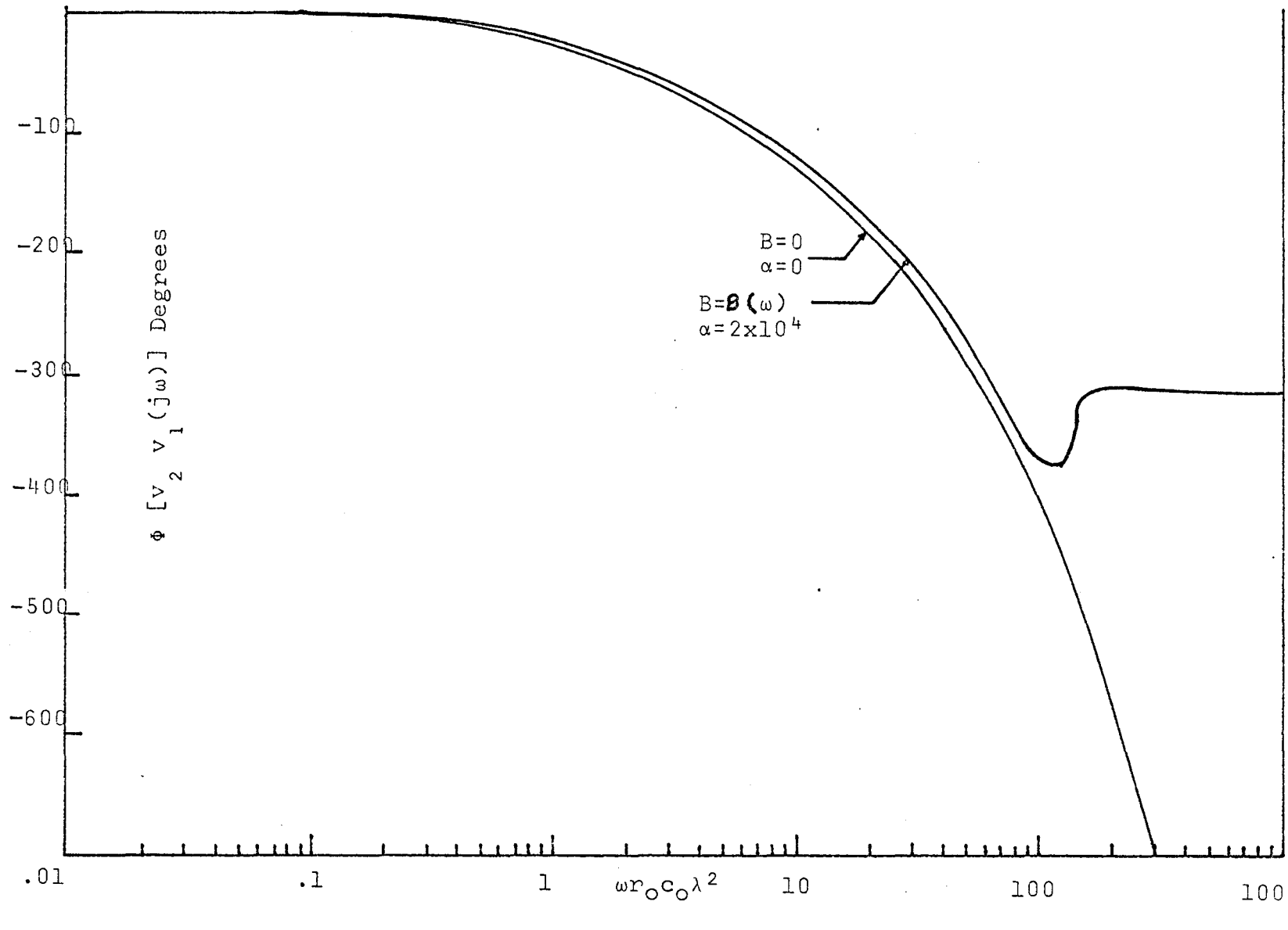
-100
-200
-300
-400
-500
-600
Φ [v2 v1(jω)] Degrees
B=0
α=0
B=β(ω)
α=2x10^4
.01
.1
1
ωr0c0λ^2
10
100
1000

FIGURE 5:11

Magnitude of the voltage transfer function of a $\overline{URC}$ notch filter taking dielectric loss into consideration.

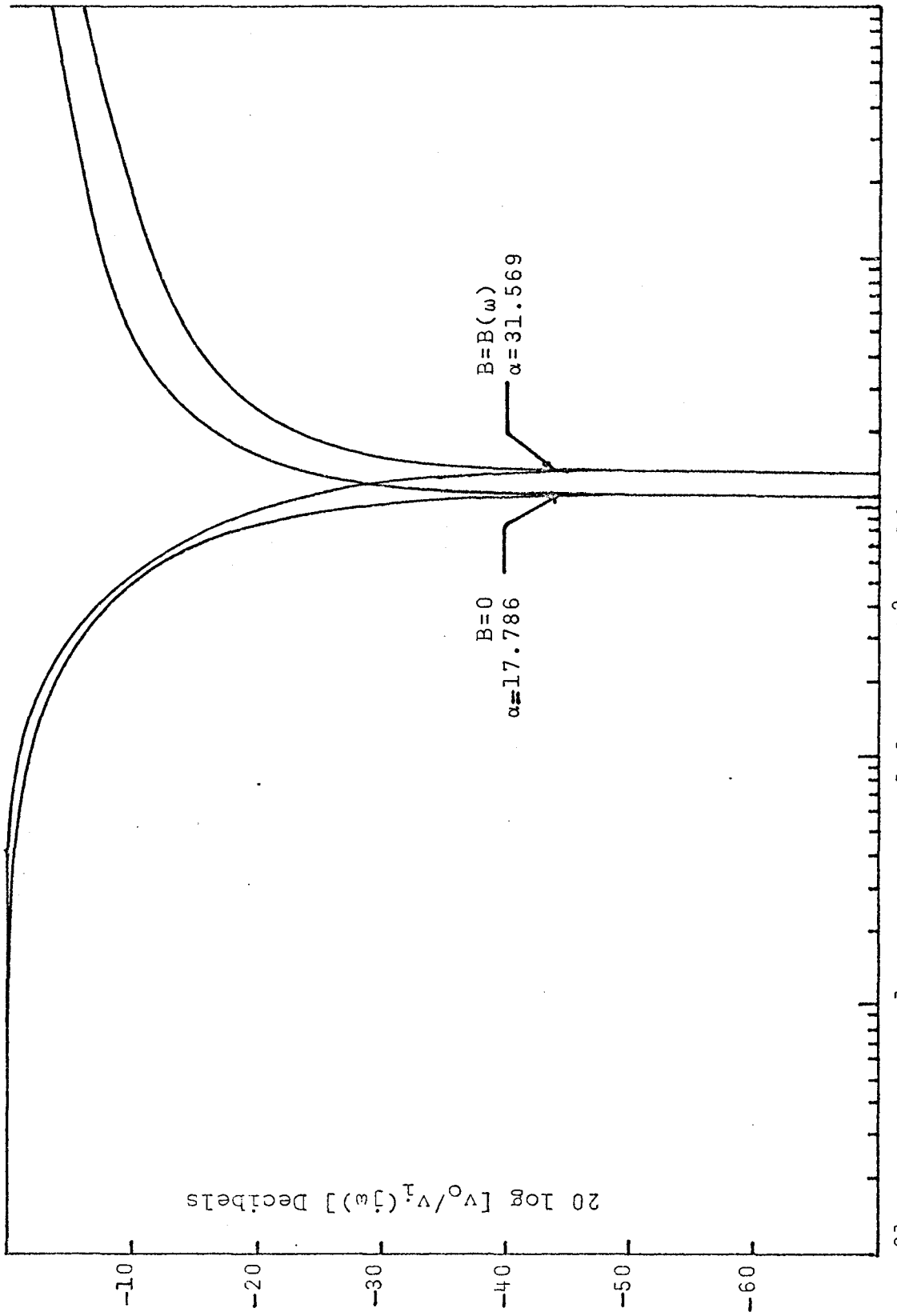
B=B(ω)
α=31.569
B=0
α=17.786
20 log [v_o/v_i(jω)] Decibels
-10
-20
-30
-40
-50
-60
.01
.1
1.0
10
100
1000
ωr_o c_o λ^2

FIGURE 5:12

Phase of the voltage transfer function of a $\overline{URC}$ notch filter taking dielectric loss into consideration.

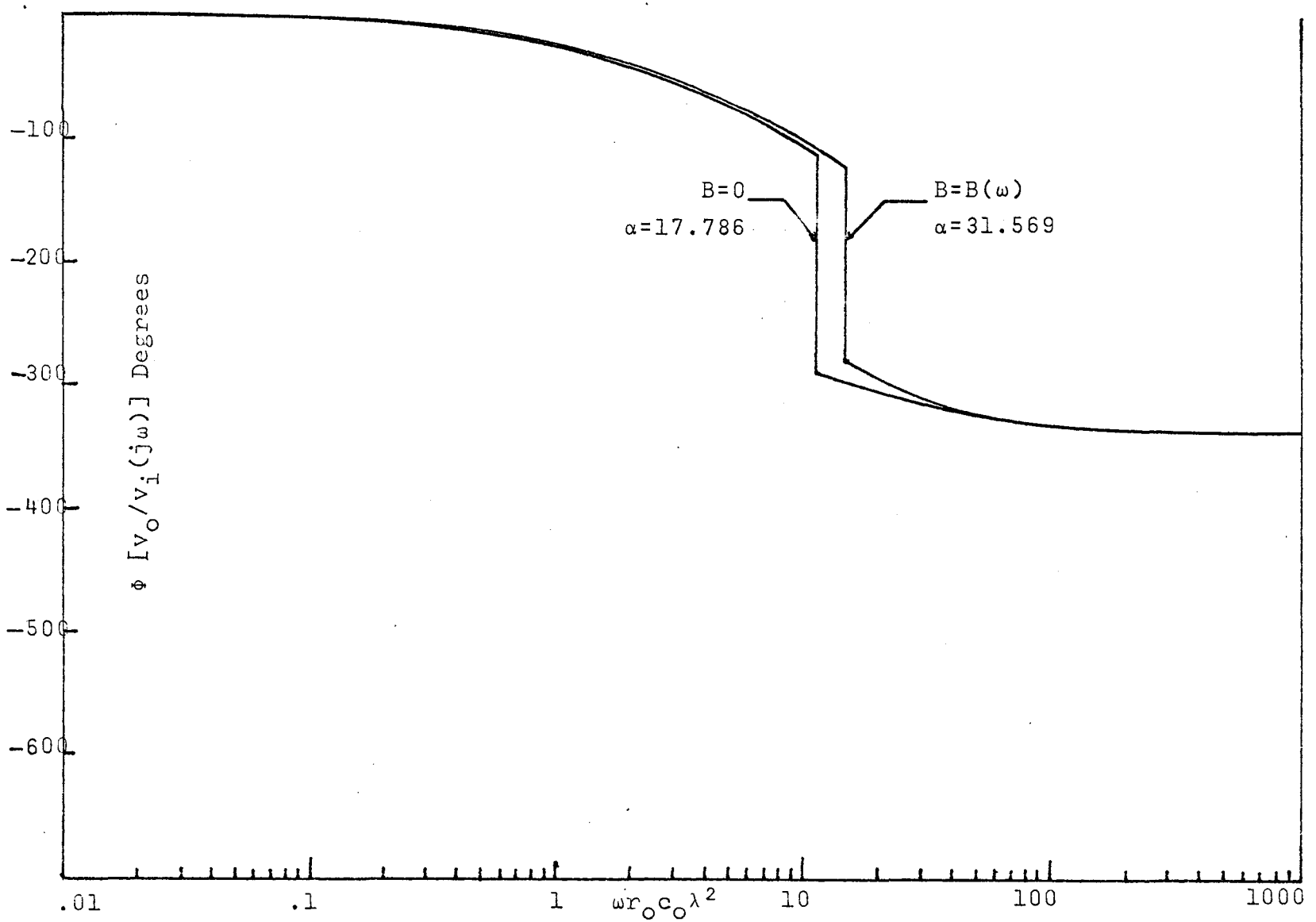
-100
-200
-300
-400
-500
-600
Φ [V_o/V_i(jω)] Degrees
B=0
α=17.786
B=B(ω)
α=31.569
.01
.1
1
ωr_o c_o λ^2
10
100
1000

5.3 Measured Effect of Dielectric Loss on a $\overline{URC}$ Notch Filter

The voltage transfer function for the $\overline{URC}$ notch filter was determined in Section 3.3 where the dielectric loss was taken into consideration. Knowing the measured value of R (17.6KΩ), B(ω) could be determined from Figure 5:2. The measured value of R_N required for an optimum notch was 556.6 ohms. By taking the contact resistance into consideration we get a value for R_N of 557.48 ohms. The resultant value of α will then be 31.569. The ideal (B=0, α=17.786) and non-ideal (B-B(ω), α=31.569) curves are as shown in Figures 5:11 and 5:12. By observing Figure 5:11, one can see that the dielectric loss causes an expansion of the rejection band width of the notch filter and increases the position of optimum notch from a normalized frequency of 11.19 to 14.08.

5.4 Measured Effect of Dielectric Loss on an $\overline{ERC}$ Network.

The voltage transfer function for the $\overline{ERC}$ low pass filter was derived in Chapter III where the dielectric loss was taken into consideration. The network tested had a taper of D equal to one so this respective response will be the only one considered. The values for $R_S(\omega)$ as shown in Figure 5:2 were also used for the $\overline{ERC}$ network. The thickness of the dielectric layer for the $\overline{ERC}$ network is the same as it was for the $\overline{URC}$ network, however, the surface

FIGURE 5:13

Magnitude of the voltage transfer function of an $\overline{ERC}$ low pass filter taking dielectric loss into consideration.

-10
-20
-30
-40
-50
-60
20 log[V2/V1(jω)] Decibels
0.1
.1
1
10
100
ωr0c0λ2
B=B(ω)
B=0

FIGURE 5:14

Phase of the voltage transfer function of an $\overline{\text{ERC}}$ low pass filter taking dielectric loss into consideration.

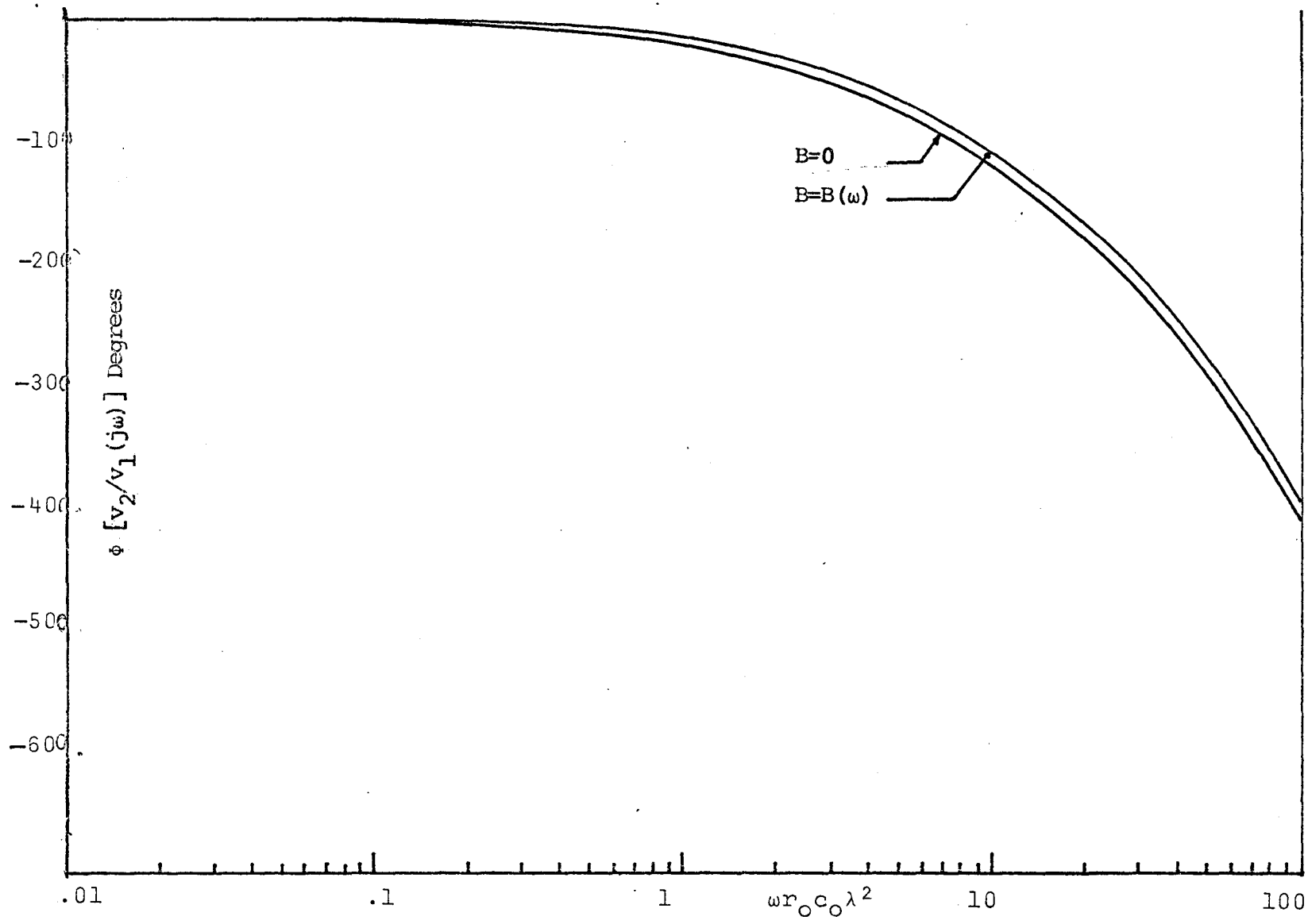
B=0
B=B(ω)
-100
-200
-300
-400
-500
-600
φ [v2/v1(jω)] Degrees
.01
.1
1
10
100
ωr0c0λ2

area is slightly smaller. This may make a small difference in the values of $R_S(\omega)$ as shown in Figure 5:2 but they should be accurate enough to give a satisfactory indication of the effect of dielectric loss on the $\overline{ERC}$ network. Knowing the measured value of R (113KΩ measured on the Type 1608A Impedance Bridge), $B(\omega)$ could now be determined and hence the voltage transfer function for the $\overline{ERC}$ low pass filter and $\overline{ERC}$ notch filter could be determined when dielectric dissipation is taken into consideration.

The ideal (B=0) and non-ideal ($B=B(\omega)$) magnitude and phase for the voltage transfer function of the $\overline{ERC}$ low pass filter are shown in Figures 5:13 and 5:14. It can be seen that the effect of dielectric loss on the $\overline{ERC}$ network is similar to the effect on the $\overline{URC}$ network. There was no notch effect noticed in the voltage transfer function of the $\overline{ERC}$ low pass filter. This is probably due to the fact that the $\overline{ERC}$ network was not tested at as high a frequency as was the $\overline{URC}$ network.

The voltage transfer function for the $\overline{ERC}$ notch filter was derived in Section 3:4 where dielectric loss was taken into consideration. Knowing the measured value of R(113KΩ), $B(\omega)$ could be determined from Figure 5:2. The measured value of R_N required for an optimum notch was 4.216 KΩ which gives a value for α of 26.8 where $\alpha=R/R_N$. The ideal (B=0, α=25.129) and non-ideal ($B=B(\omega)$, α=26.8)

FIGURE 5:15

Magnitude of the voltage transfer function of an $\overline{\text{ERC}}$ notch filter taking dielectric loss into consideration

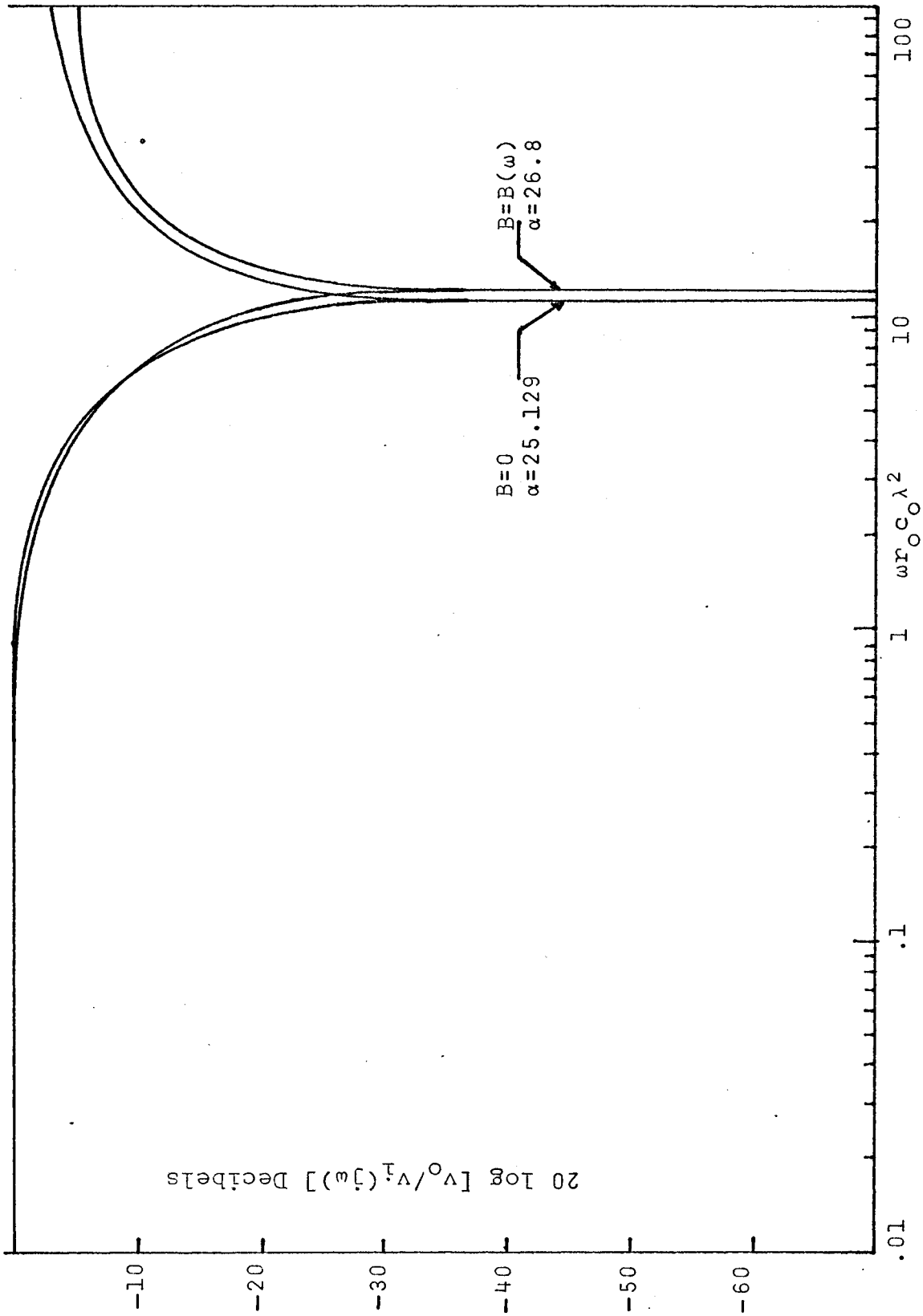
-10
-20
-30
-40
-50
-60
20 log [$v_o/v_i(j\omega)$] Decibels
.01
.1
1
10
100
$\omega r_o c_o \lambda^2$
B=0
α=25.129
B=B(ω)
α=26.8

FIGURE 5:16

Phase of the voltage transfer function of an $\overline{ERC}$ notch filter taking dielectric loss into consideration

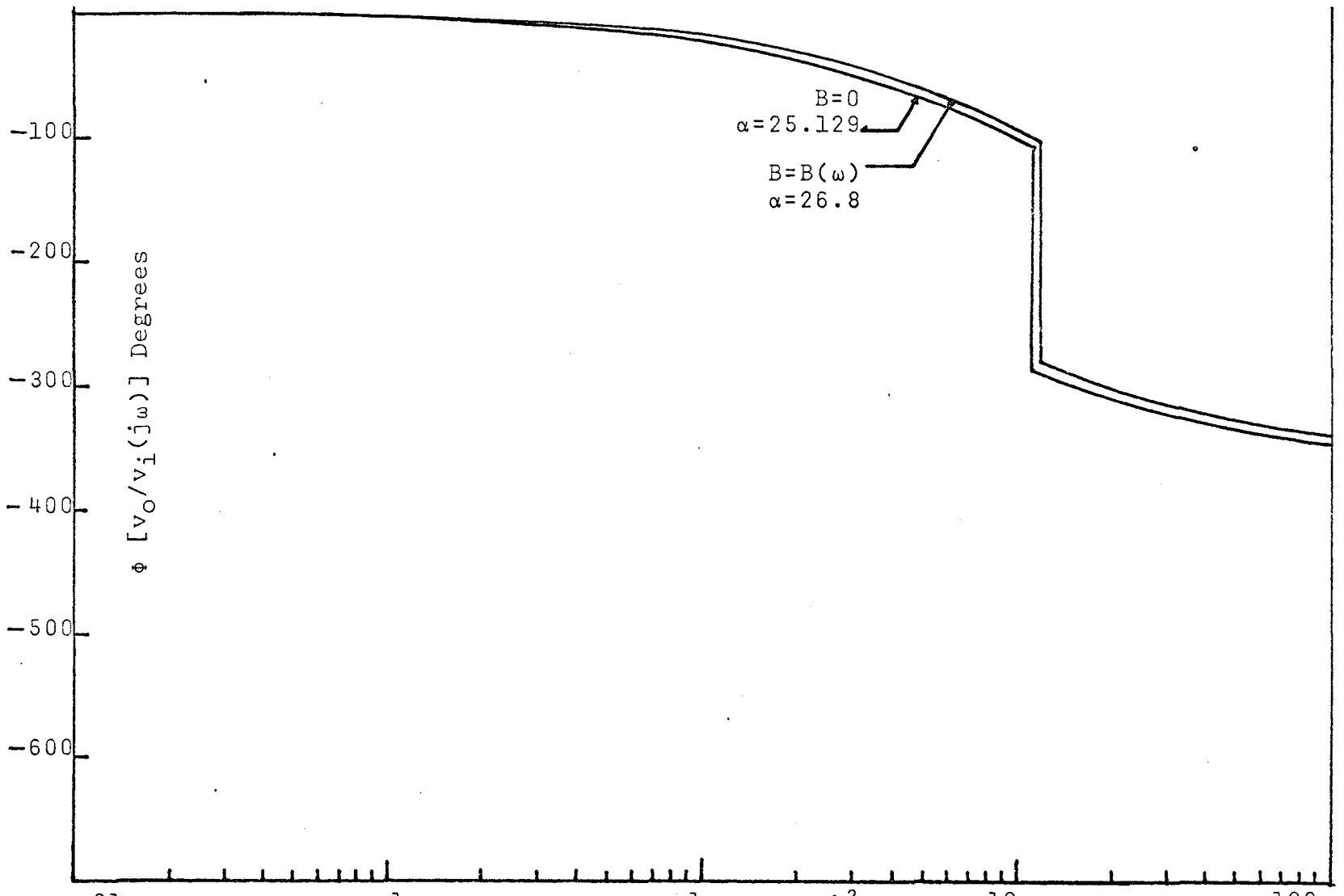
B=0
α=25.129
B=B(ω)
α=26.8
-100
-200
-300
-400
-500
-600
Φ [$v_o/v_i(j\omega)$] Degrees
.01
.1
1
$\omega r_o c_o \lambda^2$
10
100

curves are as shown in Figures 5:15 and 5:16. Once again, it can be seen that the dielectric loss causes an expansion of the rejection bandwidth of the notch filter and causes the position of optimum notch to shift from a normalized frequency of 11.72 to 12.0.

5.5 Experimental Results for the $\overline{URC}$ Network

The experimental results for the $\overline{URC}$ network consist of the driving point admittance (short circuit output) and the voltage transfer function (open circuit output) for the low pass filter and the voltage transfer function (open circuit output) for the notch filter.

The driving point admittance was measured on a General Radio Z-Y Bridge Model No.1608A for frequencies from $4H_z$ to $20KH_z$. For frequencies greater than $20KH_z$, the driving point admittance was measured on a Wayne Kerr Frequency Bridge Model No.B601. The Wayne Kerr Bridge had a frequency range of $15KH_z$ to $5MH_z$. The accuracy of the two bridges was checked by testing a lumped element RC filter composed of precision components. The bridges were found to be accurate to within 2%. The capacitance of the $\overline{URC}$ network was measured on the same bridge as the resistance and these two values were found to be 22.4nf and 17.6KΩ respectively.

The experimental results were fitted to the theoretical curves by setting the normalized frequency equal to one and

FIGURE 5:17

Theoretical and experimental results for the magnitude of the driving point admittance of a $\overline{\text{URC}}$ low pass filter

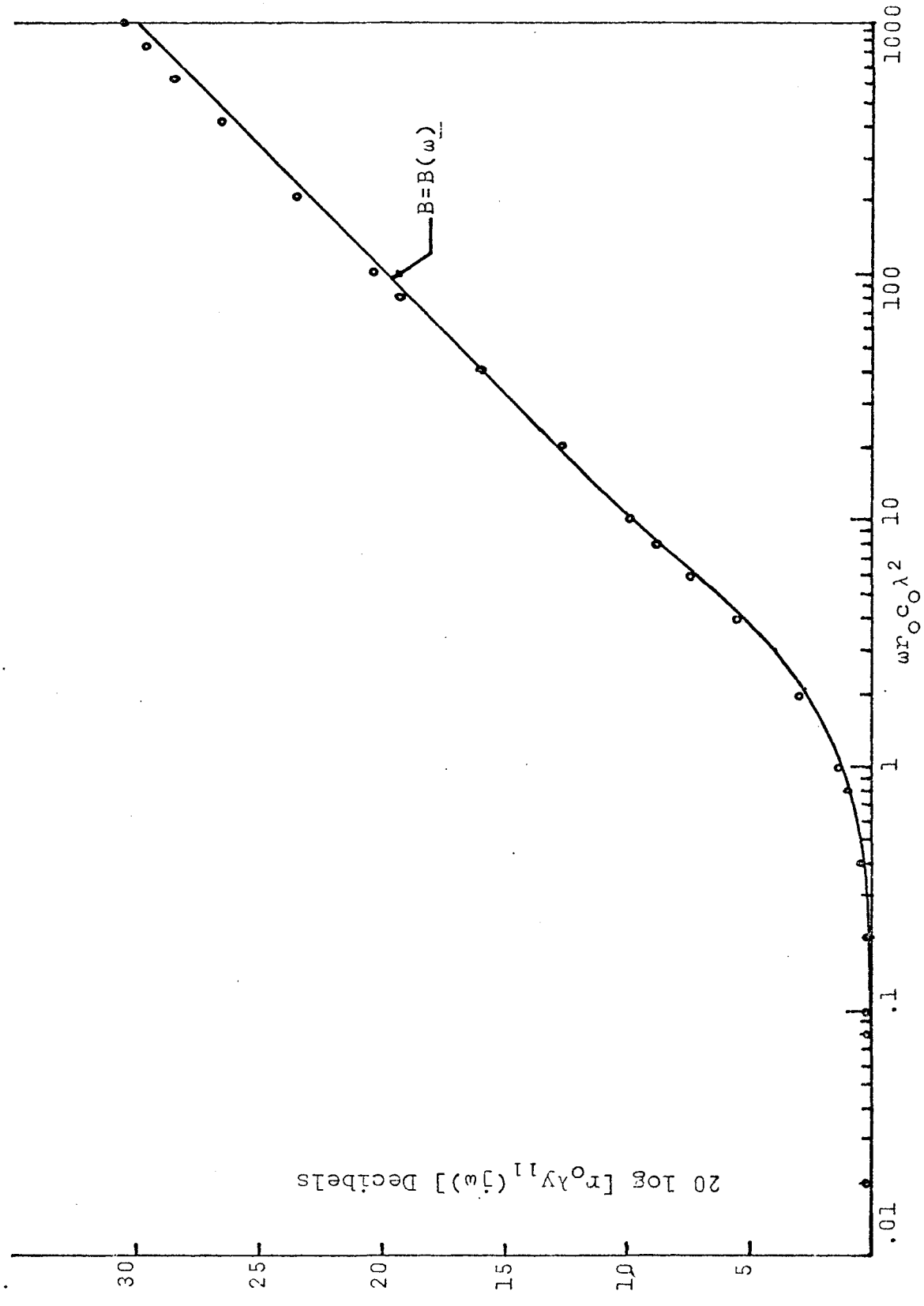
20 log [r$_o\lambda y_{11}(j\omega)$] Decibels
30
25
20
15
10
5
.01
.1
1
10
100
1000
$\omega r_o c_o \lambda^2$
B=B(ω)

FIGURE 5:18

Theoretical and experimental results for the phase of the driving point admittance of a $\overline{URC}$ low pass filter

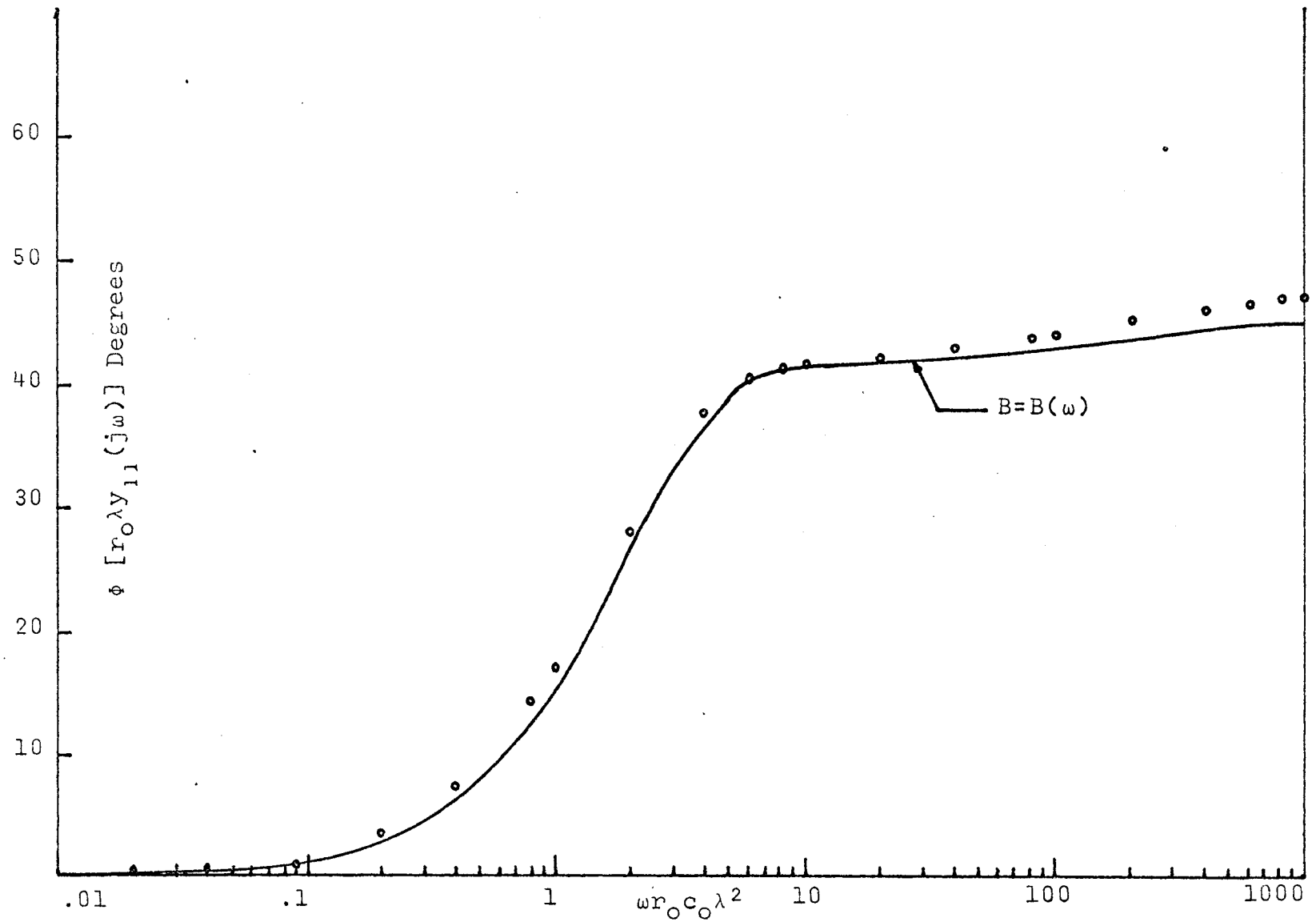
60
50
40
30
20
10
$\phi\ [r_o\lambda y_{11}(j\omega)]$ Degrees
.01
.1
1
10
100
1000
$\omega r_o c_o \lambda^2$
B=B(ω)

determining the value of real frequency at this point. The corresponding real frequency was found to be 403.7 H_z. A normalized frequency range of 0.01 to 1000 was used and the corresponding real frequency range was $4H_z$ to $400KH_z$.

The results for the driving point admittance are shown in Figures 5:17 and 5:18 where the solid line is the non-ideal theoretical curve and the circles are the experimental results. It can be seen that the experimental results are in close agreement with the theoretical results when dielectric loss is taken into consideration.

A block diagram of the equipment used to measure the voltage transfer function of the $\overline{URC}$ low pass filter and $\overline{URC}$ notch filter is shown in Figure 5:7. The input signal was supplied by a General Radio Oscillator Model No. 1310A with a frequency range of $2H_z$ to $2MH_z$. The network response was measured on a Rohde and Schwarz Type UDF twin voltmeter and type PZN phasemeter. The twin voltmeter and phasemeter had a frequency range of $10H_z$ to $100KH_z$ but this frequency range could be extended to $50MH_z$ by using a Type UFF Frequency Converter. The input impedance of the Rohde and Schwarz equipment was 1MΩ shunted by 28pf which substantiated the assumption of I_2 equal to zero in the derivation of the voltage transfer function. The accuracy of the measuring equipment was checked using a precision component lumped element RC low pass filter. The equipment was found to be

FIGURE 5:19

Theoretical and experimental results for the magnitude of the voltage transfer function of a $\overline{URC}$ low pass filter

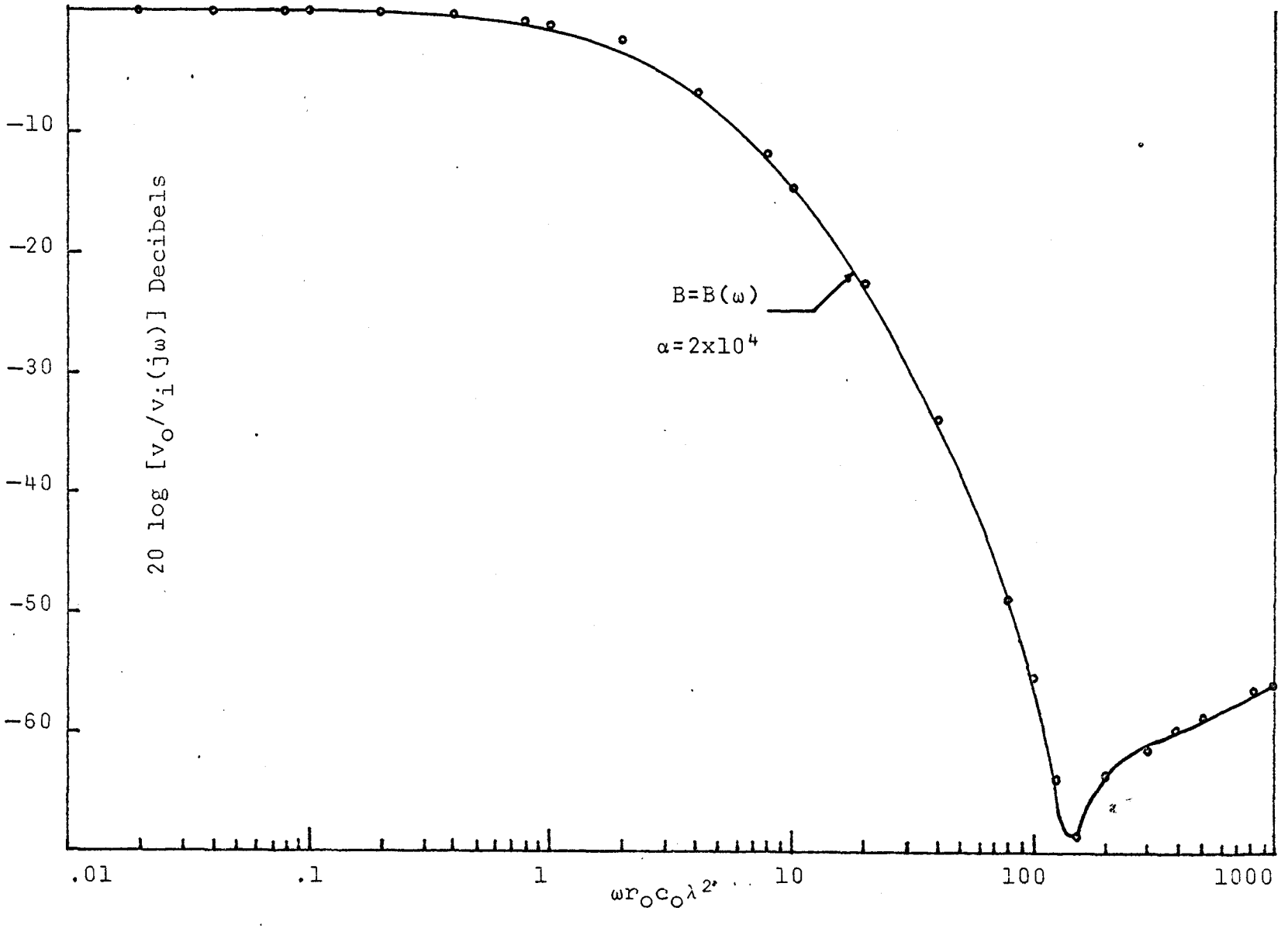
-10
-20
-30
-40
-50
-60
20 log [$v_o/v_i(j\omega)$] Decibels
B=B(ω)
α=2x10⁴
.01
.1
1
10
100
1000
$\omega r_o c_o \lambda^{2\pi}$

FIGURE 5:20

Theoretical and experimental results for the phase of the voltage transfer function of a $\overline{URC}$ low pass filter

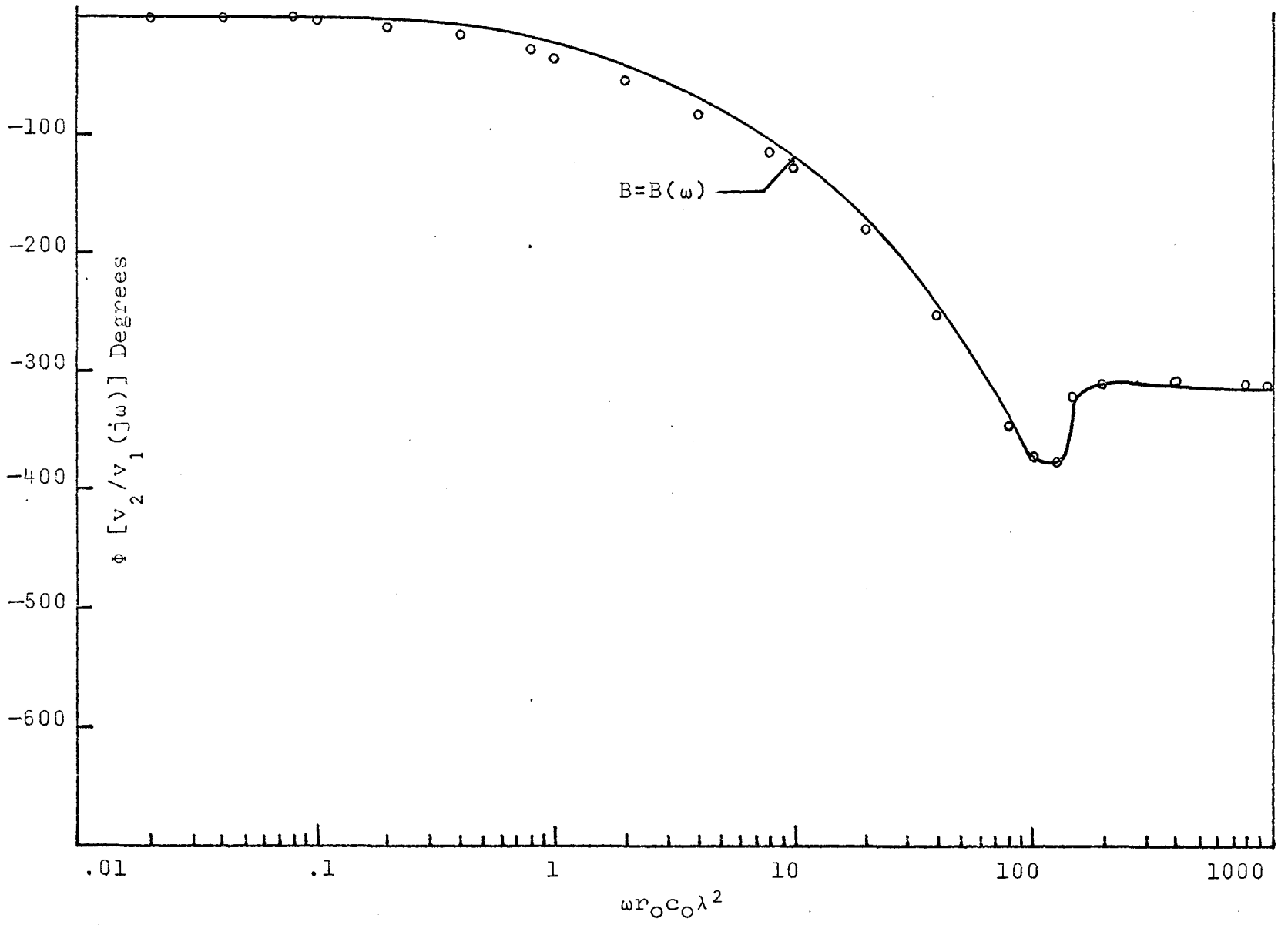
-100
-200
-300
-400
-500
-600
$\phi [v_2/v_1(j\omega)]$ Degrees
B=B(ω)
.01
.1
1
10
100
1000
$\omega r_o c_o \lambda^2$

FIGURE 5:21

Theoretical and experimental results for the magnitude of the voltage transfer function of a $\overline{\text{URC}}$ notch filter

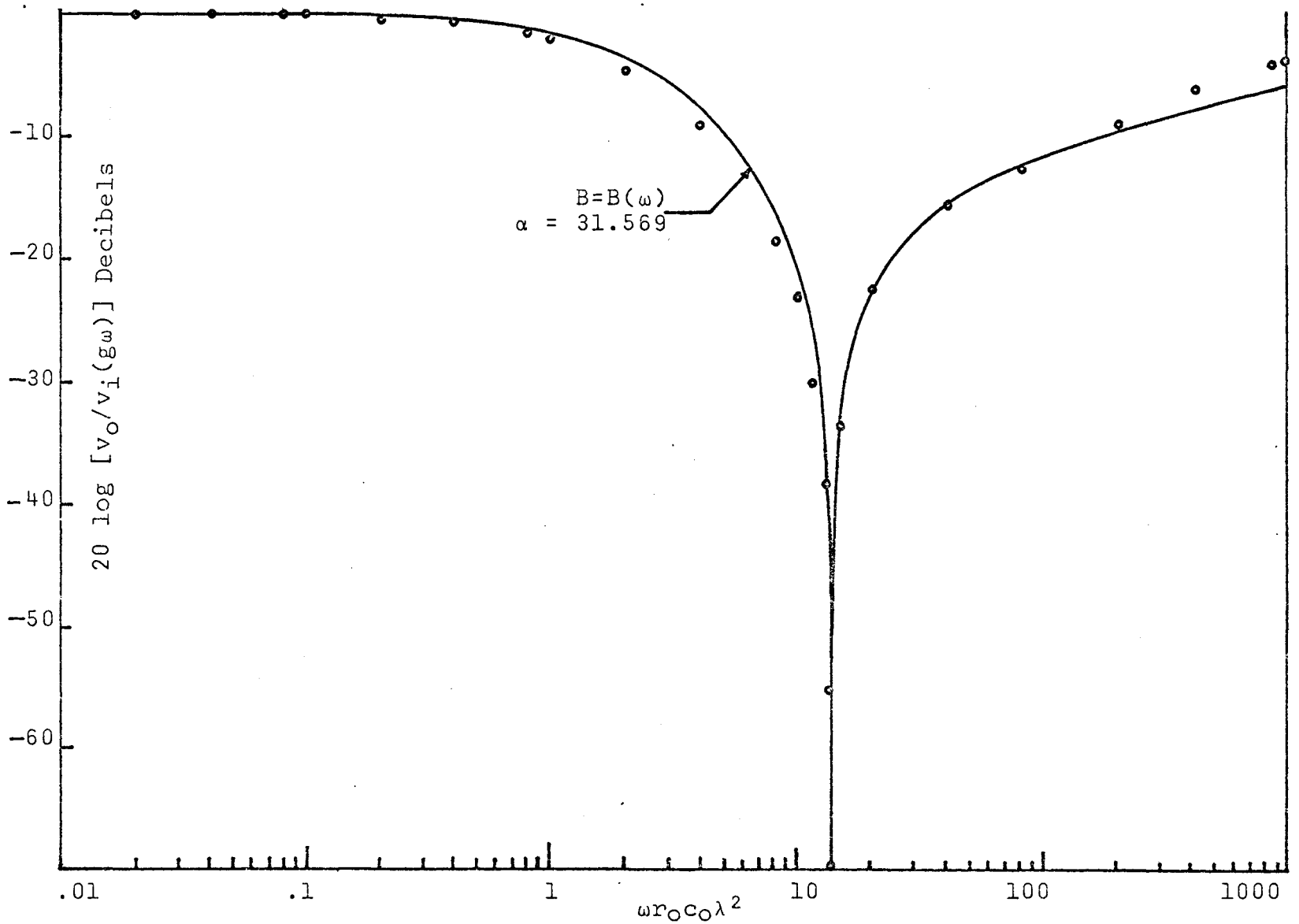
-10
-20
-30
-40
-50
-60
20 log [$v_o/v_i(g\omega)$] Decibels
B=B(ω)
α = 31.569
.01
.1
1
10
100
1000
$\omega r_o c_o \lambda^2$

FIGURE 5:22

Theoretical and experimental results for the phase of the voltage transfer function of a $\overline{URC}$ notch filter

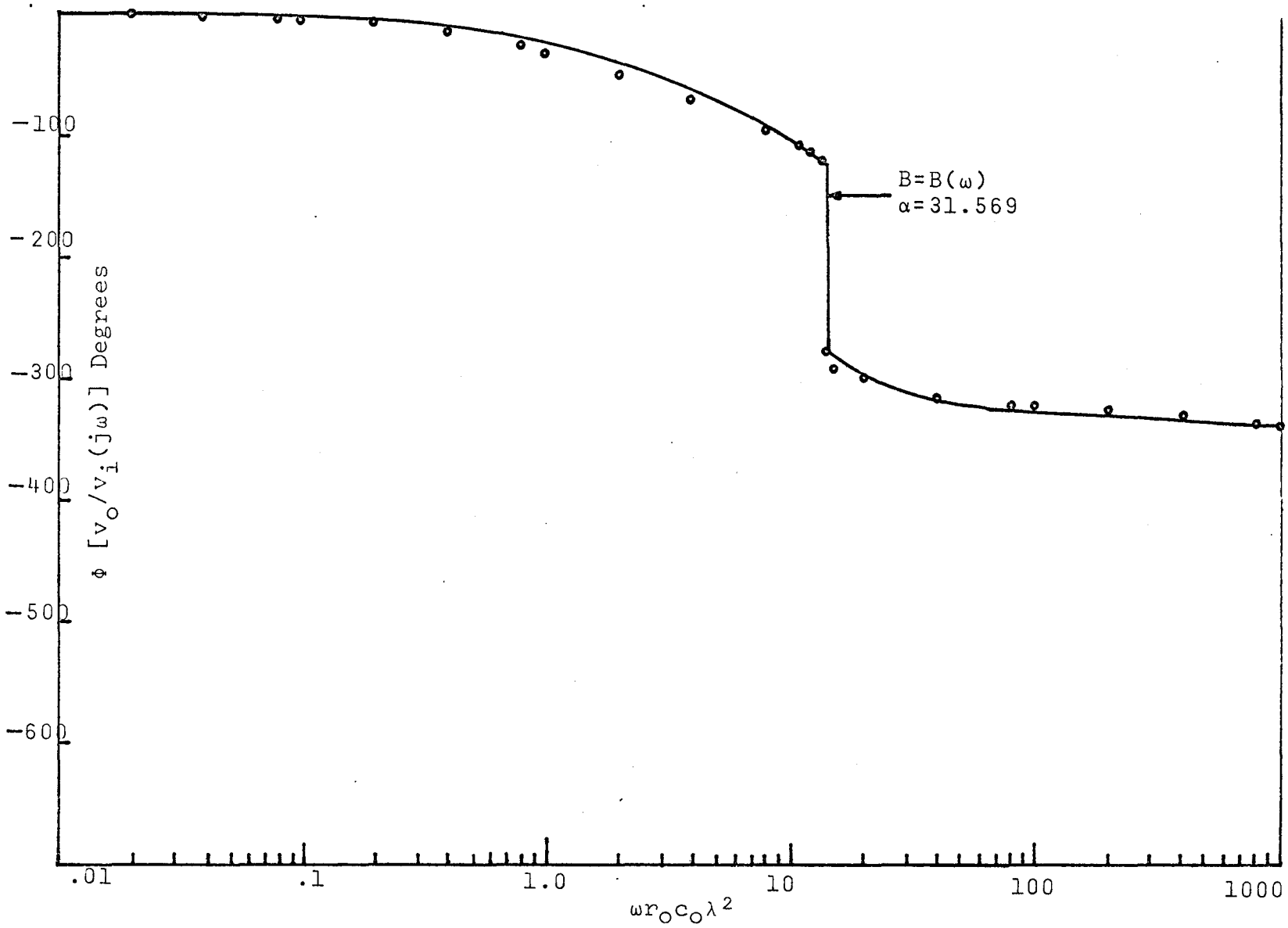
-100
-200
-300
-400
-500
-600
$\phi\ [v_o/v_i(j\omega)]$ Degrees
B=B(ω)
α=31.569
.01
.1
1.0
10
100
1000
$\omega r_o c_o \lambda^2$

very accurate with no noticeable difference between the experimental and theoretical responses of the filter.

The experimental and non-ideal theoretical results of the voltage transfer function for the $\overline{URC}$ low pass filter and $\overline{URC}$ notch filter are shown in Figures 5:19 to 5:22. By observing Figures 5:19 and 5:20, one can see that the experimental results, which are the circles, and the theoretical results, which take dielectric loss and notch effect into consideration, agree quite closely. It should be pointed out that the notch effect occurs at a normalized frequency greater than 100 which is relatively unimportant when a low pass filter is being considered.

The experimental results, and theoretical results taking dielectric loss into consideration, for the voltage transfer function of the $\overline{URC}$ notch filter are shown in Figures 5:21 and 5:22. Once again, there is a close agreement between the two curves. The experimental results show an optimum notch of 70db and a large rejection bandwidth in comparison to some lumped element notch filters. However, this undesirable feature is compensated for by using an $\overline{ERC}$ notch filter.

5.6 Experimental Results for the $\overline{ERC}$ Network

The experimental results for the $\overline{ERC}$ network consist of the voltage transfer function (open circuit output) for the low pass filter and notch filter.

FIGURE 5:23

Theoretical and experimental results for the magnitude of the voltage transfer function of an $\overline{\text{ERC}}$ low pass filter

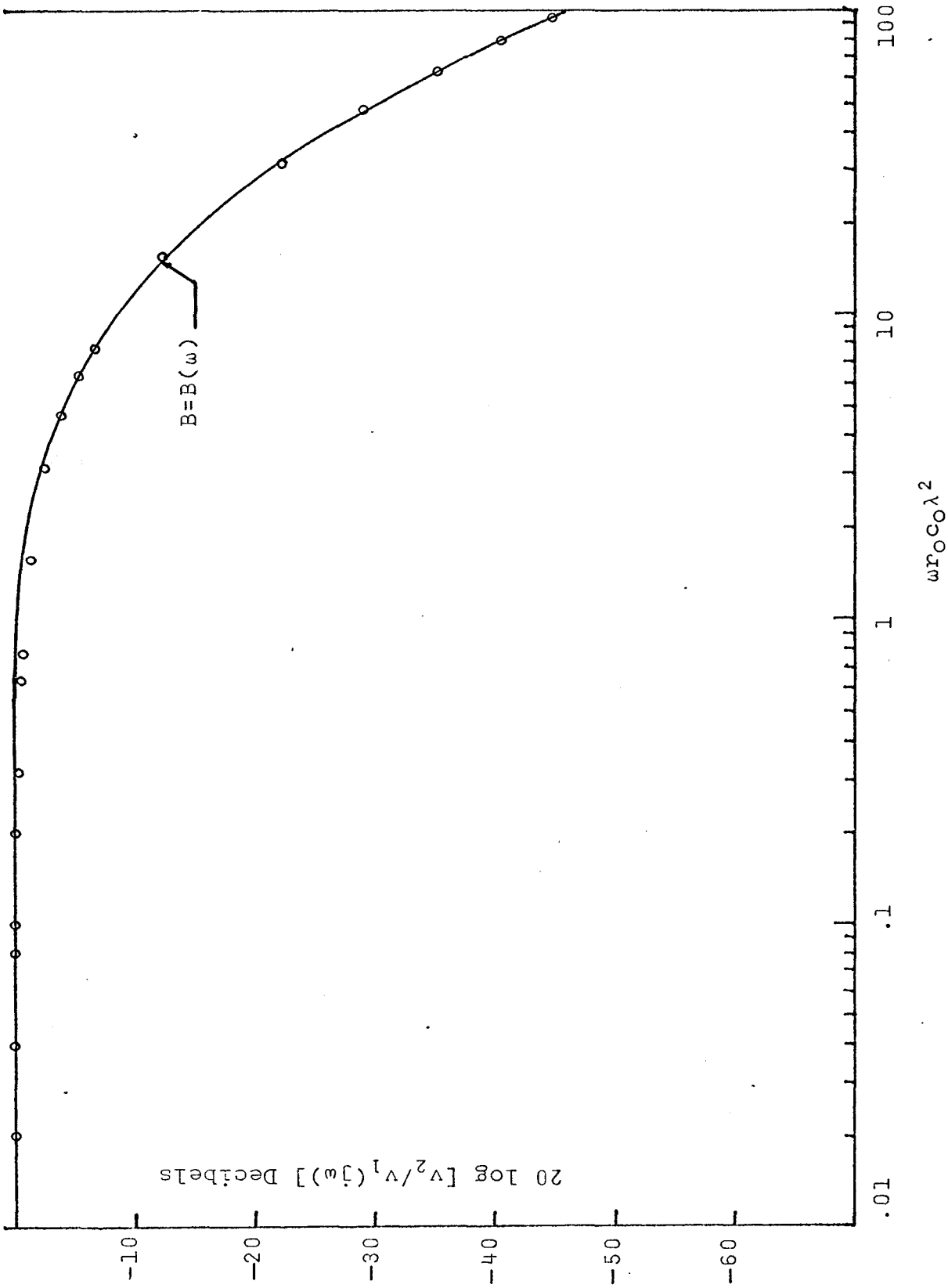
B=B(ω)
20 log [V2/V1(jω)] Decibels
-10
-20
-30
-40
-50
-60
.01
.1
1
10
100
ωr0c0λ2

FIGURE 5:24

Theoretical and experimental results for the phase of the voltage transfer function of an $\overline{\text{ERC}}$ low pass filter

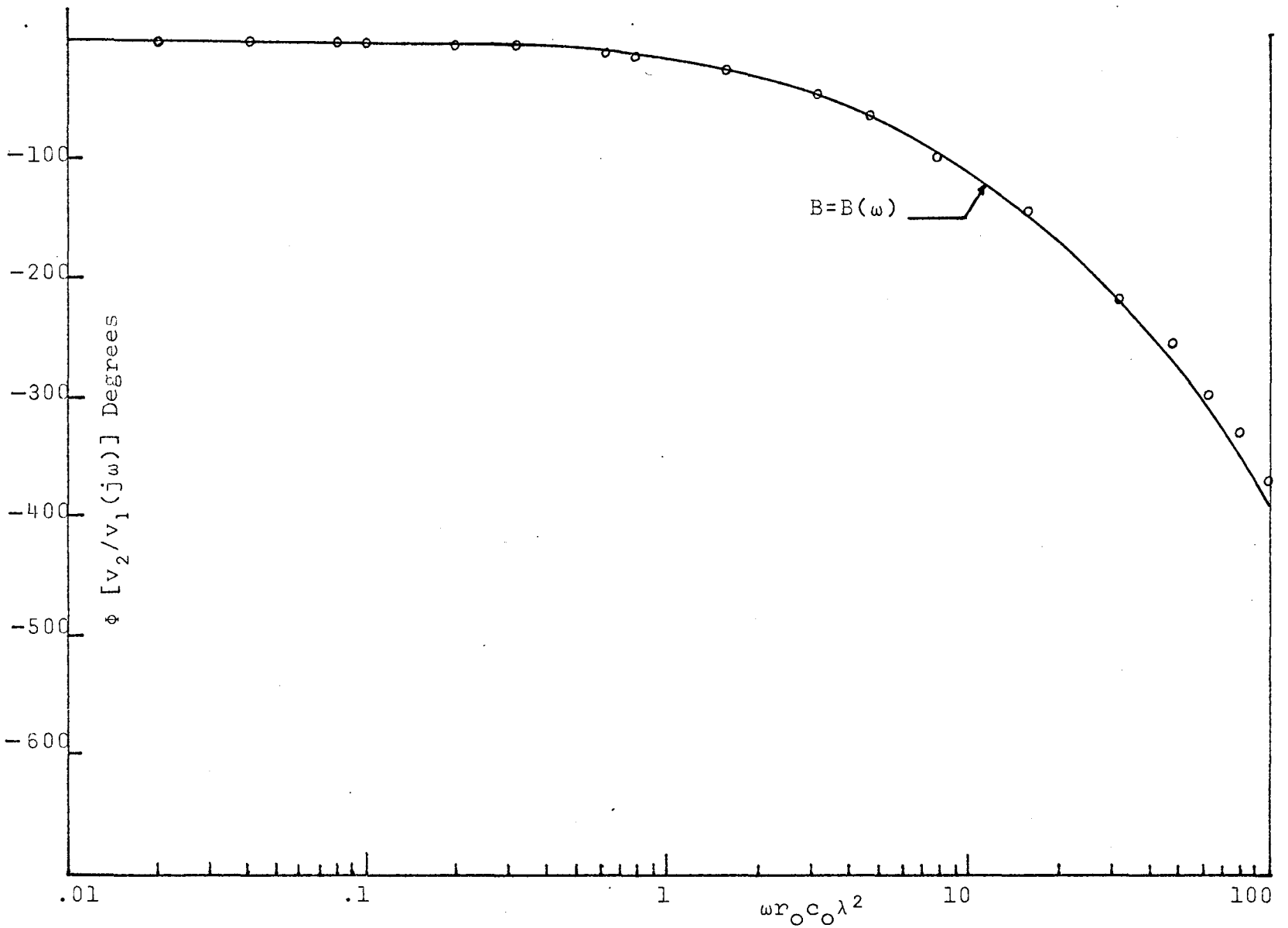
-100
-200
-300
-400
-500
-600
Φ [v2/v1(jω)] Degrees
B=B(ω)
.01
.1
1
10
100
ωr0c0λ2

FIGURE 5:25

Theoretical and experimental results for the magnitude of the voltage transfer function of an $\overline{\text{ERC}}$ notch filter

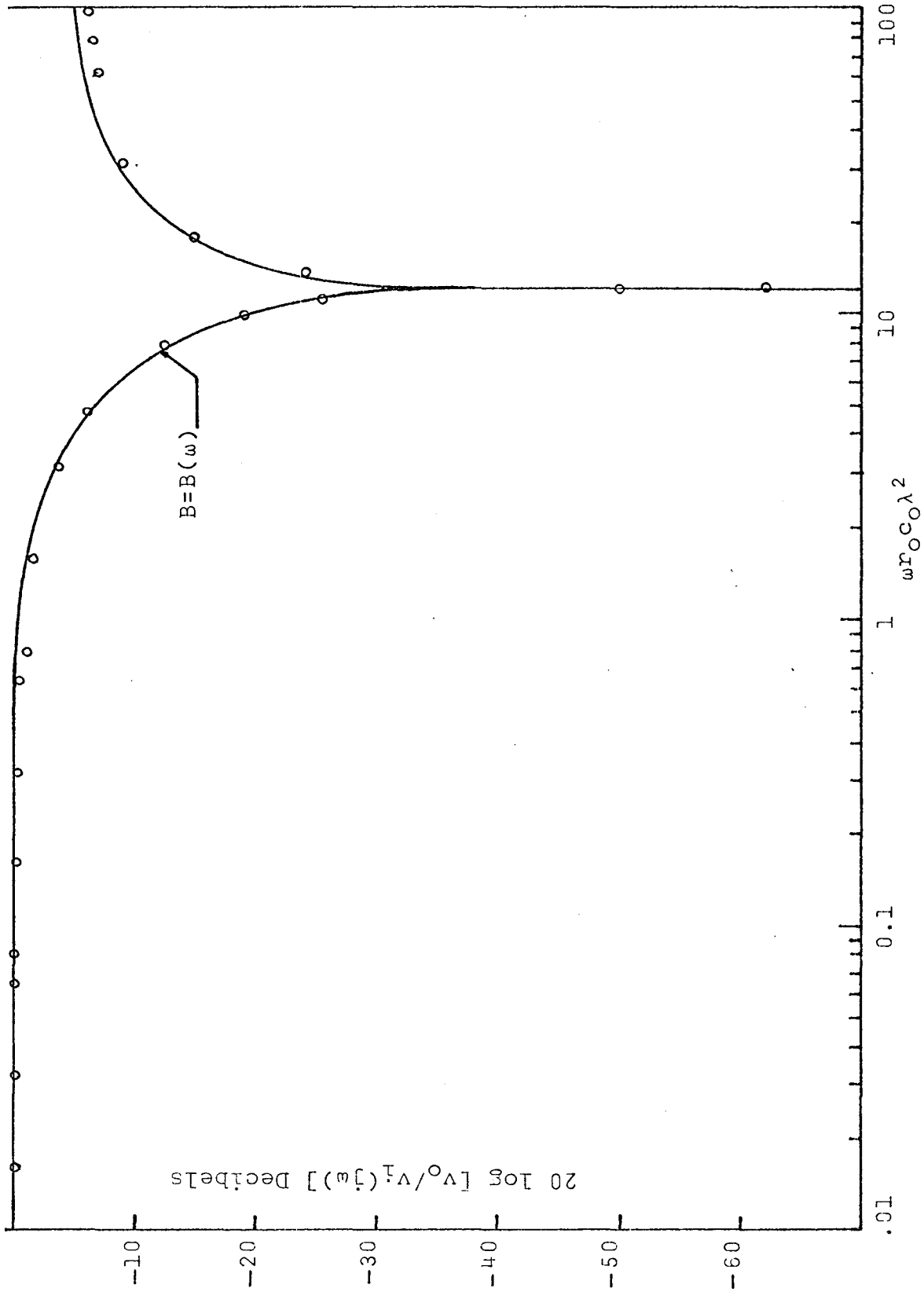
B=B(ω)
20 log [v_o/v_i(jω)] Decibels
-10
-20
-30
-40
-50
-60
.01
0.1
1
10
100
ωr_o c_o λ²

FIGURE 5:26

Theoretical and experimental results for the phase of the voltage transfer function of an $\overline{\text{ERC}}$ notch filter

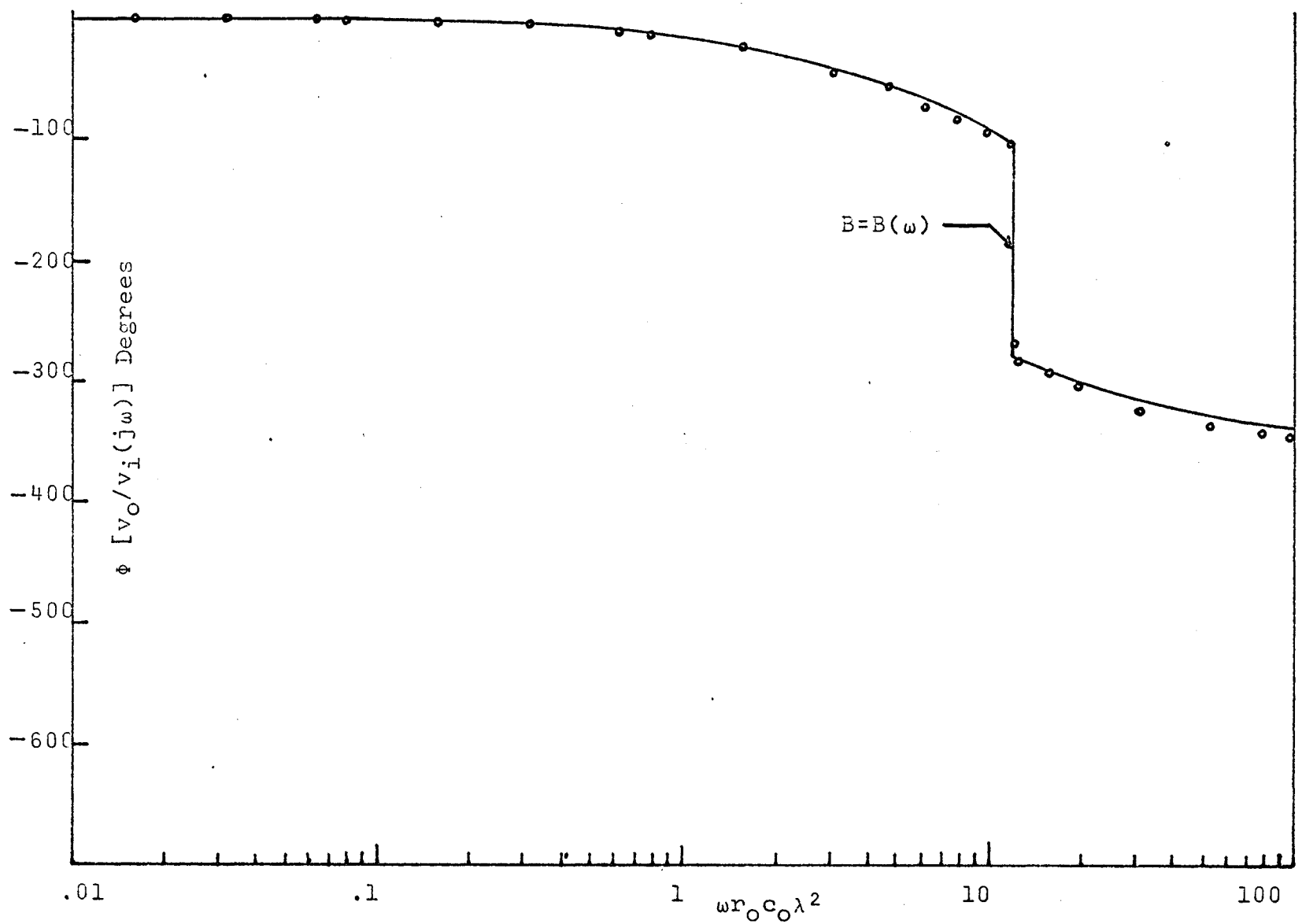
-100
-200
-300
-400
-500
-600
Φ [$v_o/v_i(j\omega)$] Degrees
B=B(ω)
.01
.1
1
10
100
$\omega r_o c_o \lambda^2$

The equipment used and the measuring techniques were identical to those used for the $\overline{URC}$ network. The measured value of R and C was 113KΩ and 9.7nf respectively. The experimental results were fitted to the theoretical curves by setting the normalized frequency equal to one and determining the value of real frequency at this point. The corresponding real frequency was found to be $199.96H_z$. A normalized frequency range of 0.01 to 100 was used and the corresponding real frequency range was $2H_z$ to $20KH_z$.

The experimental and non-ideal voltage transfer function for the $\overline{ERC}$ low pass filter and $\overline{ERC}$ notch filter are shown in Figures 5:23 to 5:26. From Figures 5:23 and 5:24, it can be seen that the experimental results and the theoretical results, which take dielectric loss into consideration are in close agreement. By comparing the response of the $\overline{ERC}$ low pass filter with that of the $\overline{URC}$ low pass filter, one can see that the $\overline{ERC}$ filter has a sharper cut-off and a greater phase shift for a given attenuation.

The experimental results, and theoretical results taking dielectric loss into consideration, for the voltage transfer function of the $\overline{ERC}$ notch filter are shown in Figures 5:25 and 5:26. Once again, there is a close agreement between the theoretical and experimental curves. The experimental results shown an optimum notch of 62db. However, there is a large improvement in the rejection bandwidth over that of the $\overline{URC}$ notch filter.

CHAPTER VI

Conclusions and Recommendations

CHAPTER VI

CONCLUSIONS AND RECOMMENDATIONS

Thin film distributed parameter RC networks were fabricated and a reasonable agreement was found between the experimental and theoretical network responses. However, it was necessary to take the dielectric loss into consideration before this agreement was obtained.

The problems with the dielectric loss would indicate the need for a thorough study of all the factors that influence the evaporation of Silicon Monoxide. It should however, be pointed out that the necessity to break vacuum after each evaporation was an influencing factor on the dielectric loss as determined in this thesis. However, it would no doubt be profitable to study other dielectrics with the possibility in mind of decreasing dielectric loss. Oxides of certain of the rare earth elements are examples of other dielectrics which could be investigated.

The exponentially tapered RC network also requires a more thorough investigation. It was shown by Oehler[6] that a "notch" produced by an exponentially tapered RC network showed discrepancies of over ten percent between the experimentally observed results and the theoretical results predicted by a one-dimensional model for the distributed network. This

would appear to be consistent with the results as obtained in this thesis which would suggest that a two-dimensional model for the distributed network be considered. A desirable feature of the $\overline{ERC}$ network is the control of the input and output impedance levels which can be used for impedance matching. This facet of the $\overline{ERC}$ network should also be investigated. It would also be advantageous to investigate the effect various amounts of taper would have on the experimental results.

Another important field of investigation is the possibility of converting the notch filter to a "tunable" notch filter. This could possibly be done by evaporating a layer of semiconductor after the dielectric layer and depositing a thin film F.E.T. in place of the notch resistance. By applying an external d.c. voltage between the upper and lower conductors, the surface capacitance of the semiconductor could be varied which should in turn vary the capacitance of the network. The value of notch resistance would be determined by the point of operation on the F.E.T. current-voltage characteristic. If this were possible, it would then be advantageous to consider minaturization of the device for encapsulation in a "TO-8 Header" or"Flat Pack".

APPENDIX A

Program for Hewlett-Packard Calculator Model 9100A to determine the effect of dielectric loss on the $\overline{\text{URC}}$ Notch Filter.

OPERATION OF PROGRAM

1. Press END
2. Press CONTINUE
3. Enter $B(\omega)$ in x
4. $x \rightarrow b$
5. Enter ε in x
6. $x \rightarrow e$

We next enter the amount by which we wish to increase X_N. To begin with, one would increase X_N by 0.001. As the imaginary part of the numerator approaches ε, X_N may be increasing by too large an amount and we may go through the minimum (i.e. pass the point where the imaginary part of the numerator is $\leq \varepsilon$). Therefore, as the imaginary part of the numerator approaches ε we stop the program and change it so X_N increases in steps of 10^{-6}.

The amount by which X_N is increased (i.e. 10^{-3}) is entered as follows:

1. GO TO 4(a)
2. SWITCH TO "PROGRAM" position.
3. ENTER 3 in x register to increase X_N by 10^{-3}.
4. SWITCH TO "RUN" position
5. PRESS END

6. PRESS CONTINUE

7. ENTER ε in x register

8. $x \rightarrow e$

9. ENTER initial value for X_N. This value must be $\leq$ the value of X_N required to make the imaginary part of the numerator $\leq \varepsilon$.

10. PRESS CONTINUE

11. WAIT FOR CONVERGENCE.

12. X_N is displayed in x register.

Once the value of X_N is determined, we can then solve for α. Alpha is solved for as follows.

1. GO TO 60

2. Press CONTINUE

3. X_N is displayed in x register
   α is displayed in y register.

Title Notch Filter with Dielectric Loss taken into Account. Calculations of Zeros (Positions of Optimum Notch) and the corresponding values of α.

Date 1 Sept. '69 Page 1

Name

$\alpha = R/R_N$

$X_N = \omega_{o,n}/\omega_o$

$B(\omega) = R_S/R = b$

Step		Key	Code	Display x	Display y	Display z	Storage f	Storage e	Storage d	Storage c	Storage b	Storage a
0	0	Clear	20									
	1	STOP	41	X_N	0	0		ϵ			b	
	2	$x\rightarrow$	23	X_N	0	0		ϵ			b	
	3	f	15	X_N	0	0	X_N	ϵ			b	
	4	↑	27	X_N	X_N	0	X_N	ϵ			b	
	5	↑	27	X_N	X_N	X_N	X_N	ϵ			b	
	6	b	14	b	X_N	X_N	X_N	ϵ			b	
	7	x	36	b	bX_N	X_N	X_N	ϵ			b	
	8	↓	25	bX_N	X_N	X_N	X_N	ϵ			b	
	9	↑	27	bX_N	bX_N	X_N	X_N	ϵ			b	
	a	x	36	bX_N	$b^2X_N^2$	X_N	X_N	ϵ			b	
	b	$x\rightarrow$	23	bX_N	$b^2X_N^2$	X_N	X_N	ϵ			b	
	c	d	17	bX_N	$b^2X_N^2$	X_N	X_N	ϵ	bX_N		b	
	d	1	01	1	$b^2X_N^2$	X_N	X_N	ϵ	bX_N		b	
1	0	+	33	1	$1+b^2X_N^2$	X_N	X_N	ϵ	bX_N		b	
	1	d	17	bX_N	$1+b^2X_N^2$	X_N	X_N	ϵ	bX_N		b	
	2	roll↑	22	X_N	bX_N	$1+b^2X_N^2$	X_N	ϵ	bX_N		b	
	3	x	36	X_N	bX_N^2	$1+b^2X_N^2$	X_N	ϵ	bX_N		b	
	4	roll↑	22	$1+b^2X_N^2$	X_N	bX_N^2	X_N	ϵ	bX_N		b	
	5	÷	35	$1+b^2X_N^2$	$\frac{X_N}{1+b^2X_N^2}$	bX_N^2	X_N	ϵ	bX_N		b	
	6	roll↑	22	bX_N^2	$1+b^2X_N^2$	$\frac{X_N}{1+b^2X_N^2}$	X_N	ϵ	bX_N		b	
	7	$x\rightleftarrows y$	30	$1+b^2X_N^2$	bX_N^2	$\frac{X_N}{1+b^2X_N^2}$	X_N	ϵ	bX_N		b	
	8	÷	35	$1+b^2X_N^2$	$\frac{bX_N^2}{1+b^2X_N^2}$	$\frac{X_N}{1+b^2X_N^2}$	X_N	ϵ	bX_N		b	
	9	↓	25	$\frac{bX_N^2}{1+b^2X_N^2}$	$\frac{X_N}{1+b^2X_N^2}$	$\frac{X_N}{1+b^2X_N^2}$	X_N	ϵ	bX_N		b	
	a	To Polar	62	A	$\angle\theta$ (rad)	$\frac{X_N}{1+b^2X_N^2}$	X_N	ϵ	bX_N		b	
	b	$\sqrt{x}$	76	$\sqrt{A}$	$\frac{\angle\theta}{X_N}$	$\frac{X_N}{1+b^2X_N^2}$	X_N	ϵ	bX_N		b	
	c	roll↓	31	$\frac{\angle\theta}{X_N}$	$\frac{X_N}{1+b^2X_N^2}$	$\sqrt{A}$	X_N	ϵ	bX_N		b	
	d	$x\rightleftarrows y$	30	$\frac{X_N}{1+b^2X_N^2}$	$\angle\theta$	$\sqrt{A}$	X_N	ϵ	bX_N		b	

Step		Key	Code	Display x	Display y	Display z	Storage f	Storage e	Storage d	Storage c	Storage b	Storage a
2	0	2	02	2	LΘ	$\sqrt{A}$	X_N	∈	b X_N		b	
	1	÷	35	2	Θ/2	$\sqrt{A}$	X_N	∈	b X_N		b	
	2	Roll↓	31	Θ/2	$\sqrt{A}$	2	X_N	∈	b X_N		b	
	3	X_R↔y TOV	30	$\sqrt{A}$	Θ/2	2	X_N	∈	b X_N		b	
	4	RECT	66	f(x)	g(x)	2	X_N	∈	b X_N		b	
	5	X→	23	f(x)	g(x)	2	X_N	∈	b X_N		b	
	6	d	17	f(x)	g(x)	2	X_N	∈	f(x)		b	
	7	y→	40	f(x)	g(x)	2	X_N	∈	f(x)	g(x)	b	
	8	C	16	f(x)	g(x)	2	X_N	∈	f(x)	g(x)	b	
	9	↑	27	f(x)	f(x)	g(x)	X_N	∈	f(x)	g(x)	b	
	a	hyper	67	f(x)	f(x)	g(x)	X_N	∈	f(x)	g(x)	b	
	b	tan	71	tanh f(x)	f(x)	g(x)	X_N	∈	f(x)	g(x)	b	
	c	roll↑	22	g(x)	tanh f(x)	f(x)	X_N	∈	f(x)	g(x)	b	
	d	X	36	g(x)	g(x) tanh f(x)	f(x)	X_N	∈	f(x)	g(x)	b	
3	0	tan	71	tan g(x)	g(x) tanh f(x)	f(x)	X_N	∈	f(x)	g(x)	b	
	1	roll↑	22	f(x)	tan g(x)	g(x) tanh f(x)	X_N	∈	f(x)	g(x)	b	
	2	X	36	f(x)	f(x) tan g(x)	g(x) tanh f(x)	X_N	∈	f(x)	g(x)	b	
	3	↓	25	f(x) tan g(x)	g(x) tanh f(x)	g(x) tanh f(x)	X_N	∈	f(x)	g(x)	b	
	4	+	33	f(x) tan g(x)	f tg + g th f	g(x) tanh f(x)	X_N	∈	f(x)	g(x)	b	
	5	e	12	∈	f tg + g th f	g(x) tanh f(x)	X_N	∈	f(x)	g(x)	b	
	6	|y|	55	∈	|f tg + g th f|	g th f	X_N	∈	f(x)	g(x)	b	
	7	X_R↔y	30	|f tg + g th f|	∈	g th f	X_N	∈	f(x)	g(x)	b	
	8	pause	51									
	9	pause	51									
	a	pause	51									
	b	pause	51									
	c	pause	51									
	d	if x>y	53	|f tg + g th f|	∈	g th f	X_N	∈	f(x)	g(x)	b	

Step		Key	Code	Display x	Display y	Display z	Storage f	e	d	c	b	a
4	0	4	04	$\lvert f t g + g t h f \rvert$	ϵ	g t h f	x_N	ϵ	f(x)	g(x)	b	
	1	5	05	$\lvert f t g + g t h f \rvert$	ϵ	g t h f	x_N	ϵ	f(x)	g(x)	b	
	2	↑	27	$\lvert f t g + g t h f \rvert$	$\lvert f t g + g t h f \rvert$	ϵ	x_N	ϵ	f(x)	g(x)	b	
	3	f	15	x_N	$\lvert f t g + g t h f \rvert$	ϵ	x_N	ϵ	f(x)	g(x)	b	
	4	STOP	41	x_N	$\lvert f t g + g t h f \rvert$	ϵ	x_N	ϵ	f(x)	g(x)	b	
4	5	1	01	1	ϵ	g t h f	x_N	ϵ	f(x)	g(x)	b	
	6	0	00	10	ϵ	g t h f	x_N	ϵ	f(x)	g(x)	b	
	7	ln x	65	ln 10	ϵ	g t h f	x_N	ϵ	f(x)	g(x)	b	
	8	↑	27	ln 10	ln 10	ϵ	x_N	ϵ	f(x)	g(x)	b	
	9	ENTER EXP	26	ln 10	ln 10	ϵ	x_N	ϵ	f(x)	g(x)	b	
4	a	3	03	10^3	ln 10	ϵ	x_N	ϵ	f(x)	g(x)	b	
	b	Cont	47	10^3	ln 10	ϵ	x_N	ϵ	f(x)	g(x)	b	
	c	Cont	47	10^3	ln 10	ϵ	x_N	ϵ	f(x)	g(x)	b	
	d	÷	35	10^3	$\frac{\ln 10}{10^3}$	ϵ	x_N	ϵ	f(x)	g(x)	b	
5	0	↓	25	x_N $\frac{\ln 10}{10^3}$	ϵ	ϵ	x_N	ϵ	f(x)	g(x)	b	
	1	e^x	74	$10^{\frac{1}{10^3}}$	ϵ	ϵ	x_N	ϵ	f(x)	g(x)	b	
	2	↑	27	$10^{\frac{1}{10^3}}$	$10^{\frac{1}{10^3}}$	ϵ	x_N	ϵ	f(x)	g(x)	b	
	3	f	15	x_N	$10^{\frac{1}{10^3}}$	ϵ	x_N	ϵ	f(x)	g(x)	b	
	4	X	36	x_N	$x_N\, 10^{\frac{1}{10^3}}$	ϵ	x_N	ϵ	f(x)	g(x)	b	
	5	y→	40	x_N	$x_N\, 10^{\frac{1}{10^3}}$	ϵ	x_N	ϵ	f(x)	g(x)	b	
	6	f	15	x_N	$x'_N = x_N 10^{\frac{1}{10^3}}$	ϵ	x'_N	ϵ	f(x)	g(x)	b	
	7	Clear x	37	0	x'_N	ϵ	x'_N	ϵ	f(x)	g(x)	b	
	8	↑	27	0	0	x'_N	x'_N	ϵ	f(x)	g(x)	b	
	9	Roll ↑	22	x'_N	0	0	x'_N	ϵ	f(x)	g(x)	b	
	a	GoTo	44	x'_N	0	0	x'_N	ϵ	f(x)	g(x)	b	
	b	0	00	x'_N	0	0	x'_N	ϵ	f(x)	g(x)	b	
	c	4	04	x'_N	0	0	x'_N	ϵ	f(x)	g(x)	b	
	d											

Step		Key	Code	Display x	Display y	Display z	Storage f	Storage e	Storage d	Storage c	Storage b	Storage a
6	0	C	16	g'(x)	/f'g+gtf/	∈	x_N	∈	f(x)	g(x)	b	
	1	↑	27	g(x)	g(x)	/f'g+gtf/	x_N	∈	f(x)	g(x)	b	
	2	sin x	70	sin g(x)	g(x)	/f'g+gtf/	x_N	∈	f(x)	g(x)	b	
	3	X	36	sin g(x)	g(x) sin g(x)	/f'g+gtf/	x_N	∈	f(x)	g(x)	b	
	4	d	17	f(x)	g(x) sin g(x)	/f'g+gtf/	x_N	∈	f(x)	g(x)	b	
	5	hyper	67	f(x)	g(x) sin g(x)	/f'g+gtf/	x_N	∈	f(x)	g(x)	b	
	6	cos x	73	cosh f(x)	g(x) sin g(x)	/f'g+gtf/	x_N	∈	f(x)	g(x)	b	
	7	X	36	cosh f(x)	g sg(ch f)	/f'g+gtf/	x_N	∈	f(x)	g(x)	b	
	8	d	17	f(x)	g sg(ch f)	/f'g+gtf/	x_N	∈	f(x)	g(x)	b	
	9	↑	27	f(x)	f(x)	g sg(ch f)	x_N	∈	f(x)	g(x)	b	
	a	hyper	67	f(x)	f(x)	g sg(ch f)	x_N	∈	f(x)	g(x)	b	
	b	sin x	70	sinh f(x)	f(x)	g sg(ch f)	x_N	∈	f(x)	g(x)	b	
	c	X	36	sinh f(x)	f(x) sinh f(x)	g sg(ch f)	x_N	∈	f(x)	g(x)	b	
	d	C	16	g(x)	f(x) sinh f(x)	g sg(ch f)	x_N	∈	f(x)	g(x)	b	
7	0	cos x	73	cos g(x)	f(x) sinh f(x)	g sg(ch f)	x_N	∈	f(x)	g(x)	b	
	1	X	36	cos g(x)	f sh f(cg)	g sg(ch f)	x_N	∈	f(x)	g(x)	b	
	2	↓	25	f sh f(cg)	g sg(ch f)	g sg(ch f)	x_N	∈	f(x)	g(x)	b	
	3	−	34	f sh f(cg)	g sg(ch f) − f sh f(cg)	g sg(ch f)	x_N	∈	f(x)	g(x)	b	
	4	f	15	x_N	α	g sg(ch f)	x_N	∈	f(x)	g(x)	b	
	5	roll↑	22	g sg(ch f)	x_N	α	x_N	∈	f(x)	g(x)	b	
	6	clear x	37	0	x_N	α	x_N	∈	f(x)	g(x)	b	
	7	roll↓	31	x_N	α	0	x_N	∈	f(x)	g(x)	b	
	8	stop	41	x_N	α	0	x_N	∈	f(x)	g(x)	b	
	9	END	46	x_N	α	0	x_N	∈	f(x)	g(x)	b	
	a											
	b											
	c											
	d											

APPENDIX B

Program for Hewlett-Packard Calculator Model 9100A to determine the effect of dielectric loss on the $\overline{\text{ERC}}$ Notch Filter.

OPERATION OF PROGRAM

1. Press END
2. Press CONTINUE
3. Enter $B(\omega)$ in x
4. $x \rightarrow b$
5. Enter D in x
6. $x \rightarrow a$
7. Enter ε in x
8. $x \rightarrow e$

We next enter the amount by which we wish to increase X_N. To begin with, one would increase X_N by 0.001. As the imaginary part of the numerator approaches ε, X_N may be increasing by too large an amount and we may go through the minimum (i.e. pass through the point where the imaginary part of the numerator is $\leq \varepsilon$). Therefore, as the imaginary part of the numerator approaches ε we stop the program and change it so X_N increases in steps of 10^{-6}.

The amount by which X_N is increased (i.e. 10^{-3}) is entered as follows:

1. GO TO 5(C)
2. Switch to "PROGRAM" position
3. Enter 3 in x register to increase X_N by 10^{-3}.

4. Switch to "RUN" position
5. Press END
6. Press CONTINUE
7. Enter ε in x register
8. $x \rightarrow e$
9. Enter initial value for X_N. This value must be $\leq$ the value of X_N required to make the imaginary part of the numerator $\leq \varepsilon$.
10. Press CONTINUE
11. Wait for convergence
12. X_N is displayed in x register

Once the value of X_N is determined, we can then solve for α. Alpha is solved for as follows

1. GO TO 6(d)
2. Press CONTINUE
3. X_N is displayed in x register
   α is displayed in y register.

Title Notch Filter with Dielectric Loss taken into Account. Calculations of Zeros (Positions of Optimum Notch) and the corresponding values of α.

Date 11 Nov. '69 Page 1

Name

$\alpha = R/R_N$

$X_N = \omega_{o,n}/\omega_o$

$B(\omega) = R_S/R = b$

Step		Key	Code	Display x	Display y	Display z	Storage f	Storage e	Storage d	Storage c	Storage b	Storage a
0	0	Clear	20									
	1	STOP	41	X_N	0	0	X_N	ϵ			b	D
	2	↑	27	X_N	X_N	0	X_N	ϵ			b	D
	3	a	13	D	X_N	0	X_N	ϵ			b	D
	4	hyper	67	D	X_N	0	X_N	ϵ			b	D
	5	Sin	70	$\sinh D$	X_N	0	X_N	ϵ			b	D
	6	X	36	$\sinh D$	$X_N \sinh D$	0	X_N	ϵ			b	D
	7	X	36	$\sinh D$	$X_N \sinh^2 D$	0	X_N	ϵ			b	D
	8	a	13	D	$X_N \sinh^2 D$	0	X_N	ϵ			b	D
	9	÷	35	D	$\frac{X_N \sinh^2 D}{D}$	0	X_N	ϵ			b	D
	a	÷	35	D	$\frac{X_N \sinh^2 D}{D^2}$	0	X_N	ϵ			b	D
	b	b	14	b	$\frac{X_N \sinh^2 D}{D^2}$	0	X_N	ϵ			b	D
	c	X	36	b	$bX_N \frac{\sinh^2 D}{D^2}$	0	X_N	ϵ			b	D
	d	/	01	1	$bX_N \frac{\sinh^2 D}{D^2}$	0	X_N	ϵ			b	D
1	0	To Polar	62	A	$L\Phi$ (rad)	0	X_N	ϵ			b	D
	1	x→	23	A	$L\Phi$	0	X_N	ϵ			b	D
	2	c	16	A	$L\Phi$	0	X_N	ϵ		A	b	D
	3	π	56	π	$L\Phi$	0	X_N	ϵ		A	b	D
	4	↑	27	π	π	$L\Phi$	X_N	ϵ		A	b	D
	5	2	02	2	π	$L\Phi$	X_N	ϵ		A	b	D
	6	÷	35	2	π/2	$L\Phi$	X_N	ϵ		A	b	D
	7	↓	25	π/2	$L\Phi$	$L\Phi$	X_N	ϵ		A	b	D
	8	x⇄y	30	$L\Phi$	π/2	$L\Phi$	X_N	ϵ		A	b	D
	9	−	34	$L\Phi$	$\pi/2 - \Phi$	$L\Phi$	X_N	ϵ		A	b	D
	a	c	16	A	$\pi/2 - \Phi$	$L\Phi$	X_N	ϵ		A	b	D
	b	↑	27	A	A	Θ	X_N	ϵ		A	b	D
	c	f	15	X_N	A	Θ	X_N	ϵ		A	b	D
	d	x⇄y	30	A	X_N	Θ	X_N	ϵ		A	b	D

Step		Key	Code	Display x	Display y	Display z	Storage f	Storage e	Storage d	Storage c	Storage b	Storage a
2	0	÷	35	A	x_N/A	Θ	x_N	∈		A	b	D
	1	↓	25	x_N/A	Θ	Θ	x_N	∈		A	b	D
	2	TO RECT	66	a′	j b′	Θ	x_N	∈		A	b	D
	3	x→	23	a′	j b′	Θ	x_N	∈		A	b	D
	4	C	16	a′	j b′	Θ	x_N	∈		a′	b	D
	5	a	13	D	j b′	Θ	x_N	∈		a′	b	D
	6	↑	27	D	D	j b′	x_N	∈		a′	b	D
	7	X	36	D	D^2	j b′	x_N	∈		a′	b	D
	8	C	16	a′	D^2	j b′	x_N	∈		a′	b	D
	9	+	33	a′	$a'+D^2$	j b′	x_N	∈		a′	b	D
	a	↓	25	$a'+D^2$	j b′	j b′	x_N	∈		a′	b	D
	b	TO POLAR	62	x	⌊π	j b′	x_N	∈		a′	b	D
	c	√x	76	√x	⌊π	j b′	x_N	∈		a′	b	D
	d	x⇄y	30	⌊π	√x	j b′	x_N	∈		a′	b	D
3	0	↑	27	⌊π	⌊π	$x^{1/2}$	x_N	∈		a′	b	D
	1	2	02	2	⌊π	$x^{1/2}$	x_N	∈		a′	b	D
	2	÷	35	2	⌊π/2	$x^{1/2}$	x_N	∈		a′	b	D
	3	ROLL↓	31	⌊π/2	$x^{1/2}$	2	x_N	∈		a′	b	D
	4	x⇄y	30	$x^{1/2}$	⌊π/2	2	x_N	∈		a′	b	D
	5	TO RECT	66	f(x)	j g(x)	2	x_N	∈		a′	b	D
	6	x→	23	f(x)	j g(x)	2	x_N	∈		a′	b	D
	7	C	16	f(x)	j g(x)	2	x_N	∈		f(x)	b	D
	8	y→	40	f(x)	j g(x)	2	x_N	∈		f(x)	b	D
	9	d	17	f(x)	j g(x)	2	x_N	∈	g(x)	f(x)	b	D
	a	↑	27	f(x)	f(x)	g(x)	x_N	∈	g(x)	f(x)	b	D
	b	hyper	61	f(x)	f(x)	g(x)	x_N	∈	g(x)	f(x)	b	D
	c	tan	71	tanh f(x)	f(x)	g(x)	x_N	∈	g(x)	f(x)	b	D
	d	x	36	tanh f(x)	f(x) tanh f(x)	g(x)	x_N	∈	g(x)	f(x)	b	D

Step		Key	Code	Display x	Display y	Display z	Storage f	Storage e	Storage d	Storage c	Storage b	Storage a
4	0	↓	25	f(x) tanh f(x)	g(x)	g(x)	x_N	∈	g(x)	f(x)	b	D
	1	x⇆y	30	g(x)	f(x) tanh f(x)	g(x)	x_N	∈	g(x)	f(x)	b	D
	2	↑	27	g(x)	g(x)	f(x) tanh f(x)	x_N	∈	g(x)	f(x)	b	D
	3	tan	71	tan g(x)	g(x)	f(x) tanh f(x)	x_N	∈	g(x)	f(x)	b	D
	4	X	36	tan g(x)	g(x) tan g(x)	f(x) tanh f(x)	x_N	∈	g(x)	f(x)	b	D
	5	↓	25	g(x) tan g(x)	f(x) tanh f(x)	f(x) tanh f(x)	x_N	∈	g(x)	f(x)	b	D
	6	+	33	g(x) tan g(x)	g tg + f th f	f(x) tanh f(x)	x_N	∈	g(x)	f(x)	b	D
	7	e	12	∈	g tg + f th f	f(x) tanh f(x)	x_N	∈	g(x)	f(x)	b	D
	8	|y|	55	∈	|g tg + f th f|	f(x) tanh f(x)	x_N	∈	g(x)	f(x)	b	D
	9	x⇆y	30	|g tg + f th f|	∈	f(x) tanh f(x)	x_N	∈	g(x)	f(x)	b	D
	a	Pause	57									
	b	"	57									
	c	"	57									
	d	"	57									
5	0	"	57									
	1	if x>y	53	|g tg + f th f|	∈	f(x) tanh f(x)	x_N	∈	g(x)	f(x)	b	D
	2	5	05									
	3	7	07									
	4	↑	27	|g tg + f th f|	|g tg + f th f|	∈	x_N	∈	g(x)	f(x)	b	D
	5	f	15	x_N	|g tg + f th f|	∈	x_N	∈	g(x)	f(x)	b	D
	6	STOP	41	x_N	|g tg + f th f|	∈	x_N	∈	g(x)	f(x)	b	D
5	7	81	01	1	∈	f(x) tanh f(x)	x_N	∈	g(x)	f(x)	b	D
	8	0	00	10	∈	f(x) tanh f(x)	x_N	∈	g(x)	f(x)	b	D
	9	ln x	65	ln 10	∈	f(x) tanh f(x)	x_N	∈	g(x)	f(x)	b	D
	a	↑	27	ln 10	ln 10	∈	x_N	∈	g(x)	f(x)	b	D
	b	ENTER EXP	26	ln 10	ln 10	∈	x_N	∈	g(x)	f(x)	b	D
5	c	3	03	10^3	ln 10	∈	x_N	∈	g(x)	f(x)	b	D
	d	÷	35	10^3	(ln 10)/10^3	∈	x_N	∈	g(x)	f(x)	b	D

Step		Key	Code	Display x	Display y	Display z	Storage f	Storage e	Storage d	Storage c	Storage b	Storage a
6	0	↓	25	$(\ln 10)/10^3$	ϵ	ϵ	x_N	ϵ	$g(x)$	$f(x)$	b	D
	1	e^x	74	$10^{\frac{1}{10^3}}$	ϵ	ϵ	x_N	ϵ	$g(x)$	$f(x)$	b	D
	2	↑	27	$10^{\frac{1}{10^3}}$	$10^{\frac{1}{10^3}}$	ϵ	x_N	ϵ	$g(x)$	$f(x)$	b	D
	3	f	15	x_N	$10^{\frac{1}{10^3}}$	ϵ	x_N	ϵ	$g(x)$	$f(x)$	b	D
	4	X	36	x_N	x_N'	ϵ	x_N	ϵ	$g(x)$	$f(x)$	b	D
	5	y→	40	x_N	x_N'	ϵ	x_N	ϵ	$g(x)$	$f(x)$	b	D
	6	f	15	x_N	x_N'	ϵ	x_N'	ϵ	$g(x)$	$f(x)$	b	D
	7	clear x	37	0	x_N'	ϵ	x_N'	ϵ	$g(x)$	$f(x)$	b	D
	8	↑	27	0	0	x_N'	x_N'	ϵ	$g(x)$	$f(x)$	b	D
	9	roll↑	22	x_N'	0	0	x_N'	ϵ	$g(x)$	$f(x)$	b	D
	a	GoTo	44	x_N'	0	0	x_N'	ϵ	$g(x)$	$f(x)$	b	D
	b	0	00									
	c	2	02									
6	d	a	13	D	/gtg+fthf/	ϵ	x_N	ϵ	$g(x)$	$f(x)$	b	D
7	0	e^x	74	e^D	/gtg+fthf/	ϵ	x_N	ϵ	$g(x)$	$f(x)$	b	D
	1	↑	27	e^D	e^D	ϵ	x_N	ϵ	$g(x)$	$f(x)$	b	D
	2	X	36	e^D	e^{2D}	ϵ	x_N	ϵ	$g(x)$	$f(x)$	b	D
	3	1	01	1	e^{2D}	ϵ	x_N	ϵ	$g(x)$	$f(x)$	b	D
	4	-	34	1	$e^{2D}-1$	ϵ	x_N	ϵ	$g(x)$	$f(x)$	b	D
	5	a	13	D	$e^{2D}-1$	ϵ	x_N	ϵ	$g(x)$	$f(x)$	b	D
	6	÷	35	D	$(e^{2D}-1)/D$	ϵ	x_N	ϵ	$g(x)$	$f(x)$	b	D
	7	f	15	x_N	$(e^{2D}-1)/D$	ϵ	x_N	ϵ	$g(x)$	$f(x)$	b	D
	8	X	36	x_N	$x_N \frac{e^{2D}-1}{D}$	ϵ	x_N	ϵ	$g(x)$	$f(x)$	b	D
	9	C	16	$f(x)$	$x_N \frac{e^{2D}-1}{D}$	ϵ	x_N	ϵ	$g(x)$	$f(x)$	b	D
	a	hyper	47									
	b	Cos	73	$\cosh f(x)$	$x_N \frac{e^{2D}-1}{D} = H$	ϵ	x_N	ϵ	$g(x)$	$f(x)$	b	D
	c	X	36	$\cosh f(x)$	$H \cosh f(x)$	ϵ	x_N	ϵ	$g(x)$	$f(x)$	b	D
	d	d		$g(x)$	$H \cosh f(x)$	ϵ	x_N	ϵ	$g(x)$	$f(x)$	b	D

Title _____ Date _____ page 5 of 5

Name _____

Step		Key	Code	Display x	Display y	Display z	Storage f	Storage e	Storage d	Storage c	Storage b	Storage a
8	0	Sin	70	Sin g(x)	H cos h f(x)	∈	x_N	∈	g(x)	f(x)	b	D
	1	X	36	Sin g(x)	H ch f sg	∈	x_N	∈	g(x)	f(x)	b	D
	2	C	16	f(x)	H ch f sg	∈	x_N	∈	g(x)	f(x)	b	D
	3	÷	35	f(x)	H ch f sg/f	∈	x_N	∈	g(x)	f(x)	b	D
	4	2	02	2	H ch f sg/f	∈	x_N	∈	g(x)	f(x)	b	D
	5	÷	35	2	H ch f sg/2f	∈	x_N	∈	g(x)	f(x)	b	D
	6	a	13	D	H ch f sg/2f	∈	x_N	∈	g(x)	f(x)	b	D
	7	e^x	74	e^D	H ch f sg/2f	∈	x_N	∈	g(x)	f(x)	b	D
	8	÷	35	e^D	$\frac{H\ ch\ f\ sg}{2\ f\ c^D}$	∈	x_N	∈	g(x)	f(x)	b	D
	9	Clear x	37	0	α	∈	x_N	∈	g(x)	f(x)	b	D
	a	Roll↑	22	∈	0	α	x_N	∈	g(x)	f(x)	b	D
	b	f	15	x_N	0	α	x_N	∈	g(x)	f(x)	b	D
	c	Roll↓	22	α	x_N	0	x_N	∈	g(x)	f(x)	b	D
	d	x⇄y	30	x_N	α	0	x_N	∈	g(x)	f(x)	b	D
9	0	STOP	41	x_N	α	0	x_N	∈	g(x)	f(x)	b	D
	1	END	46	x_N	α	0	x_N	∈	g(x)	f(x)	b	D
	2											
	3											
	4											
	5											
	6											
	7											
	8											
	9											
	a											
	b											
	c											
	d											

BIBLIOGRAPHY

1. M. S. Ghausi and J. J. Kelly, "Introduction to Distributed Parameter Networks With Application to Integrated Circuits", Holt Rinehart & Winston, Inc., New York, N.Y., 1968.

2. S. S. Haykim, "Active Network Theory", (To be Published).

3. J. J. Kelly and M. S. Ghausi, "Tapered Distributed RC Networks with Similar Immittances", I.E.E.E. Trans., CT-12, p.554 (1965).

4. H. C. Lin, "Integrated Electronics", Holden-Day Inc., San Francisco, California, 1967.

5. W. M. Kaufman, "Theory of a Monolithic Null Device and some Novel Circuits", Proc. I.R.E., Vol. 48, p.1330, 1961.

6. K. Oehler, "Analysis and Synthesis of Distributed Parameter Circuits", Ph.D. Thesis, University of Texas, 1964.

7. M. J. Hellstrom, "Symmetrical RC Distributed Networks", Proc. I.R.E. Vol. 50, pp.97-98 (1962).

8. W. M. Kaufman and S.J. Garrett, "Tapered Distributed Filters", I.R.E. Trans. P.G.C.T., Vol. 9, p.1330-1331 (1962).

9. S. Tolansky, "Multiple Beam Interferometry of Surfaces and Films", Oxford University Press, Oxford, 1962.

10. R. C. Dynes, "A Tunneling Investigation of the Mechanisms Determining Superconductivity in Simple Metals and Alloys," Ph.D. Thesis, McMaster University, 1968.

11. W. P. Mason, "Piezoelectric Crystals and their Application to Ultrasonics," D. Van Nostrand Co. Inc., New York, 1950.

12. F. J. Vallo, "Performance Enhancement of Evaporated Thin Film Field Effect Transistors", M. Eng. Thesis, McMaster University, 1969.

13. A. D. Moore, "Mapping Techniques Applied to Fluid Mapper Patterns", A.I.E.E. Transactions, Vol. 71, p.1-6 (1952).

14. M. G. Miksic, E. J. Schlig and R. R. Haering, "Solid State Electronics", I, 39, 1964.

15. R. W. Berry, P. M. Hall and M. T. Harris, "Thin Film Technology", D. Van Nostrand Co.Inc., Princeton, New Jersey, 1968.